A MOLECULAR ANALYSIS OF *SRC64* AND ITS IMPACT ON CYTOSKELETAL REORGANIZATION IN THE DROSOPHILA EMBRYO

by

TAYLOR CLINTON STRONG, B.S.

A THESIS

IN

CELL & MOLECULAR BIOLOGY

Submitted to the Graduate Faculty of
Texas Tech University Health Sciences Center
in Partial Fulfillment of the Requirements
for the Degree of

MASTER OF SCIENCE

Advisory Committee

Jeffery Thomas (Chairperson)
Dan Webster
Simon Williams

Accepted

Barbara C. Pence, Ph.D.
Associate Dean of the Graduate School of Biomedical Sciences
Texas Tech University Health Sciences Center

May 2007

ACKNOWLEDGMENTS

I would first like to thank my graduate mentor Dr. Jeffrey Thomas for his guidance, leadership, and assistance during my time spent in his laboratory and at Texas Tech University Health Sciences Center. I would also like to thank my committee members: Dr. Daniel Webster, and Dr. Simon Williams for their valuable input into this project. For their assistance in the laboratory I would like to thank Erin Anderson and Ralph Rosales.

For locating and providing *Src64* mutations, I would like to thank The Seattle TILLING Project, a joint project run by the Fred Hutchison Cancer Research Center and the University Of Washington Department Of Biology. For providing the anti-alpha zipper RB 78 anti-myosin II heavy chain antibody I would like to thank A. Sokac.

I would also like to thank my wife Desiree and my parents for the support that they have given me.

TABLE OF CONTENTS

ABSTRACT

Src-family kinases are involved in many processes related to development. As regulators of development, Src-family kinases are involved in cell motility, cell proliferation, and neo-angiogenesis. Src-family kinase activity has also been implicated in a number of cancers. *Src64* in Drosophila encodes a non-receptor tyrosine kinase that is homologous to human Src family kinases. *Src64* is involved in processes related to cell proliferation and apoptosis. Additionally, specific roles for Src64 have been identified in ring canal growth, dorsal closure, and salivary gland invagination. Our lab is specifically looking at the role of *Src64* in microfilament ring constriction during cellularization. The $Src64^{\Delta 17}$ mutation deletes the first two exons of the gene and eliminates all but trace amounts of Src64 protein, suggesting that there is an alternate transcriptional start site that is unaffected by the $Src64^{\Delta 17}$ mutation. This alternate transcript may be responsible for the phenotypic differences observed between *Src64* deficient flies and $Src64^{\Delta 17}$ flies. Semi-quantitative RT-PCR confirmed the presence of low levels of *Src64* mRNA in $Src64^{\Delta 17}$ embryos. Using 5' RACE analysis of $Src64^{\Delta 17}$ embryos we located the alternate transcriptional start site and identified a previously unknown exon located 13,100 base pairs downstream of the primary transcriptional start site, and 12,113 bp downstream of the two exons deleted in $Src64^{\Delta 17}$. To further investigate the role of *Src64* in development we identified ten missense mutations in the *Src64* coding region. This approach has allowed us to isolate several *Src64* mutations in an unbiased manner that disrupt the SH2 and tyrosine kinase domains. We analyzed embryos affected by these *Src64* mutations for defects related to *Src64* activity. In our analysis we identified defects to the cellularization front and microfilament rings of varying strength depending on the specific *Src64* mutation.

LIST OF TABLES

LIST OF FIGURES

CHAPTER I
INTRODUCTION

1.1 Src-family kinases

The Src-family of kinases is a large family of related non-receptor tyrosine kinase proteins found in nearly all metazoan organisms that share a common structure and are active in similar pathways (Boggon and Eck, 2004). All Src-family kinases contain an SH3, an SH2 and a tyrosine kinase domain. Additionally, the proteins have an SH4 domain at the amino terminus that is a myristoylation site for targeting of the protein to the plasma membrane, and a regulatory tyrosine near the C-terminus (Roskoski, 2004). v-Src was the first Src-family kinase discovered. The gene was identified in the Rous sarcoma virus in chickens which gave the protein family its name (Roskoski, 2004). Nine members of the Src-family of kinases have been discovered in humans: Src, Lck, Hck, Fyn, Blk, Lyn, Fgr, Yes, and Yrk. The human gene Src is representative of the prototypical Src-family kinase and is the most studied of the human Src-family kinases (Summy and Gallick, 2006). Src is also well known as the first discovered proto-oncogene (Bishop, 1985).

The multi-domain structure of Src allows the proteins to bind to a large number of substrates and interact in a large number of pathways (Pawson, 2004). The SH3 domain allows Src-family kinases to bind to proteins with the RxxPxP motif. The SH2 domain allows the protein to bind specific phospho-tyrosine residues in target proteins; though Src SH2 domains bind preferentially to the pYEEI motif (Boggon and Eck, 2004). The tyrosine kinase domain catalyzes the phosphorylation of specific tyrosine residues in target proteins and allows the protein to participate in signaling cascades (Roskoski, 2004).

Src activity is regulated by the activity of various upstream kinases and phosphorylases. Inhibition of Src activity occurs mainly through the activity of the protein C-terminal Src kinase (CSK) (Roskoski, 2004). Src protein has two forms, the active form and the auto-inhibited form (Boggon and Eck, 2004). Phosphorylation of the regulatory C-terminal tyrosine by CSK allows the Src SH2 domain to bind the regulatory C-terminal tyrosine. This places the protein in an auto-inhibited shape that prevents

substrate binding in the SH3 and SH2 domains and blocks the tyrosine kinase domain catalytic site (Boggon and Eck, 2004). Src protein can be activated by dephosphorylation of the regulatory C-terminal tyrosine and phosphorylation of a regulatory A-loop tyrosine in the tyrosine kinase domain by upstream kinases. Dephosphorylation of the regulatory C-terminal tyrosine prevents binding to the SH2 domain. This opens the SH3 and SH2 domains up for substrate binding and allows for tyrosine kinase catalytic activity (Roskoski, 2004). Phosphorylation of the A-loop tyrosine places the tyrosine kinase activation loop in the active conformation allowing for Src kinase activity (Roskoski, 2004).

Src-family kinases are active in a large number of cell signaling pathways (Thomas and Brugge, 1997). Src, specifically, is known to be involved in signaling pathways related to cell proliferation (Baumeister et al. 2005), cell motility (Yeo et al, 2006), cell adhesion (Thomas and Brugge, 1997), and neo-angiogenesis (Summy and Gallick, 2006).

Src is known to regulate cell motility and cell adhesion at focal adhesions. Focal adhesions are integrin rich plasma membrane structures that link the actin cytoskeleton to the extra-cellular matrix and participate in the process of cell motility (Parsons, 2003). Src is known to associate with focal adhesions. Specifically, both the Src SH2 and SH3 domains are able to localize Src to focal adhesions by binding to the focal adhesion associated adapter protein paxillin (Kaplan et al., 1994; Schaller, 2001). The Src SH2 domain is also involved in recruitment of the protein focal adhesion kinase (FAK) to focal adhesions (Kaplan et al., 1994; Yeo et al., 2006). FAK controls cell motility by regulating the formation of new focal adhesions, and by acting on proteins, such as vinculin, that link integrins to the actin cytoskeleton (Pawson, 2003). FAK is a target of Src kinase activity at tyrosine residues 576/577 (Sieg et al., 1999). Src-dependent phosphorylation of FAK at these residues is necessary for full enzymatic activity (Schaller et al., 1999). FAK activity leads to an increase in focal adhesion turnover, which can result in decreased in cell adhesion and increased cell motility. Additionally, there appears to be a kinase-independent function for Src at focal adhesions. The SH3 and SH2 domains are sufficient to cause structural changes to focal adhesions. During

this process the SH3 and SH2 domains are thought to work in a scaffolding role, though the specifics of kinase-independent activity is not known (Kaplan et al., 1994).

Src can also regulate cell motility by direct regulation of the actin cytoskeleton (Frame et al. 2002). Cortactin is an actin binding protein present in actin-rich structures called lamellipodia commonly present at the leading edge of motile cells. Cortactin is a Src substrate that is activated by phosphorylation by Src kinase activity (Huang et al., 1997; Wu et al., 1991). Src activation of cortactin leads to ARP2/3 (actin related protein) activation, and an increase in actin filament nucleation. The increase in actin filament polymerization provides the force necessary to move the leading edge of the cell forward (Higgs and Pollard, 2001). Many of the specifics roles for Src during this process have yet to be discovered and the specific roles of the SH3 and SH2 domains during this process are still under investigation.

Src also regulates cell proliferation and neo-angiogenesis through its role of a regulator of adherens junctions. Adherens junctions are cell-cell junctions in epithelial cells that are comprised of transmembrane cadherin proteins that bind the cells together, and catenins, that bind the cell-cell junction to the cytoskeleton. Adherens junctions provide stability to epithelial tissues and are responsible for contact inhibition of cell proliferation (Baumeister et al., 2005). Cadherin-catenin junction stability is regulated by tyrosine phosphorylation at the tyrosine 685 residue. Stimulation of endothelial cells by vascular endothelial growth factor (VEGF) leads to Src-dependent phosphorylation of VE-cadherin, disruption of cell-cell junctions, and an increase in cell proliferation (Schwartz et al., 1981; Wallez et al., 2007). This pathway is important in the process of neo-angiogenesis (the creation of new blood vessels) (Baumeister et al., 2005). As in Src activation of cortactin, specific roles for the SH3 and SH2 domains during this process have not been identified.

1.2 Relevance

The role that Src-family kinases can play in cancer development has been well established (Summy and Gallick, 2006). Src activity has been shown to be elevated in a wide range of cancers including colon, breast, and pancreatic cancers (Irby and Yeatman,

2000). An increase in Src activity can lead to increases in cell motility, cell proliferation, and neo-angiogenesis beyond the level seen in normal cells (Irby and Yeatman, 2000). At their extremes these traits are characteristic of the transformed phenotype and are important steps in the progression to malignancy (Irby and Yeatman, 2000). Increased Src activity can result from elevated upstream signaling activity, increased Src transcription, and activating mutations in Src (Summy and Gallick, 2006).

Endothelial cells provide a good model for how an elevation in Src activity can affect normal cell activity. CSK inhibits Src activity by phosphorylation of the regulatory C-terminal tyrosine (Rokoski, 2004). Normally, CSK associates with VE-cadherin and works to inhibit Src activity (Baumeister et al. 2005); however, Src mutants have been identified in which CSK is unable to inhibit Src activity due to a mutation of the regulatory C-terminal tyrosine (Irby et al. 1999). This mutation leads to elevated Src activity, increased VE-cadherin phosphorylation (Wallez et al. 2007), and loss of cell stability leading to the loss of contact inhibition of cell proliferation and the increased vascular permeability that is characteristic of malignant cells (Irby et al. 1999). This is a current area of clinical research for Src inhibitors. Supporting the role of Src in the regulation of angiogenesis is the recent identification of a Src kinase inhibitor that inhibits VEGF induced endothelial cell proliferation (Ali et al., 2005).

The multi-domain structure of Src allows the protein to function in a large number of complex pathways (Thomas and Brugge, 1997). Due to this complexity there is still a lot that is unknown about Src activity. Specifically, how does Src activity differ in the various signaling pathways in which it is involved? Control of Src transcription is another area in which little is known about Src regulation. Src transcription is important because the level of Src in a cell can be the difference between normal cell activity and progression towards malignancy (Summy and Gallick, 2006).

The *Drosophila* embryo is an ideal model for the study of Src family kinases and their activity during normal development. By using the *Drosophila* embryo we are able to combine the classical genetic approach of working with *Drosophila* with the ability to make direct observations of the cytoskeleton in the developing embryo. There are two Src-family kinases in *Drosophila*. One of them, *Src64*, is a close homolog to human Src

and is known to be involved in aspects of embryonic development specifically related to the actin cytoskeleton. This makes *Src64* activity a good model for Src-family kinase regulation of the actin cytoskeleton. Using the *Drosophila* embryo we are able to see how alteration of *Src64*, either at the genetic level or at the protein level, will affect the development of the embryo. In this analysis of *Src64*, we look at both transcriptional regulation of *Src64* and Src64 protein activity during development. This research could be important in discovering how Src family kinases are controlled in humans during normal development, as well as how Src activity is altered in the progression towards malignancy.

1.3 Drosophila embryo development

Drosophila embryo development is a 16-stage process that takes approximately 22 hours to complete (Roberts, 1998). Development begins in the egg chamber before embryogenesis. Nurse cells connected to the oocyte deposit transcription factors and RNA transcripts into the embryo through structures called ring canals (Robinson and Cooley, 1996). Ring canals are actin-rich cytoskeletal structures formed as a result of incomplete cytokinesis during the cellular divisions that form the oocyte and the 15 surrounding nurse cells (Robinson and Cooley, 1986). Maternally deposited transcription factors and RNA transcripts control the beginning stages of embryo development during which time zygotic transcription is silenced (Edgar and Schubinger, 1996). After pro-nuclear fusion, development proceeds through the first three embryonic stages during which nine rapid rounds of nuclear division without cytokinesis forms the multi-nucleate pre-blastoderm (Roberts, 1998) (Figure 1.1). During embryonic stage four the nuclei migrate towards the periphery of the embryo and proceed through five more rounds of nuclear division without cytokinesis (Roberts, 1998). It is during stage four, approximately during the 11^{th} or 12^{th} nuclear division cycle, that zygotic transcription begins. By the 14^{th} nuclear division cycle, at the end of stage four, zygotic transcription is fully active and has taken over the main role in controlling embryo development (Edgar and Schubinger, 1986). At the end of stage four the embryo has become an approximately 6,000 nuclei syncytial blastoderm. During stage five the process of

cellularization transforms the syncytial blastoderm into a cellular blastoderm. During cellularization individual furrow canals of plasma membrane rich in actin form around each nucleus and migrate towards the interior of the embryo (Thomas and Wieschaus, 2004; Fullilove and Jacobsen, 1971). The cellularization front progresses towards the interior of the embryo separating each nucleus with newly formed cell membrane. As the cellularization front passes the nuclei, microfilament rings within the front begin to constrict and close off the interior portion of the cells (Royou et al., 2004; Schejter and Wieschaus, 1993; Thomas and Wieschaus, 2004). Stage five ends with the completion of cellularization (Figure 1.1). During the remaining stages of embryogenesis more complex processes bring about the formation of the three germ layers and begin the process of segmentation. Embryonic development is completed at approximately 21-22 hours with the hatching of the larva (Roberts, 1998).

Many of the events occurring during early Drosophila development such as ring canal formation during oogenesis, and nuclear migration, cellularization, and microfilament ring constriction in the early embryo are complex processes that are performed through precise control of actin filaments (Sullivan et al., 1993). The molecular mechanisms that control these processes are currently poorly understood; however, the non-receptor tyrosine kinase *Src64* has emerged as one candidate protein that is important in the control of these processes (Dodson et al., 1998; Thomas and Wieschaus, 2004). These actin-mediated developmental events are a good model for the study of Src-family kinase regulation of the actin cytoskeleton.

1.4 *Src64* and associated mutations

Src64 is a 31.6kbp gene located at 64B11-12 on chromosome 3L. The gene is transcribed into a 2-3kbp mRNA transcript depending on alternately spliced exons in the 5’ untranslated region. *Src64* is translated into a 552 amino acid, 60 kD, protein that is comprised of an SH3, SH2 and a tyrosine kinase domain (Brody, 1995) (Figure 1.2). Like all Src-family kinases the protein has a myristoylation site near the amino terminus that localizes the protein to plasma membrane, and a regulatory inhibitory tyrosine near the carboxyl terminus (Boggon and Eck, 2004). Regulation of *Src64* activity is similar to

regulation of human Src. Src64 activity is inhibited by the kinase activity of CSK on the regulatory C-terminal tyrosine, and activated by phosphorylation of the regulatory A-loop tyrosine in the tyrosine kinase domain (O'Reilly et al., 2006; Pedraza et al., 2004; Roskoski, 2004).

Two mutations in *Src64* have been useful in the study of the gene's activity. The $Src64^{\Delta 17}$ mutation was produced by and previously described by Dodson, Guarnieri, and Simon (Dodson et al., 1998). The mutation is an imprecise P-element excision of the first two exons of *Src64*, which includes the transcriptional start site (Figure 1.3). $Src64^{\Delta 17}$ is a strong reduction-of-function allele that reduces but does not completely remove Src64 protein from affected flies. Over-exposed western blots of protein isolated from $Src64^{\Delta 17}$ embryos show trace amounts of Src64 protein (Dodson et al., 1998; O'Reilly et al., 2006).

The $Src64^{KO}$ mutation was produced by, and previously described by A. M. O'Reilly (O'Reilly et al., 2006). The mutation was produced via "ends out" homologous recombination (Gong and Golic, 2003) and replaces 5550 bp of *Src64* from 802 bp upstream of the start codon and 971 bp downstream of the stop codon with the *white* gene (O'Reilly et al., 2006; Gong and Golic, 2003) (Figure 1.3). Unlike $Src64^{\Delta 17}$, the mutation removes all traces of Src64 protein from affected flies. $Src64^{KO}$ flies show similar but more pronounced defects than $Src64^{\Delta 17}$ flies (O'Reilly et al., 2006).

The $Src64^{\Delta 17}$ and $Src64^{KO}$ mutations provided the first evidence for an alternate transcriptional start site for *Src64*. The over-exposed western blots that showed trace amounts of Src64 protein in $Src64^{\Delta 17}$ flies suggest that there is some alternate method of *Src64* transcription (Dodson et al., 1998). Additionally, the ring canal, embryo yield, and hatch rate defects seen in $Src64^{KO}$ flies and embryos appear more severe than those identified in $Src64^{\Delta 17}$ flies and embryos (O'Reilly et al., 2006). In the absence of an alternate transcriptional start site, the $Src64^{\Delta 17}$ mutation would be expected to cause the same defects as seen in the $Src64^{KO}$ mutation.

1.5 *Src64* activity

In addition to its role in cell proliferation and cell motility (Pedraza et al., 2004), *Src64* activity has been linked to a number of specific processes during embryo development. During Drosophila oogenesis F-actin is localized to the cleavage furrows during the four rounds of mitotic division that give rise to the 15 nurse cells and the oocyte (Tilney et al., 1996). An accumulation of actin to the cleavage furrows arrests the cleavage process and prevents the completion of cytokinesis. This allows for the transfer of materials from the nurse cells into the oocyte (Guarnieri et al., 1998). During oogenesis the ring canals grow from 0.5μl to approximately 10μl in diameter (Dodson et al., 1998). Both $Src64^{\Delta 17}$ and $Src64^{KO}$ mutant females have ring canals with a reduced diameter, though the defect seen in $Src64^{KO}$ is greater than that seen in $Src64^{\Delta 17}$(O'Reilly et al., 2006). It is thought that the action of the protein Kelch, an actin cross-linking protein, leads to this expansion of the ring canals (Kelso et al., 2002). Both the $Src64^{\Delta 17}$ mutant and a non-phosphorylatable mutant for Kelch show similar defects in ring canal morphology. The phosphorylated form of Kelch does not interact with actin, thus it is thought that *Src64* kinase activity is necessary to dissociate Kelch from actin (Kelso et al., 2002). Thus far no research has uncovered a specific role for the Src64 SH3 or SH2 domains in the protein's interaction with Kelch. Interestingly, the actin remodeling protein cortactin has also been identified in ring canal formation (Somogyi and Rorth, 2004). Src-family kinases are known to phosphorylate cortactin in humans. *Src64* may regulate the activity of cortactin during the process of ring canal growth; however, the two have not yet been linked.

Another gene that has emerged as a key mediator of ring canal morphogenesis is Tec29. Tec kinases are known targets of Src family kinases, and are similar to Src family kinases both in their structure and in their regulation of the cytoskeleton (Smith et al., 2001). Src64 is required for localization of Tec29 to ring canals, and the activity of the SH3 and SH2 domains is sufficient to localize Tec29 to ring canals (Guarnieri et al., 1998; Lu et al., 2004). Additionally, Src64 has been shown to phosphorylate Tec29, though the specific role of Tec29 in the formation of ring canals is not yet known (Lu et al., 2004).

During cellularization and microfilament ring constriction *Src64* is also thought to work through the controlled reorganization of actin microfilaments as it does during ring canal formation. The cellularization front at the base of each furrow canal is rich in both F-actin and myosin (Thomas and Wieschaus, 2004; Royou et al., 2004). These proteins could provide the contractile force required for the progression of the cellularization front and constriction of the microfilament rings. The cellularization front also shows increased levels of Src64 protein in a region that overlaps regions with elevated levels of myosin (Thomas and Wieschaus, 2004). $Src64^{\Delta 17}$ mutants do not show this elevated level of *Src64* at the cellularization front and have defects to the cellularization front that appear as a wavy, imprecise cellularization front and a reduced circularity (a normalized ratio of area to perimeter) of the microfilament rings; however, despite the reduced level of Src64 protein in $Src64^{\Delta 17}$ embryos, cellularization front progression and some microfilament ring constriction still occur (Thomas and Wieschaus, 2004). Similar to the formation of ring canals, Tec29 is involved in the cellularization process, however during cellularization Tec29 localizes to the cellularization front independent of Src64 activity (Thomas and Wieschaus, 2004).

As is the case with Src activity in humans, there is still a lot that is unknown about *Src64* activity in *Drosophila*. Specifically, questions remain about specific roles for the SH3 and SH2 domains during *Src64* activity. In our analysis of *Src64*, we hoped to gain a greater understanding of the roles that specific protein domains have during *Src64* activity and during Src-family kinase activity in general.

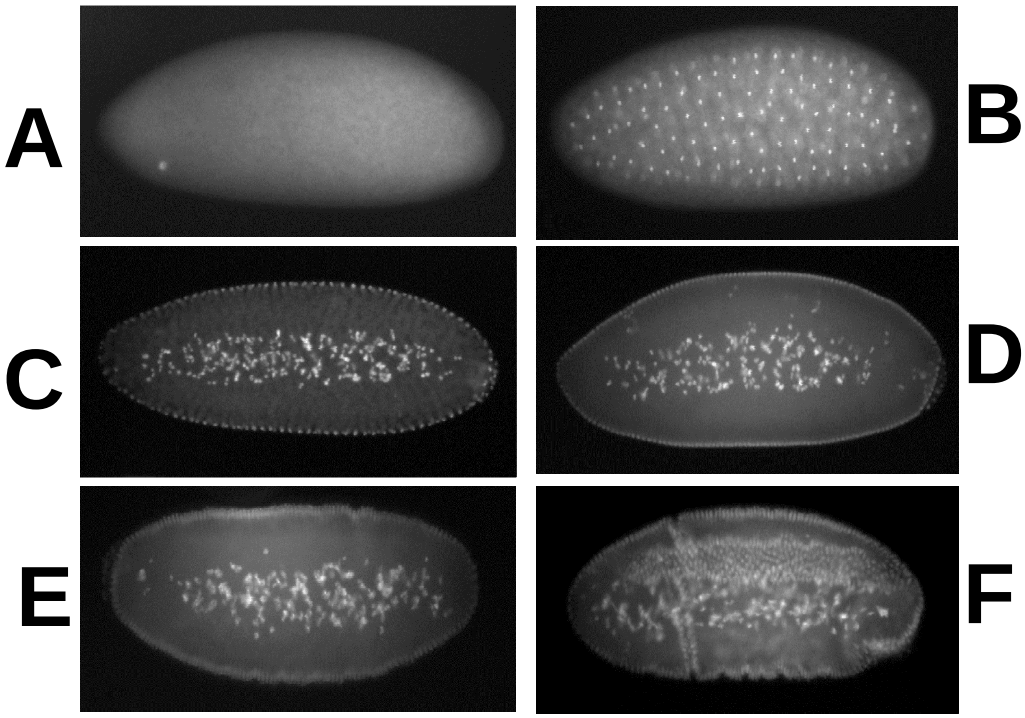

Figure 1.1: Early embryo development. *Drosophila* embryo development is a 16-stage process taking approximately 22 hours to complete. Development begins with pronuclear fusion during stage 1 (A). During the first 90 minutes and the first three stages of embryonic development, nine rounds of rapid nuclear division without cytokinesis result in a multinucleate pre-blastoderm (B). Stage 4 lasts for approximately 60 minutes and begins with nuclear migration as the majority of the nuclei migrate towards the periphery of the embryo (C). Four more rounds of nuclear division result in a 6000 nuclei syncytial blastoderm (D). Zygotic transcription begins during this stage. Cellularization marks the beginning of stage 5 in which the syncytial blastoderm is transformed into a cellular blastoderm (E). The process of cellularization takes approximately 60 minutes. At the conclusion of cellularization, during stage 6, the cephalic and ventral furrows form and posterior mid-gut invagination begins (F).

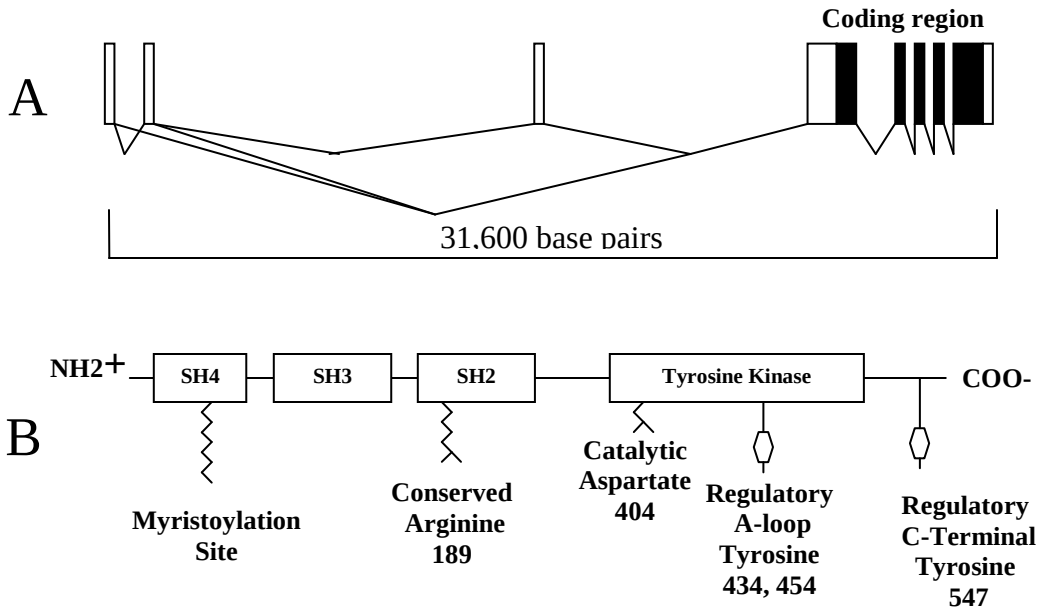

Figure 1.2: *Src64* splicing pattern and protein domains. *Src64* is a 31.6 kb gene located at 64B11-12 on chromosome 3L. The gene is transcribed into a 2-3kb mRNA transcript depending on alternately spliced 5' un-translated exons (A). The gene is translated into a 552 amino acid, 60kD protein comprised of an SH3, SH2, and tyrosine kinase domain (B). There is a myristoylation site (SH4 domain) at the amino terminus that localizes the protein to the plasma membrane. Regulation of the protein is primarily through inhibition by phosphorylation of the regulatory C-terminal tyrosine. Src64 can be activated by phosphorylation of the regulatory A-loop tyrosine in the catalytic domain (B). The catalytic aspartate residue is necessary for tyrosine kinase catalytic activity in the tyrosine kinase domain (B). In the SH2 domain the conserved arginine residue is important in recognition of the binding motif in the target protein (B).

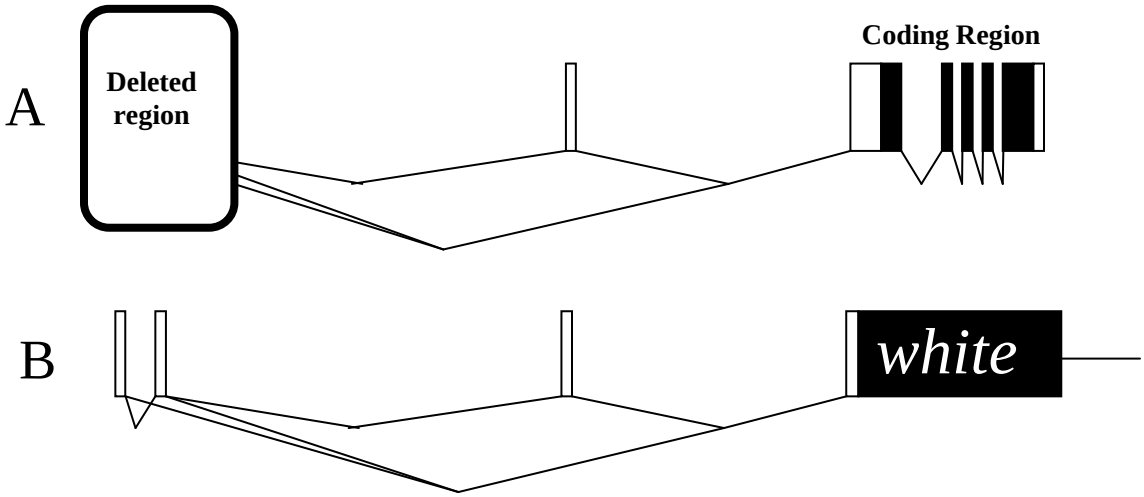

Figure 1.3: The *Src64* mutations $Src64^{\Delta 17}$ and $Src64^{KO}$. $Src64^{\Delta 17}$ is a mutation that deletes the first two exons of Src64 including the transcriptional start site (A). The mutation is a result of an imprecise P-element excision of the first two exons of *Src64.* The $Src64^{KO}$ mutation deletes the entire coding region of *Src64* with the *white* gene. (B). *white* was inserted in a reverse orientation to *Src64*. The mutation was produced by "ends out" homologous recombination.

CHAPTER II
MATERIALS AND METHODS

2.1 Drosophila stocks: strains, food, and care

In all experiments the OregonR strain of *Drosophila melanogaster* was used as the wild-type strain. Flies were fed a mixture of sugar, cornstarch, yeast and agar, and were stored in an incubator at 23˚ C with a humidity level between 50%-70%. The $Src64^{\Delta 17}$ strain was provided to our lab by G. S. Dodson (Dodson et al., 1998). The $Src64^{KO}$ strain was provided to our lab by A. M. O'Reilly (O'Reilly et al., 2006). *Src64* mutants with point mutations in the SH2 and tyrosine kinase domains were provided to our lab by the Seattle TILLING Project and the Charles Zuker lab. All other strains were obtained from the Bloomington Stock Center and described in Flybase (The Flybase Consortium, 2003)

2.2 Embryo collection and RNA isolation

For amplification with the exon one primer pair and the coding primer pair, RNA was isolated from embryos collected after overnight incubations on apple juice/agar plates with yeast as a food source. The embryos were collected in a mesh basket and prepared by dissolving the eggshell with a 50% bleach solution for approximately 2 minutes (Roberts, 1998). Embryos were washed in PTw (1X phosphate buffered saline pH 6.5 plus 0.1% Tween20) and examined under the stereoscopic microscope. Embryos were sorted by age and collected at the developmental stages of pre-cellularization (stage 4), early-cellularization (stage 5), late-cellularization (stage 5), and early-gastrulation (stage 6). Sorted embryos were immediately frozen in liquid nitrogen and were kept at -80 degrees until the RNA isolation step.

For amplification with the alternate exon one primer pair, RNA was isolated from embryos separated into pre-zygotic transcription and post-zygotic transcription. Embryos were sorted by timed collections. Maternal RNA was isolated from embryos immediately after a one-hour embryo collection on apple juice/agar plates. Zygotic RNA was isolated from embryos after a one-hour embryo collection on apple juice/agar plates followed by a one-hour incubation at 23˚C.

The RNAqueous-4PCR kit (Ambion) was used for RNA isolation. Embryos were disrupted in a microcentrifuge tube by using a melted 200µl micropipette tip as a pestle. The tip was heated briefly and pushed into a microcentrifuge tube, forming it into a pestle with the shape of the inside of a microcentrifuge tube. The cells were lysed and passed through a silica filter in a microcentrifuge at 13.6 rcf. After two washes the RNA was eluted with 100 µl of 1X TE (tris buffer pH 8.0 plus EDTA). RNA concentration was determined using a UV spectrophotometer and the RNA was stored at -80 degrees.

2.3 RT-PCR and Semi-quantitative RT-PCR

RT-PCR was performed using the Retroscript kit (Ambion). cDNA synthesis was performed on either 400ng or 1µg of RNA (depending on the specific experiment) in a 20µl reaction. Random decamers were used to prime for the reverse transcription reaction using MM-LV reverse transcriptase (Ambion).

mRNA transcripts containing the *Src64* exon one were amplified using the exon one primer pair, with a forward primer located in exon one and a reverse primer located in exon six (Table 2-1; Figure 2-1 A). We amplified 2µl of cDNA, at a concentration of 20ng/µl, in a 25 µl PCR reaction containing the exon one primer pair for 30 cycles at an annealing temperature of 60˚C. The products of this PCR reaction were run on a 1% agarose gel for visual analysis

mRNA transcripts containing the *Src64* coding region were amplified using the coding primer pair, with a forward primer located in exon six and a reverse primer located in exon eight (Table 2-1; Figure 2-1 A). We amplified 2µl of cDNA, at a concentration of 20ng/µl, in a 25µl PCR reaction containing the coding region primer set for 35 cycles at an annealing temperature of 58˚C. We ran the products of this PCR reaction on a 1% agarose gel for visual analysis

Semi-quantitative RT-PCR was performed on *Src64* transcripts containing the coding region using the QuantumRNA 18S Internal Standards (Ambion). For the linear range analysis we performed an eight-tube PCR reaction amplifying 2µl of cDNA, at a concentration of 20ng/µl, in a 25µl PCR reaction containing the coding primer pair. One tube was removed from the thermocycler every other cycle beginning at cycle number 25. The products from the PCR reaction were run on a 1% agarose gel for analysis. We used

the Alpha Innotech FluorChem 8000 UV gel imaging system and densitometer readings taken from each of the eight samples in the gel to determine the maximum number of cycles in which amplification of the target transcript remained in the linear range. We performed the 18S ratio test by amplifying 2µl of cDNA, at a concentration of 20ng/µl, in a 25 µl, five-tube PCR containing the coding primer pair and a variable ratio of 18S primers to 18S competitive primers. The optimal ratio of 18S primers to 18S competitive primers amplified 18S rRNA at approximately the same level as the coding primer pair. Semi-quantitative RT-PCR of the coding region was performed on RNA isolated from wild-type and *Src64*$^{\Delta 17}$ pre-cellularization, early cellularization, late cellularization, and early gastrulation embryos. 2µl of cDNA, at a concentration of 20ng/µl, was amplified in a in a 25 µl PCR reaction. We ran the results on a 2% agarose gel for visual analysis, and used the Alpha Innotech FluorChem 8000 UV gel imaging system to determine relative RNA amounts in the eight samples.

Semi-quantitative RT-PCR was performed on *Src64* transcripts containing the alternate exon one using the QuantumRNA 18S Internal Standards (Ambion) and the alternate exon one primer pair, with a forward primer located in the alternate exon one and a reverse primer located in exon four (Table 2.1; Figure 2.1 B). For the linear range analysis we performed an ten-tube PCR reaction amplifying 2µl of cDNA, at a concentration of 50ng/µl, in a 25µl PCR reaction containing the alternate exon one primer pair. One tube was removed from the thermocycler every other cycle beginning at cycle 24. The products from the PCR reaction were run on a 1% agarose gel for analysis. We used the Alpha Innotech FluorChem 8000 UV gel imaging system and densitometer readings taken from each of the ten samples to determine the maximum number of cycles in which amplification of the target transcript remained in the linear range. The optimal 18S primer/competitive primer ratio was determined empirically, by performing a series of semi-quantitative RT-PCR reactions. Semi-quantitative RT-PCR of *Src64* transcripts containing the alternate exon one was performed on RNA isolated from wild-type and *Src64*$^{\Delta 17}$ pre-zygotic transcription and post-zygotic transcription embryos. 2µl of cDNA, at a concentration of 50ng/µl, was amplified in a in a 25 µl PCR reaction. We ran the

results on a 2% agarose gel for visual analysis, and used the Alpha Innotech FluorChem 8000 UV gel imaging system to determine relative RNA amounts in the eight samples.

2.4 5'RACE

Rapid amplification of cDNA ends (5'RACE) analysis was performed using the FirstChoice RLM-RACE kit (Ambion). One microgram of total RNA was treated with calf intestinal alkaline phosphatase to remove the free 5'-phosphate from the 5'end of rRNA, tRNA, fragmented mRNA, and fragmented DNA. The RNA was then treated with tobacco acid pyro-phosphotase to remove the cap from full-length mRNA. The 5' Adapter was then ligated to the 5' end of the mRNA using T4 RNA ligase (Figure 2.2). cDNA was made by reverse transcription reaction priming with random primers. Two rounds of nested PCR using outer and inner forward primers located in the 5'Adapter and outer and inner reverse primers located in exon 4 were used to amplify the specific *Src64* transcripts (Table 2.1; Figure 2.2).

We cloned one microgram of the amplified 5' transcript into the *pCRII* vector (Invitrogen) using the TA Cloning kit (Figure 2.2) (Mead et al., 1991). Clones were transformed into competent *E.coli* cells using OneShot Competent Cells (Invitrogen) and grown overnight at 37˚C on LB (Luria broth) plates treated with IPTG (Isopropyl β-D-1-thiogalactopyranoside) and X-gal (5-bromo-4-chloro-3-indolyl- beta-D-galactopyranoside). We used blue/white selection to select transformed colonies, and selected a total of 70 colonies for overnight amplification in 2mL LB. We isolated plasma DNA from the amplified colonies using the FastPlasmid Mini kit (Eppendorf). The isolated DNA was sequenced by the Texas Tech University Biotechnology Core Facility DNA sequencing lab. Identified sequences were compared to the known *Src64* sequence, the 5'adapter sequence, and the *pCRII* vector sequence using the Vector NTI sequence analysis program ContigExpress.

We performed an analysis of the promoter region upstream of the alternate transcriptional start site using the program TFSEARCH (Akiyama, 1999).

2.5 Isolation of *Src64* mutants

TILLING (Targeting Induced Localized Lesions in Genomes) was performed by the Seattle TILLING Project, a joint project run by the Fred Hutchinson Cancer Research Center and the University Of Washington Department of Biology. Mutations were located based on primers provided by our lab that encompassed the majority of the SH3 domain and the entire SH2 and tyrosine kinase domains. The forward primer was located in exon five, and the reverse primer was located in exon eight (Table 2.1; Figure 2.3). Identified *Src64* mutants were provided to our lab as balanced heterozygous mutant strains in either single mutant stocks or stocks with a mixed population of mutant chromosomes.

To isolate the *Src64* mutant chromosome from the mixed chromosome stock a single male from each of the mutant lines was crossed to balanced heterozygous *PrDr/TM6B* females. DNA was isolated from progeny confirmed to have the mutant chromosome *($Pr^{+}Dr^{+}$)* for detection of the *Src64* mutation by restriction mapping or direct sequence analysis. We isolated DNA from the progeny using the Genomic DNA Purification kit (PureGene) by using the single fly DNA isolation protocol (PureGene) scaled up to a three fly reaction, and amplified the DNA using the same primers provided to the Seattle TILLING Project (Table 2.1; Figure 2.3). For the restriction mapping analysis we used the enzymes *BccI*, *Eco57I*, *NruI*, and *BamHI* depending on the mutation and the specific restriction site lost (Table 2.3). Amplified DNA was digested in a 25µl reaction containing 1µg of amplified DNA and one unit of enzyme. The reactions were incubated at 37˚C for 2 hours and run on a 2% agarose gel at 80 volts. Restriction fragment length polymorphisms (RFLPs) in the amplified sequence allowed us to confirm the presence of the mutant chromosome. For mutations that do not produce an RFLP, the presence of the mutation was confirmed by direct sequence analysis. Sequencing was performed by the Texas Tech University Biotechnology Core Facility DNA sequencing lab and compared to the known *Src64* sequence using the Vector NTI sequence analysis program ContigExpress.

To reduce the number of background mutations in the *Src64* mutants, we performed a three step recombination cross using the *rucuca* (*ru h th st cy sr e^{s} ca*) strain

of flies (Table 2.2; Figure 2.4). The same recombination was performed on the *Src64*^{KO} strain to standardize the genetic background. *rucuca* flies have a variety of mutations to genes at known locations along the length of chromosome 3 that produce visible phenotypes. By crossing to *rucuca* and selecting progeny flies with a specific phenotype we were able to select flies that had experienced a recombination event between the regions of 66D and 72D on chromosome 3 (Figure 2.4). This recombination replaced approximately 70-85% of chromosome 3 with the *rucuca* chromosome but retained the original mutated *Src64* region of chromosome 3. The recombinant mutant chromosomes were balanced over the *TM6B* balancer chromosome and established as stable heterozygous lines

We used restriction mapping, DNA sequencing, and standard PCR analysis as was previously described for the isolation of the mutant chromosome to confirm the presence of the *Src64* mutant allele after the recombination (Table 2.3). To confirm the *Src64*^{KO} recombination, we amplified isolated DNA using a forward primer for the *white* gene that was inserted into *Src64* and the reverse primer located 1,274 base pairs downstream from the stop codon and outside of the region replaced by the *white* gene (Table 2.1; Figure 2.5). Only in *Src64*^{KO}, in which the coding region of *Src64* has been replaced with the *white* gene, will this primer combination successfully amplify isolated DNA.

2.6 Mutant Analysis

We collected embryos for analysis of nuclear fallout, embryo size, cellularization front, and microfilament rings from approximately 50 homozygous males crossed to approximately 50 homozygous females. Flies were allowed to lay eggs for either 6 hour periods or overnight on apple juice/agar plate with yeast as the food source. We collected the embryos from the plate by washing into a mesh basket. Collected embryos were treated with bleach for approximately two minutes to dissolve the outer shell and heat-fixed in a boiling 1X triton salt solution for 10 seconds (Roberts, 1998). To remove the vitelline membrane, the embryos were then immersed in a heptane/methanol mixture and

vortexed for 5-10 seconds. Embryos were washed 3 times in methanol and stored in methanol at -4^{o} C (Roberts, 1998).

For the analysis of nuclear fallout we stained the heat-fixed embryos with Hoechst dye. Heat fixed embryos were rehydrated for forty minutes in 1%BSA/PBT (Phosphate buffered saline pH 6.5 plus 0.1% Triton X-100 and 1% BSA) and incubated for three minutes in Hoechst dye diluted 1:1000 in PTw (1X phosphate buffered saline pH 6.5 plus 0.1% Tween20). Stained embryos were washed three times in PTw and mounted on slides using Aquapolymount (Polysciences) (Roberts, 1998). We dried the slides overnight in the dark at room temperature and stored them at 4˚C (Roberts, 1998). We conducted our analysis of embryos for nuclear fallout using the Zeiss AxioImager.A1 fluorescence microscope and a DAPI filter. Images were captured using the Zeiss Axiocam MRm camera at a magnification of 200X. Assessment of nuclear fallout was done using the ImageJ program (Rasband, NIH; http://rsb.info.nih.gov/ij/). We sorted the embryos by nuclear division cycle during stage four and counted nuclei in a region defined by the middle 2/3 of the length of the embryo and ¼ of the width of the embryo from the perimeter of the embryo (Figure 2.6). This method allowed us to standardize the area counted for different sized embryos and avoid counting nuclei at the anterior and posterior regions of the embryo, where it becomes difficult to distinguish yolk nuclei from fallout nuclei. For a statistical analysis of nuclear fallout we performed un-paired T-tests on the number of nuclei counted and compared each sample to wild-type. This allowed us to determine if a specific *Src64* mutation resulted in a significant increase in the incidence of nuclear fallout.

We performed our analysis of embryo size using the same Hoechst stained, 200X magnification photos used in the analysis of nuclear fallout. Maximum length and width were determined using the program ImageJ. ImageJ measurements were converted to micrometers using the length conversion provided by the imaging program (AxioVision 4.4 by Zeiss). Length and width measurements were taken from all embryos found in stage 4, and were not sorted by nuclear division cycle.

Staining for analysis of cellularization front and microfilament ring defects was done using the anti-zipper Rb 78 anti-myosin II heavy chain antibody, a gift from A.

Sokac (A. Sokac, personal communication; Royou el al., 2004). Heat-fixed embryos were rehydrated for 2X 20 minutes in 1% BSA/PBT. Embryos were blocked for 2 hours in 10% BSA/PBT and stained overnight at 4˚C in primary antibody diluted to 1:1000 in 5% BSA/PBT. Primary antibody was not pre-absorbed before use and was used to stain no more than two samples. Embryos were then rinsed 3X in PBT and washed for 4X 15 minutes in PBT. Embryos were stained using Alexa Fluor 546 goat-anti-rabbit antibody (Molecular Probes) as a secondary antibody diluted 1:200 in 5% BSA/PBT for two hours at room temperature. After staining, the embryos were washed four times in PTw and mounted on slides using Aquapolymount (Polysciences) (Roberts, 1998). Analysis of embryos for cellularization front and microfilament ring defects was performed using the Zeiss AxioImager.A1 fluorescence microscope using a rhodamine filter. 200X, 400X, and 630X magnification images were captured using Zeiss Axiocam MRm camera.

The cellularization front was analyzed using the 200X and 400X magnification images. Early cellularization embryos were analyzed for uniformity of depth of the cellularization front as described by Thomas and Wieschaus (Thomas and Wieschaus, 2004) (Figure 2.7). Analysis of the cellularization front was done by visual inspection and comparison the cellularization front in wild-type embryos (negative control), and the cellularization front in *Src64*$^{\Delta 17}$ embryos (positive control).

Microfilament rings were analyzed using the 630X magnification images. Microfilament rings in early and late cellularization embryos were measured for circularity and area encompassed by the rings. Circularity (measured as $c=4\pi A/p^2$ where c=circularity, A=area, and p=perimeter) is a normalized ratio of area to perimeter that measures how similar a measured ring is to a true circle. A circularity of 1 is representative of a true circle. Ten rings were measured in the mid-section of each embryo identified (Figure 2.8) by tracing the rings with the freehand drawing tool in the ImageJ program (Rasband, NIH; http://rsb.info.nih.gov/ij/).

Analysis of embryo yield and hatch rate was performed by crossing an equal number of 2-5 day old virgin female flies with an equal number of wild-type (WT) males. The flies were allowed to lay embryos on apple juice/agar plates with yeast for 24-hour periods at a temperature of 23˚C. We counted the embryos every 24 hours after which

the plates were incubated for an additional 40-45 hours at which time we re-examined the plates to determine the hatch rate.

To compare data from embryo size, microfilament ring circularity, embryo yield, and hatch rate we performed the Tukey-Kramer Multiple Comparison Test. This test compares every set of data to each of the other sets of data. This allowed us to identify statistical groupings and rate defects identified in *Src64* mutants by strength as a moderate or severe defect.

Table 2.1: Primers used in RT-PCR, semi-quantitative RT-PCR, and 5'RACE experiments

Primer name	Sequence	Exon
64RTe1A	5'-ttttcggcggcttcttatcg-3'	1
64RTR3	5'-atgaccaaggcctgaagcg-3'	6
64B3F2	5'-tcgtgcgaccttcagagc-3'	6
64B2R2	5'-ggacatgtactcctgcacg-3'	8
Alt Ex1F	5'-gtgaaaatgtgcatggatgg-3'	Alternate 1
64E4R1	5'-ttggagggcatttgctttag-3'	4
TILLING 1F	5'-atcgacgacaccgagtccgattg-3'	5
TILLING 1R	5'-cgacgtgaccgagaaggactcgaagt-3'	8
5RACEouter-reverse	5'-tggagggcatttggctttagt-3'	4
5RACEinner-reverse	5'-aaaaacgcatttcgttctgg-3'	4
Src64^{KO} reverse	5'-caatgtgtcaacgtccttcg-3'	*
White1R	5'-caatgtgtcaacgtccttcg-3'	*
5-Prime adapter forward-outer	5'-gctgatggcgatgaatgaacactg-3'	#
5-Prime adapter forward-inner	5'-cgcggatccgaacactgcgtttgctggctttgatg-3'	#

* Primers used to amplify the recombined region of *Src64*^{KO}. The forward primer primes to the complimentary strand of *white*. The reverse primer is located 1,273 bp downstream of the *Src64* stop codon.
# Primers located in the 5'adapter ligated to the 5' end of the alternate transcriptional start site

Table 2.2: The *rucuca* strain: genes, alleles, cytological locations and recombination distance

Gene	Allele	Cytological Location	Recombination distance
roughoid	*Ru*^{1}	61F8	3-0.0
hairy	*h*^{1}	66D10	3-26.5
thread	*th*^{1}	72D1	3-42.3
scarlet	*st*^{1}	73A3	3-44
curled	*cu*^{1}	86D3-4	3-50.0
stripe	*sr*^{1}	90E4-F1	3-62.0
ebony	*e*^{s}	93C7-D1	3-70.7
claret	*ca*^{1}	99C2	3-100.7

Table 2.3: Methods for confirmation of recombinant genotype for *Src64* point mutations and $Src64^{KO}$

Mutant	Method of confirmation	Restriction enzyme used
$Src64^{P190L}$	Restriction mapping	*Eco57I*
$Src64^{D204V}$	Sequencing	-
$Src64^{G208E}$	Restriction mapping	*BccI*
$Src64^{R217C}$	Sequencing	-
$Src64^{C259Y}$	Sequencing	-
$Src64^{D372N}$	Restriction mapping	*BccI*
$Src64^{H402L}$	Restriction mapping	*BccI*
$Src64^{R403C}$	Restriction mapping	*BccI*
$Src64^{D404N}$	Restriction mapping	*NruI*
$Src64^{S440F}$	Restriction mapping	*BamHI*
$Src64^{KO}$	PCR	-

- No restriction site lost from mutant

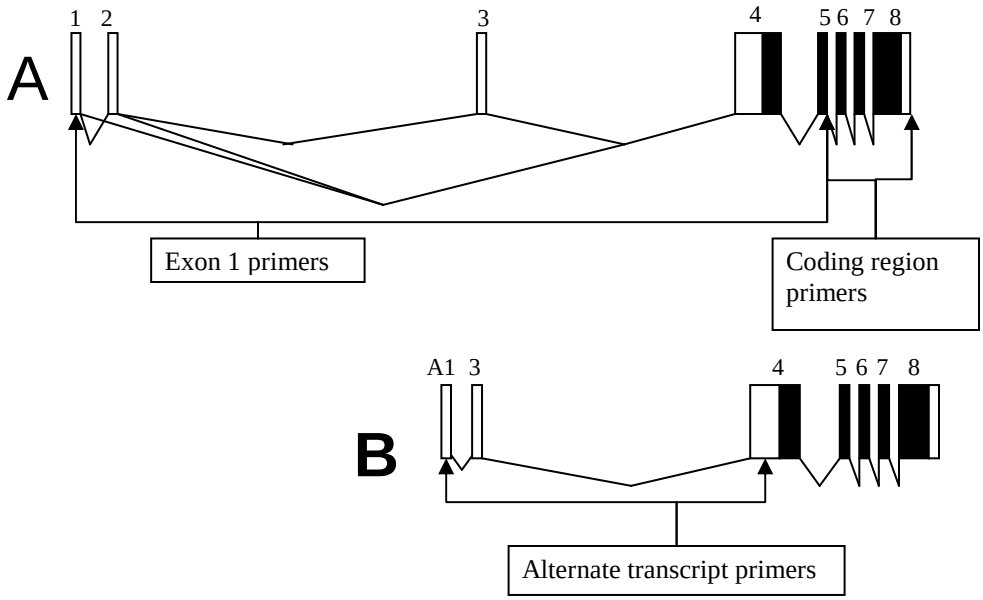

Figure 2.1: Primers associated with amplification of the primary transcriptional start site, coding region, and alternate transcriptional start site. The primary transcript was amplified with a forward primer located in exon 1 and a reverse primer located in exon 6 (A). The coding region was amplified with a forward primer located in exon 6 and a reverse exon located in exon 9 (A). The alternate transcriptional start site was amplified with a forward primer located in the alternate exon 1 and a reverse primer located in exon 4 (B) .

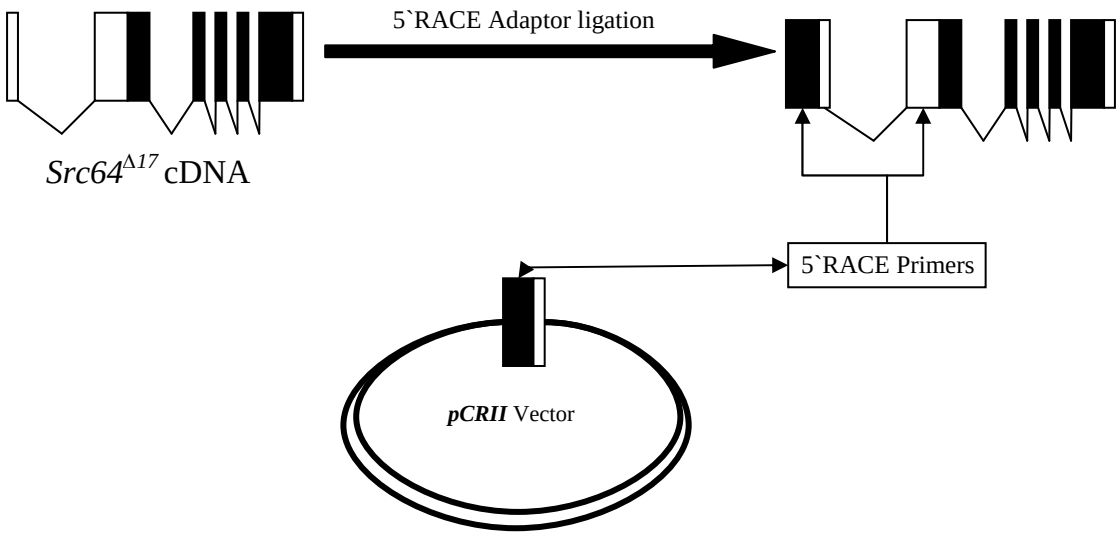

Figure 2.2: 5'RACE of *Src64*$^{\Delta 17}$ mRNA. RNA isolated from *Src64*$^{\Delta 17}$ mutant embryos was treated with TAP and CIP. The 5'adapter was ligated and after the reverse transcription reaction the alternate transcript was amplified with two rounds of nested PCR. The amplified fragment was cloned into the *pCRII* vector using TA cloning. Cloned plasmid was used to transform competent *E.coli* cells. 70 colonies were isolated via blue/white screening. The colonies were grown overnight in 2 ml LB broth. Plasmid DNA was isolated from the grown plasmids and sequenced by the Texas Tech University Biotechnology Core Facility DNA sequencing lab.

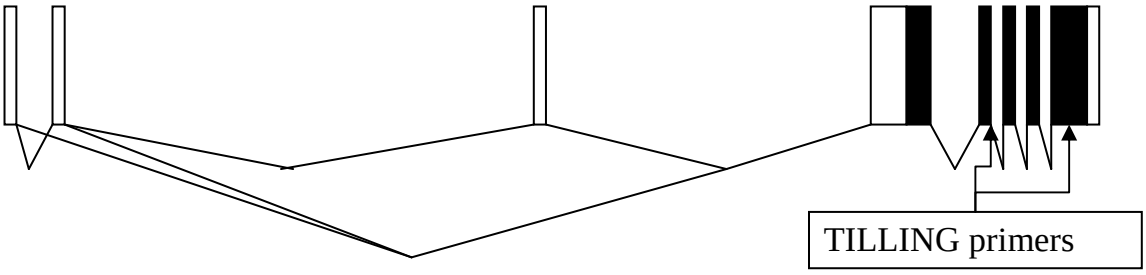

Figure 2.3: Primers for amplification of *Src64* for TILLING analysis. A forward primer located in exon 5 and a reverse primer located in exon 8 were used to amplify *Src64* DNA for analysis of the TILLING region. The amplified region contains part of the SH3, the SH2, and the tyrosine kinase domains.

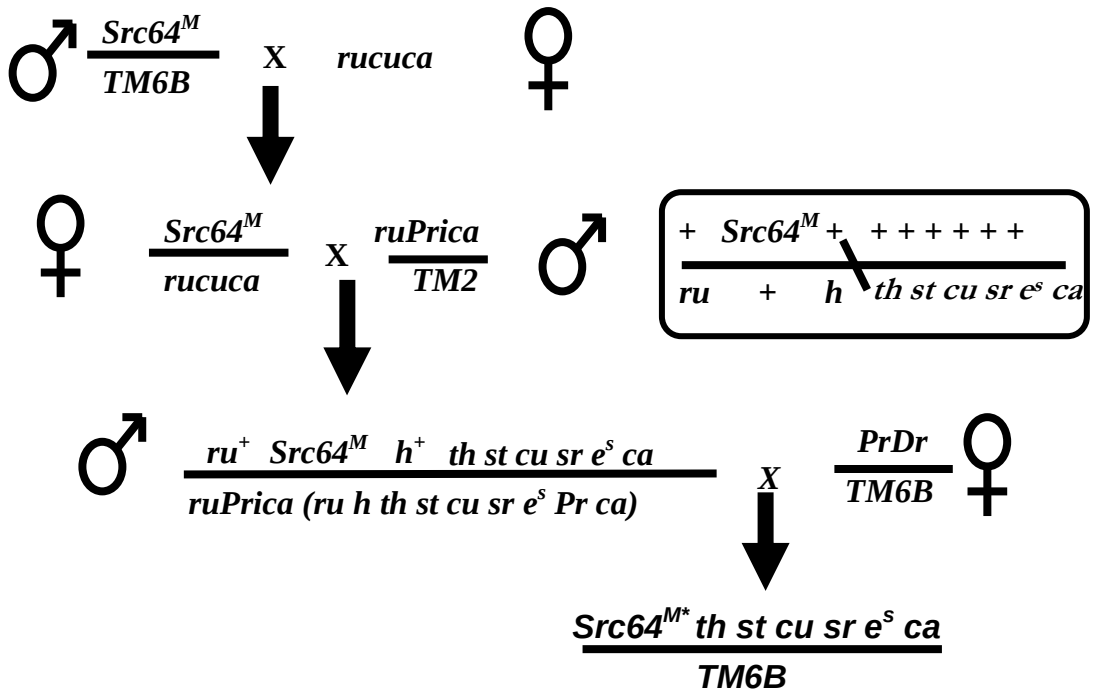

Figure 2.4: Generation of recombinant chromosomes carrying *Src64***.** A three step recombination cross was performed on the mutant stocks provided by the Seattle TILLING Project. The *rucuca* strain was used to recombine with the Src64 mutant chromosome. During the recombination cross flies were examined for the specific phenotype indicating a crossover between *Src64* and the mutation *thread (th).* A successful recombination would remove 70-85% of the mutant chromosome and replace it with the *rucuca* chromosome. The recombinant mutant lines were then balanced over the *TM6B* balancer chromosome and established as stocks.

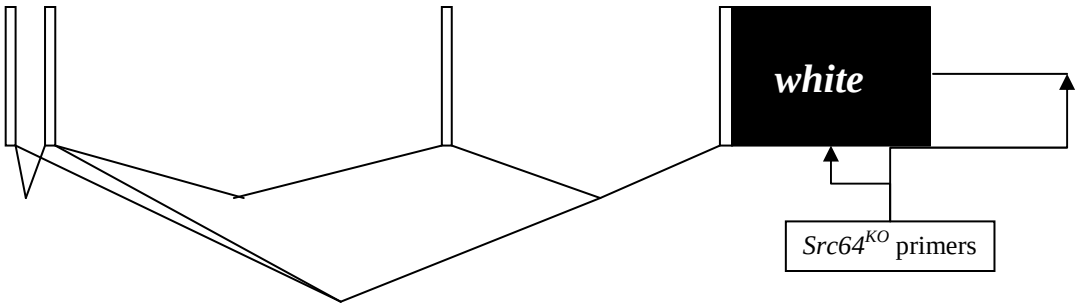

Figure 2.5: Primers for amplification of *Src64*^{KO}. *Src64*^{KO} genomic DNA was amplified with a forward primer located in the inserted *white* gene and a reverse primer located 1,273 base pairs downstream of the stop codon. The *white* gene replaced *Src64* from 802 base pairs upstream of the start codon to 971 base pairs downstream of the stop codon.

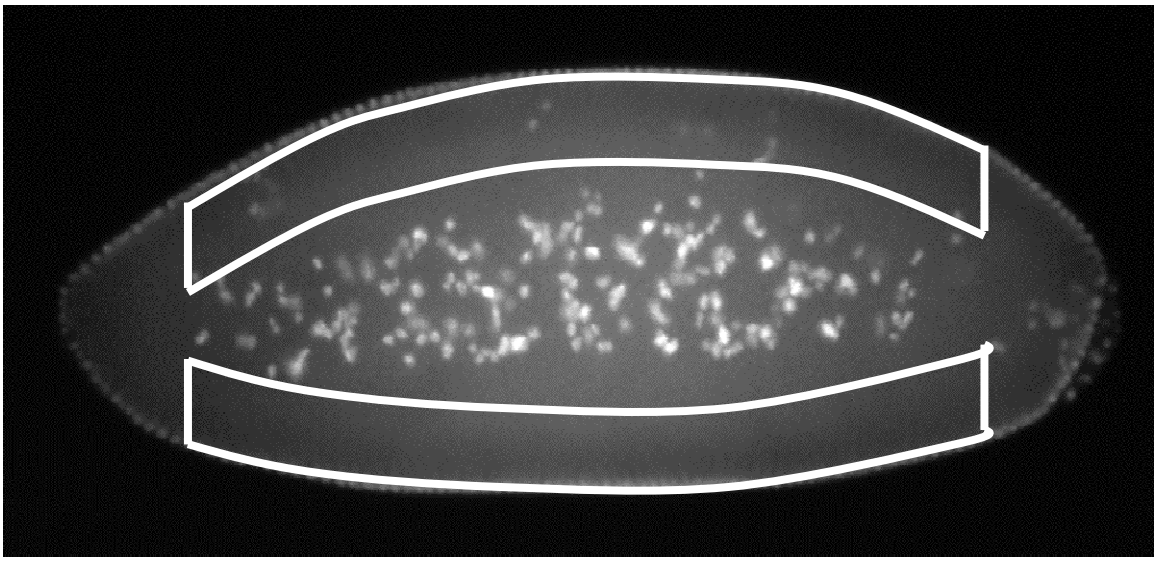

Figure 2.6: Analysis of nuclear fallout. Embryos were stained with Hoechst dye diluted 1:1000 in PTw for 3 minutes. Embryos were mounted on slides and viewed under the fluorescence microscope using a DAPI filter at 200X magnification. Nuclei were counted in a region defined by the middle 1/3 of embryo length within 1/4 of embryo width from the perimeter. This standardized the analyzed area for varying embryo size and avoided the anterior and posterior regions of the embryo where it can be difficult to determine fallout nuclei from yolk nuclei.

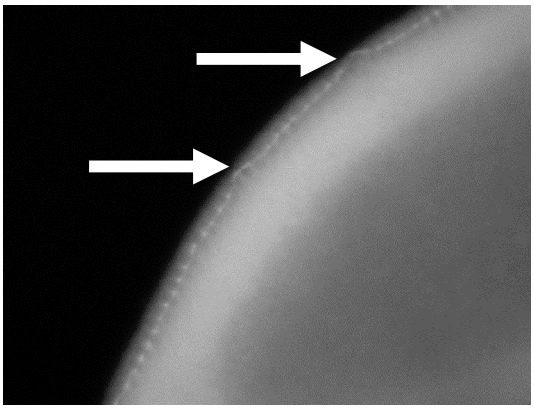

Figure 2.7: Analysis of the cellularization front. The cellularization front was analyzed using images taken with the fluorescence microscope. Images were taken at 400X magnification. Embryos were compared during early cellularization, before the cellularization front had passed the nuclei on its progression towards the interior of the embryo. Analysis of the cellularization front consisted of visual inspection of the cellularization front for abnormalities. In this *Src64*$^{\Delta 17}$ embryo abnormalities of the cellularization front are marked with arrows.

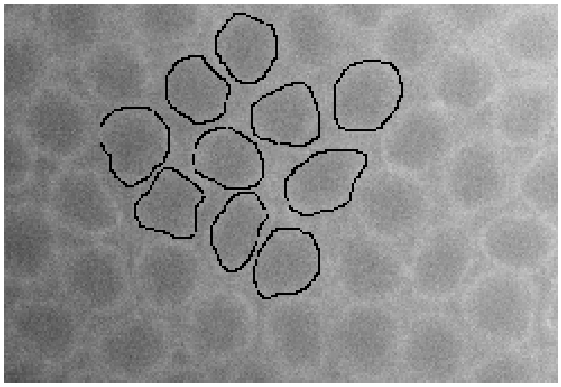

Figure 2.8: Analysis of microfilament rings. Microfilament rings were analyzed for circularity using images taken on the fluorescence microscope at 630X magnification. Ten rings were selected from each embryo in early and late cellularization. The ten rings were selected in a group within the middle of the embryo avoiding any rings within or anterior to the pre-cephalic furrow region. The ten selected microfilament rings were analyzed using the ImageJ program at 200% zoom. Rings were traced using the freehand selection tool and measured for circularity and area.

.

CHAPTER III
MOLECULAR ANALYSIS OF *Src64*

3.1 Introduction

Previous analyses of the *Src64* mutations $Src64^{\Delta 17}$ and $Src64^{KO}$ (described in Chapter1, section 1.2) have suggested the presence of trace amounts of *Src64* protein in $Src64^{\Delta 17}$ flies (Dodson et al., 1998), while the $Src64^{KO}$ mutation removes all traces of *Src64* protein (O'Reilly et al., 2006). Additionally, ring canal, embryo yield, and hatch rate defects identified in $Src64^{\Delta 17}$ flies and embryos were not as severe as the defects identified in $Src64^{KO}$ flies and embryos (O'Reilly et al., 2006). These results suggest two possibilities that could account for the differences identified between $Src64^{\Delta 17}$ flies and embryos and $Src64^{KO}$ flies and embryos. One possibility is that promoter elements may remain that could be sufficient enough to initiate transcription near the deleted region in $Src64^{\Delta 17}$ mutants. Another possibility is the presence of an alternate transcriptional start site located outside of the deleted region of the $Src64^{\Delta 17}$ mutation. Such an alternate transcriptional start site could be responsible for a small percentage of *Src64* transcription in wild-type flies, and thus could be responsible for the trace amounts of Src64 protein in *Src64* mutants and the phenotypic differences observed between $Src64^{\Delta 17}$ and $Src64^{KO}$ mutants.

Our hypothesis is that there is an alternate transcriptional start site located outside of the deleted region in the $Src64^{\Delta 17}$ mutation. We propose that an alternate transcriptional start is responsible for the trace amounts of Src64 protein present in $Src64^{\Delta 17}$ flies and embryos, and is responsible for the reduced severity of ring canal, embryo yield, and hatch rate defects observed in $Src64^{\Delta 17}$ flies and embryos.

To test this hypothesis we performed a semi-quantitative RT-PCR analysis of *Src64* mRNA levels in RNA isolated from wild-type and $Src64^{\Delta 17}$ embryos. Semi-quantitative RT-PCR is a method of estimating the relative RNA levels between two samples. By using primers for 18S rRNA as a loading control we can confirm that two sets of RNA samples have approximately the same amount of RNA, and we can measure the relative difference in the levels of a specific mRNA transcript. Semi-quantitative RT-PCR is performed in a PCR reaction confirmed to be in the linear range, and includes 18S

competitive primers that reduce the level of 18S amplification approximately to the level of gene specific amplification. We used 18S rRNA levels as a control because other commonly used controls such as β-actin and metabolic genes were considered unacceptable due to the changing environment within the embryo.

Additionally, we identified the source of the *Src64* mRNA present in *Src64*$^{\Delta 17}$ embryos by performing a 5'RACE (Rapid Amplification of cDNA Ends) analysis on RNA specifically isolated from *Src64*$^{\Delta 17}$ embryos. 5'RACE is a method of identifying the 5' end of specific mRNA transcripts by ligating an adapter to the 5' end of all mRNA transcripts in an RNA sample and amplifying a specific transcript in a PCR reaction with forward primers located in the adapter and gene specific reverse primers. The amplified transcript can be cloned and amplified for direct sequencing analysis and identification of the 5' end.

3.2 Results

3.2.1 Semi-quantitative RT-PCR determined that *Src64* mRNA was present in *Src64*$^{\Delta 17}$ embryos

We performed RT-PCR and semi-quantitative RT-PCR experiments on RNA isolated from wild-type and *Src64*$^{\Delta 17}$ embryos. To determine if there is *Src64* mRNA in *Src64*$^{\Delta 17}$ embryos, the first step in our analysis of *Src64* transcription in wild-type and *Src64*$^{\Delta 17}$ embryos was to confirm that *Src64*$^{\Delta 17}$ embryos lacked *Src64* mRNA transcripts containing exon one (deleted in the *Src64*$^{\Delta 17}$ mutation). We accomplished this by amplifying wild-type and *Src64*$^{\Delta 17}$ cDNA with the exon one primer pair (Chapter 2, Section 2.3). We identified a number of *Src64* transcripts of varying size in the four wild-type samples while the four *Src64*$^{\Delta 17}$ samples failed to amplify with the exon one primer pair (Figure 3.1 A). This confirmed that *Src64*$^{\Delta 17}$ embryos do not have any *Src64* mRNA transcripts derived from exon one. The multiple bands in the four wild-type sample represent the alternate splicing in the 5' un-translated region of *Src64*. Exons one and six span the region of alternate splicing. We did not identify any significant differences between wild-type and *Src64*$^{\Delta 17}$ in the four embryo ages in the analysis.

The next step of our analysis of *Src64* was to determine if *Src64*$^{\Delta 17}$ embryos contain *Src64* mRNA transcripts despite the deletion of the first two exons. We

accomplished this by amplifying wild-type and *Src64*$^{\Delta 17}$ cDNA with the coding primer pair. We identified a single transcript in both the wild-type and *Src64*$^{\Delta 17}$ samples; however, the level of *Src64* mRNA containing the coding region was severely reduced in the *Src64*$^{\Delta 17}$ samples compared to the wild-type samples (Figure 3.1 B). Again, we did not identify any significant differences between the four embryo ages in this analysis in the wild-type or *Src64*$^{\Delta 17}$ samples.

We determined the linear range of amplification and the 18S primer/competitive primer ratio before the semi-quantitative RT-PCR of the coding region (Chapter 2, Section 2.3). From the linear range analysis we determined that the maximum number of cycles in which DNA amplification remained in the linear range was 30 cycles when amplifying wild-type cDNA with the coding primer pair (Figure 3.2 A, B). From the ratio test we determined that an 18S primer/competitive primer ratio of 0.5:9.5 would amplify 18S rRNA to approximately the same level as amplification with the coding primer pair (Figure 3.2 C). We performed the semi-quantitative RT-PCR on RNA isolated from wild-type and *Src64*$^{\Delta 17}$ embryos using the determined linear range and 18S ratio. The results indicated that, in samples containing approximately equal amounts of RNA, the level of *Src64* mRNA containing the coding region was severely reduced in *Src64*$^{\Delta 17}$ samples compared to the wild-type samples (Figure 3.3). To quantify these results we used a densitometer to measure the level of RNA in each sample (Table 3.1). Statistical analysis of these results indicated a significant reduction (P=0.001) in the level of *Src64* mRNA in the *Src64*$^{\Delta 17}$ samples, and we determined that the level of *Src64* in the wild-type samples was 10-fold higher the *Src64*$^{\Delta 17}$ samples (Figure 3.4).

3.2.2 5'RACE of *Src64*$^{\Delta 17}$ cDNA identified an alternate transcriptional start site 13,100 base pairs downstream from the primary transcriptional start site

We performed a 5'RACE analysis on RNA specifically isolated from *Src64*$^{\Delta 17}$ embryos to identify the 5'-end of any *Src64* transcripts present in the RNA sample. This experiment allowed us to determine if the small amounts of Src64 mRNA in *Src64*$^{\Delta 17}$ flies is a result of a reduced *Src64* transcription near the deleted region, or the presence of an alternate transcriptional start site.

We successfully amplified the 5' end of *Src64* transcripts present in RNA isolated from wild-type and *Src64*$^{\Delta 17}$ embryos. Before the cloning step, a portion of the PCR product was run on a 1% agarose gel for visual confirmation of ligation and amplification (Figure 3.5). The results indicated successful ligation and amplification of a single *Src64* transcript in the *Src64*$^{\Delta 17}$ sample, while in the wild-type control sample there were a number of different sized transcripts, again representative of alternate splicing in the 5' un-translated region of *Src64*. After the cloning and transformation steps (Chapter 2, Section 2.4), 70 successfully transformed colonies were selected for amplification and sequencing analysis of plasmid DNA. One of the colonies failed to grow. Plasmid DNA was isolated from the remaining 69 colonies for sequencing analysis. Nine of the 69 samples analyzed indicated self-ligation of the plasmid and contained no sequences from either the 5' adapter or *Src64*. In the remaining 60 samples the 5' adapter was found ligated to the same 5' end of identical *Src64* transcripts. The alternate transcriptional start site was identified in a previously unknown, 108 base pair exon located 13,100 base pairs downstream of the primary transcriptional start site and 99 base pairs upstream of exon 3 (Figure 3.6).

3.2.3 Semi-quantitative RT-PCR identified RNA derived from the alternate transcriptional start site in wild-type and *Src64*$^{\Delta 17}$ embryos

The identification of the alternate transcriptional start site in an exon not present in *Src64* transcripts derived from the primary transcriptional start site allowed us to specifically amplify *Src64* transcripts derived from the alternate transcriptional start site. We used semi-quantitative RT-PCR to estimate the relative level of *Src64* transcription specifically derived from the alternate transcriptional start site in wild-type and *Src64*$^{\Delta 17}$ embryos (Chapter 2, Section 2.3).

We determined the linear range of amplification and 18S primer/competitive primer ratio before performing the semi-quantitative RT-PCR of *Src64* transcripts containing the alternate exon one (Chapter 2, Section 2.3). From the linear range analysis we determined that the maximum number of cycles in which DNA amplification remained in the linear range was 38 cycles when amplifying wild-type cDNA with the alternate exon one primer pair (Figure 3.7). We determined that an 18S

primer/competitive primer ratio of 0.7:9.3 would amplify 18S rRNA at approximately the same level as amplification with the alternate exon one primer pair. We performed the semi-quantitative RT-PCR on RNA isolated from wild-type and *Src64*$^{\Delta 17}$ embryos using the determined linear range and 18S ratio (Figure 3.8). Again, we used densitometer readings from the gel to compare relative amounts of mRNA transcripts derived from the alternate transcriptional start site in the two sample sets (Table 3.2). Analysis of the results indicated no significant difference (P=0.143) between the level of transcription in the wild-type samples and the *Src64*$^{\Delta 17}$ samples (Figure 3.9).

Table 3.1: Densitometer readings from semi-quantitative RT-PCR of the coding region

	Wild Type				*Src64*$^{\Delta 17}$			
	PC	EC	LC	EG	PC	EC	LC	EG
Coding primers	17697*	23920*	17889*	24150*	2601*	2461*	1653*	972*
18S primers	10077	13040	10277	10816	14222	12083	6673	5008

* Statistical analysis was performed using an unpaired T-test assuming unequal variances. Data from all four ages were included in the statistical comparison. The level of *Src64* mRNA transcripts containing the coding region is significantly lower (P=0.001) in the *Src64*$^{\Delta 17}$ samples compared to the wild-type samples.

PC: Pre-cellularization
EC: Early cellularization
LC: Late Cellularization
EG: Early Gastrulation

Table 3.2: Densitometer readings from semi-quantitative RT-PCR *Src64* transcripts derived from the alternate transcriptional start site

	Wild Type		*Src64*$^{\Delta 17}$	
	Pre-zygotic transcription	Post-zygotic transcription	Pre-zygotic transcription	Post-zygotic transcription
Coding primers	2671*	6633*	3318*	2888*
18S primers	1690	2378	3530	2419

* Statistical analysis was performed using an unpaired T-test assuming unequal variances. Data from pre- and post-zygotic transcription were included in the statistical comparison. The difference between the two sample sets is not statistically significant (P=0.143).

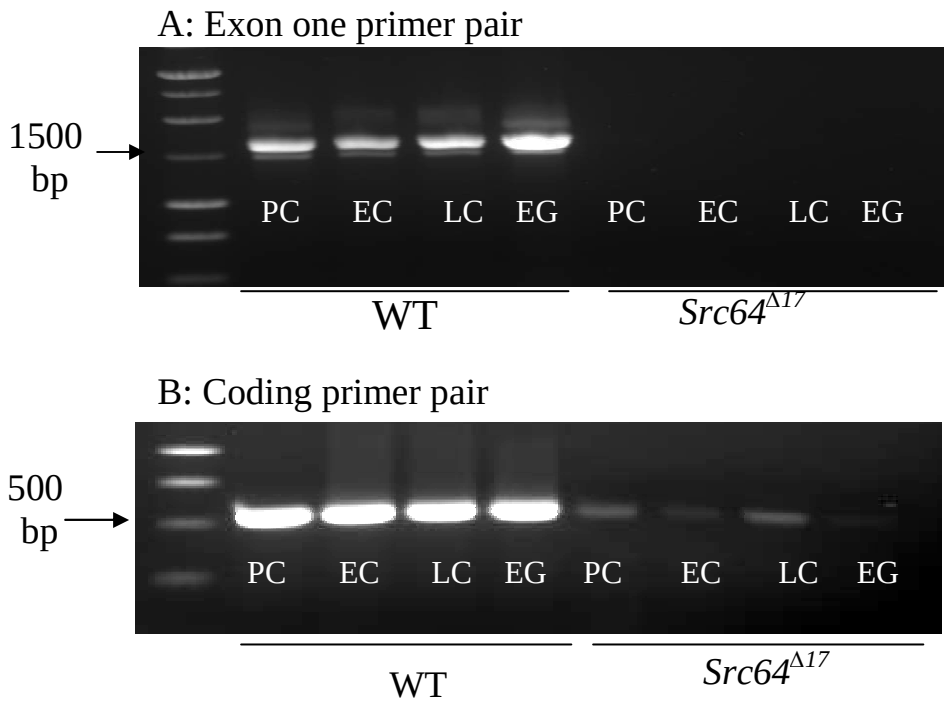

Figure 3.1: RT-PCR of RNA isolated from wild-type and *Src64*$^{\Delta 17}$ embryos. WT and *Src64*$^{\Delta 17}$ embryos were separated into the ages of pre-cellularization (PC), early cellularization (EC), late cellularization (LC), and early gastrulation (EG) for RNA isolation and RT-PCR analysis. Wild-type and *Src64*$^{\Delta 17}$ samples were tested for the presence of *Src64* transcripts containing exon one (A), and containing the coding region (B). We identified a number of differently sized *Src64* transcripts (due to alternate splicing in the 5' un-translated region) in the wild-type samples using the exon one primer pair (A). The *Src64*$^{\Delta 17}$ samples failed to amplify with the exon one primer pair due to the deletion of the first two exons of *Src64* (A). Amplification with the coding primer pair indicated the presence of a single *Src64* transcript in both the wild-type and *Src64*$^{\Delta 17}$ samples (B). The level of *Src64* RNA containing the coding region is severely reduced in the *Src64*$^{\Delta 17}$ samples when compared to the wild-type samples (B).

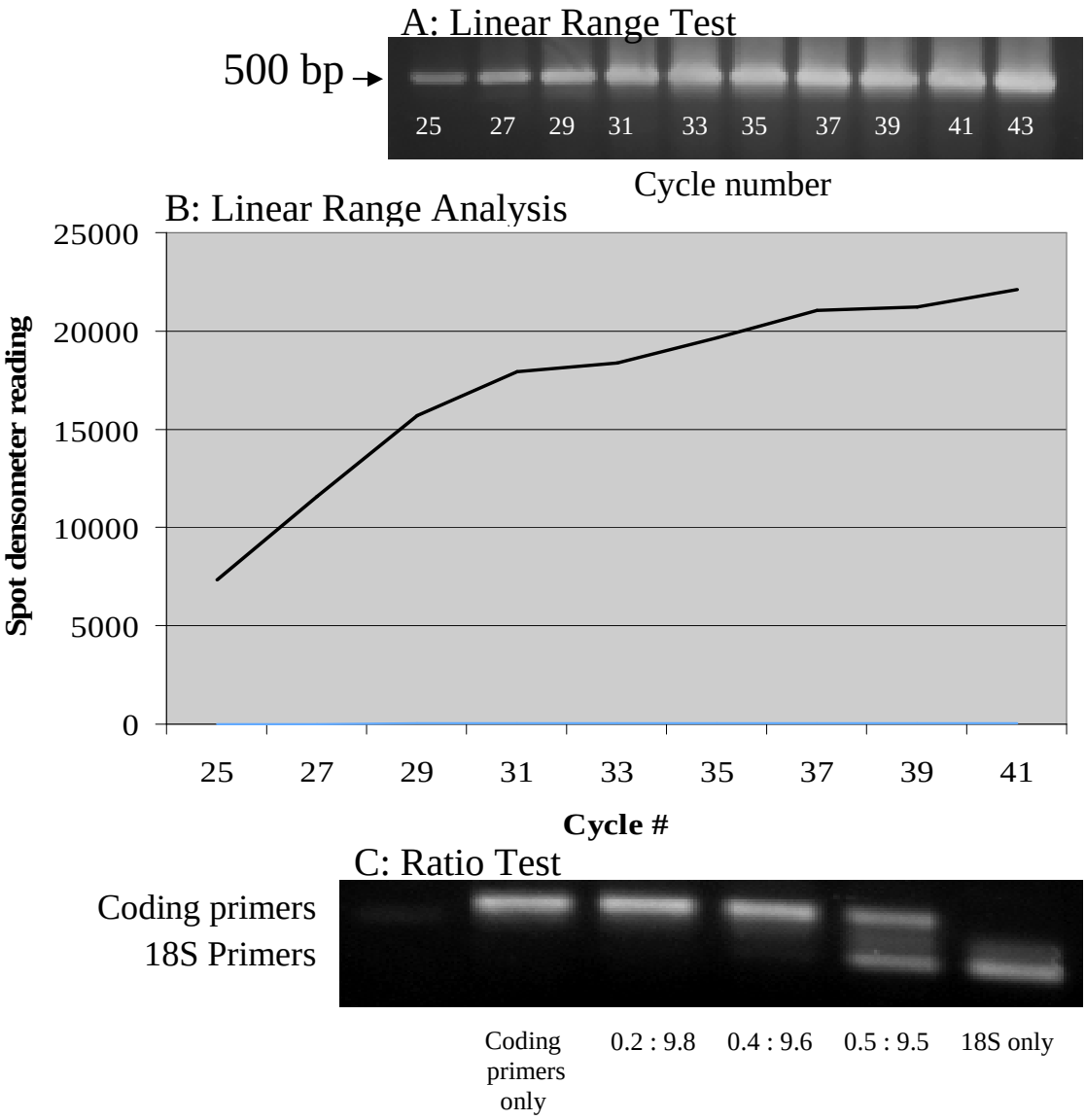

Figure 3.2: Linear range analysis and ratio test for semi-quantitative RT-PCR of the coding region. To determine the linear range of amplification wild-type cDNA was amplified in a PCR reaction containing the coding primer pair. One tube was removed every two cycles beginning with cycle 25 (A). Densitometer readings were plotted by cycle number to identify the linear range (B). We determined that PCR amplification was within the linear range between 25 and 30 cycles (B). In the ratio test, different ratios of 18S primers and competitive primers were run in parallel with the *Src64* coding primers in a 30 cycle PCR reaction with an annealing temperature of 58˚C. At the correct ratio 18S should amplify at approximately the same level as the coding primers. The ratio of 0.5 18S primers to 9.5 18S competitive primers amplified 18S rRNA at approximately the same amount as the coding primers (C).

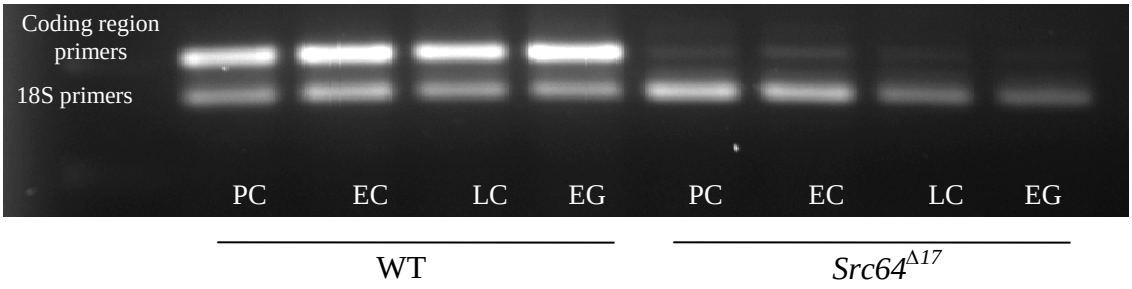

Figure 3.3: Semi-quantitative RT-PCR of the coding region primers. 2µl of cDNA was run in a PCR reaction with the coding region primer pair and the 18S primer/competitive primer mixture at a ratio of 0.5 to 9.5. The PCR was a 30 cycle reaction run at 58˚C. Comparison between the samples shows an approximately equal amount of 18S rRNA in both wild type and *Src64*$^{\Delta 17}$ samples. The *Src64*$^{\Delta 17}$ samples have a reduced amount of coding region *Src64* mRNA. Densitometer readings were taken from the gel for statistical comparison between the wild-type and *Src64*$^{\Delta 17}$ samples.

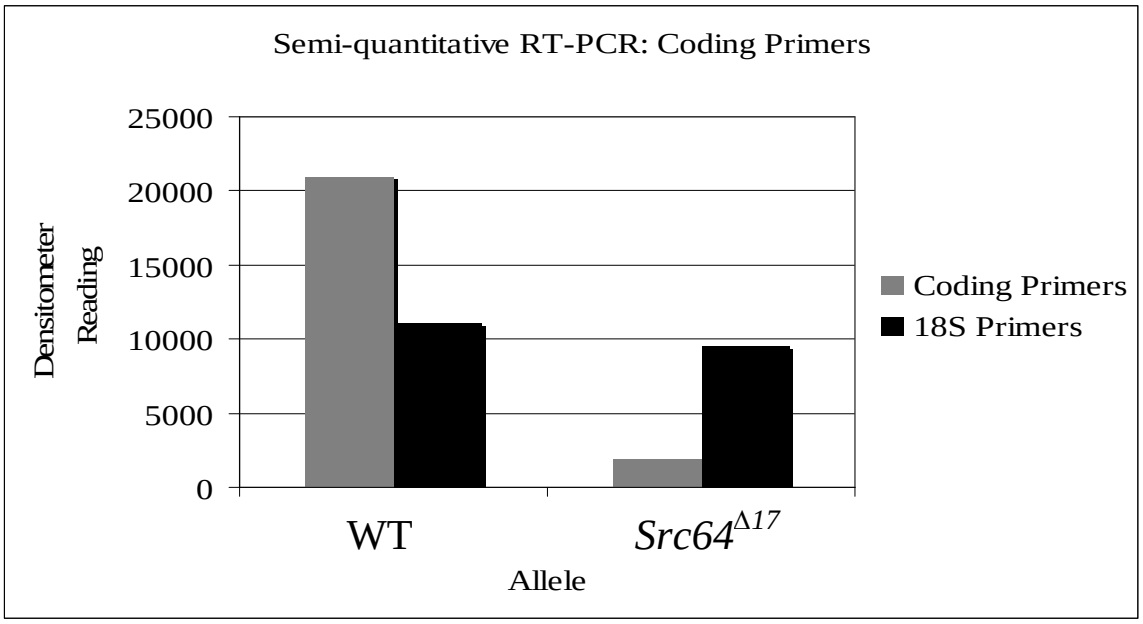

Figure 3.4: Average densitometer readings from the coding region semi-quantitative RT-PCR. Densitometer readings from the samples of different ages (Table 3.1) were averaged for comparison of the coding region to 18S. Statistical analysis indicated a significant difference (P=0.001) between the level of *Src64* RNA between the samples with an approximately 10-fold higher level of *Src64* mRNA in the wild-type samples compared to the *Src64*$^{\Delta 17}$ samples

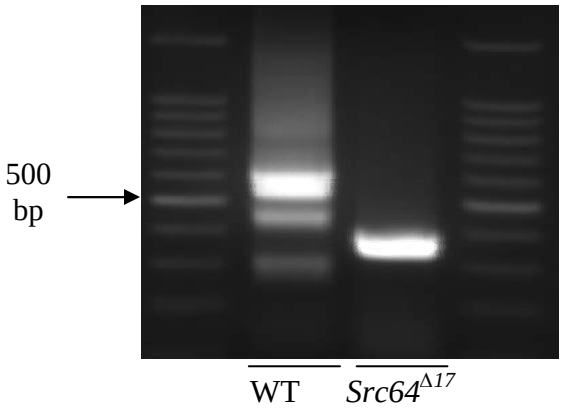

Figure 3.5: 5'RACE of wild-type and *Src64*$^{\Delta 17}$ RNA. After two rounds of amplification with forward primers located in the 5'-adapter and reverse primers located in exon four the products were run on a 1% agarose gel. The results indicated that a number of different sized transcripts had been located in the wild-type sample ranging from 200 to 600 base pairs. A single transcript was located in the *Src64*$^{\Delta 17}$ sample with a length of approximately 250 base pairs. The PCR product from the *Src64*$^{\Delta 17}$ sample was cloned and amplified for sequencing.

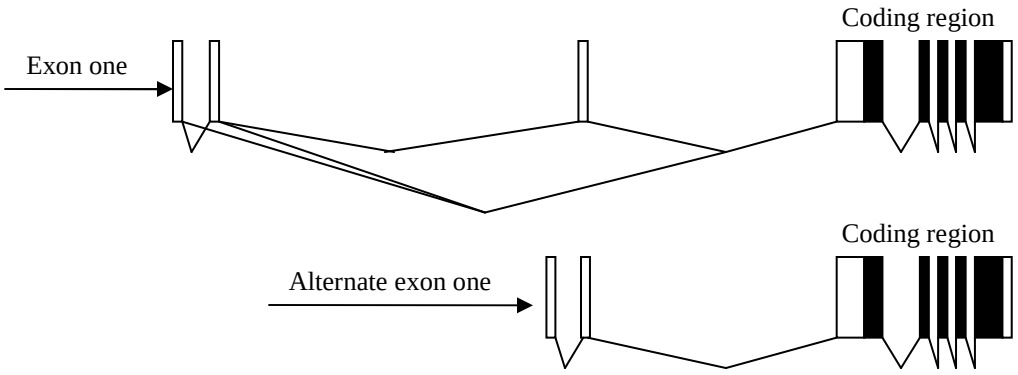

Alternate exon 1

AGTCAGAGTAAAAAACCGAGTC
AGACAGCAGCAGCTGATAAGCC
GCCATGCGGATGTGAAAATGTG
CATGGATGGATGAGGGATAGTA
ATAAATCTATTTACTTCCAT

Figure 3.6: The alternate transcriptional start site. Sequence analysis of the 70 isolated clones indicated that an alternate transcriptional start site was responsible for the *Src64* mRNA seen in $Src64^{\Delta 17}$ samples. The alternate transcriptional start site is located 13,100 base pairs downstream from the primary transcriptional start site in a previously unknown 108 base pair exon 99 base pairs upstream of exon 3

A: Linear range test

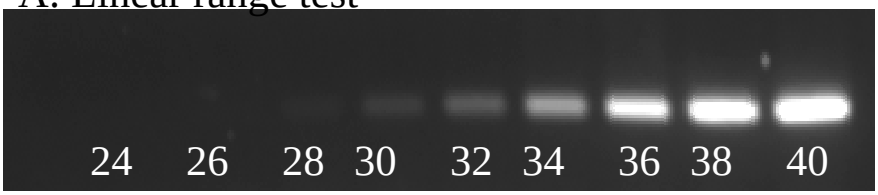

Cycle number

B: Spot densometer readings

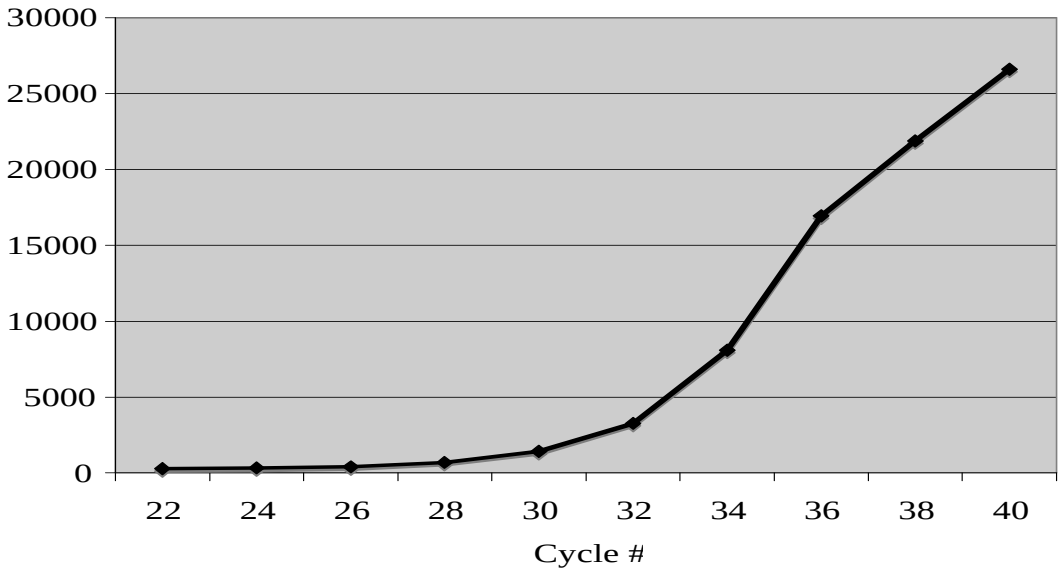

Figure 3.7: Linear range analysis for semi-quantitative RT-PCR of Src64 transcripts containing the alternate exon one. 2µl of cDNA isolated from wild type embryos was amplified in a 10 tube PCR reaction with the alternate exon primers. One tube was removed every two cycles beginning with cycle 22. After running the samples on a 1% agarose gel (A) spot densometer readings were used to compare the samples and determine the linear range of amplification (B). 38 cycles was determined to be the maximum number of cycles in the PCR reaction that remained within the linear range. The 18S primer/competitive primer ratio was determined experimentally by testing a number of different ratios in sequential semi-quantitative RT-PCR reactions

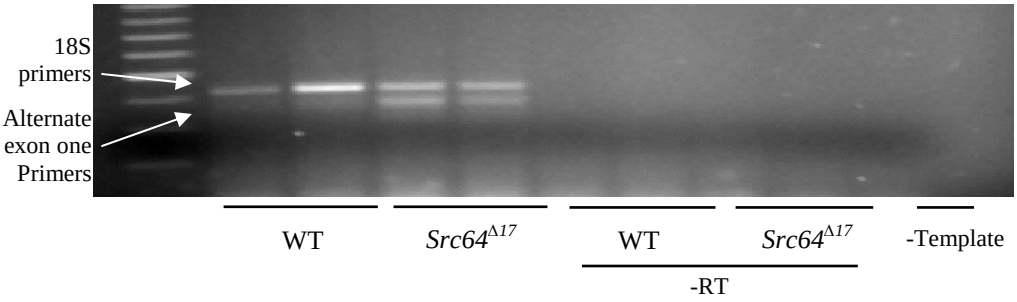

Figure 3.8: Semi-quantitative RT-PCR of Src64 transcripts containing the alternate exon one. The alternate exon primers were run in parallel with the 18S primers and 18S competitive primers at a ratio of 0.7 to 9.3. Samples were separated into RNA isolated from pre-zygotic transcription embryos and post-zygotic transcription embryos. Comparison between wild-type samples and *Src64*$^{\Delta 17}$ samples indicated the possibility of an increased level of RNA derived from the alternate transcriptional start site in *Src64*$^{\Delta 17}$ embryos in pre-zygotic transcription RNA samples and post-zygotic transcription RNA samples. Densitometer readings were taken from the gel for statistical comparison between the wild-type and *Src64*$^{\Delta 17}$ samples

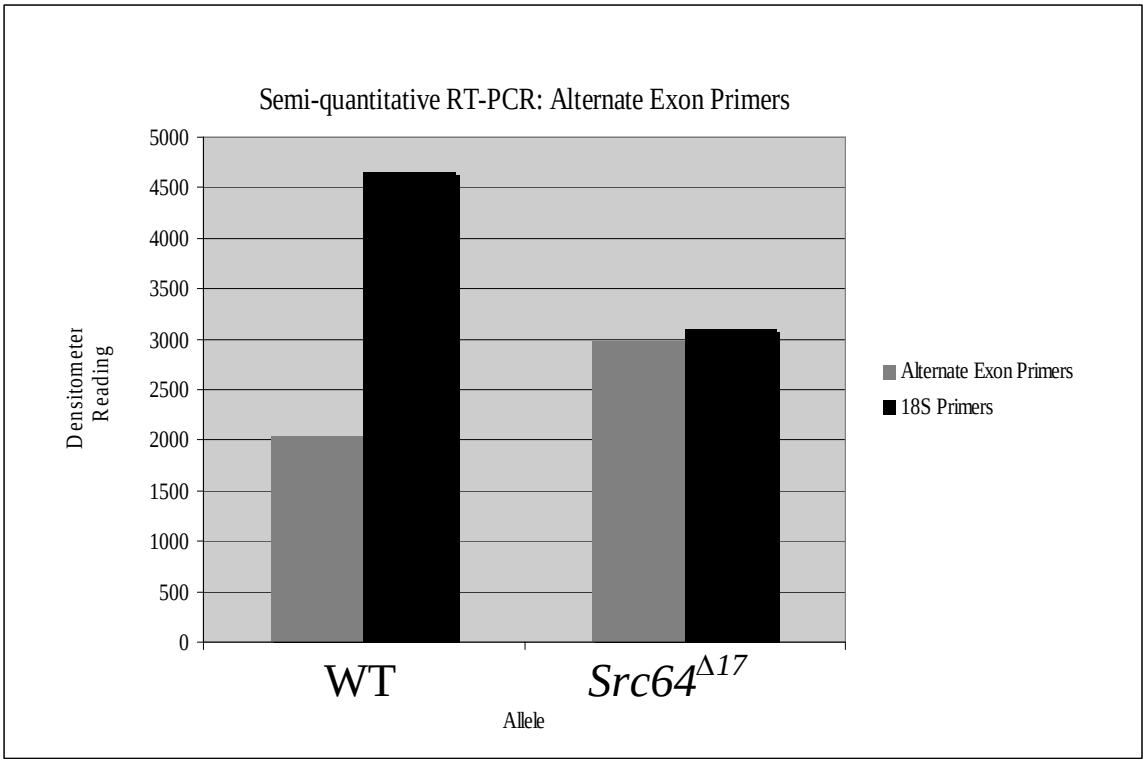

Figure 3.9: Comparison of densitometer readings from the alternate exon one semi-quantitative RT-PCR. Spot-densometer readings were averaged for comparison between wild-type and *Src64*$^{\Delta 17}$ samples. The results indicated the possibility of an increase in the level of transcription via the alternate transcriptional start site in the *Src64*$^{\Delta 17}$ samples compared to the wild-type samples. Statistical analysis of the spot-densometer readings indicated that the observed difference was not statistically significant (P=0.143).

CHAPTER IV
PHENOTYPIC ANALYSIS OF *SRC64* MUTANTS

4.1 Introduction

The multi-domain structure of Src-family kinases allows for a wide range of protein activity. Src, in particular, has been linked to signaling pathways related to cell proliferation (Baumeister et al. 2005), cell motility (Yeo et al, 2006), cell adhesion (Baumeister et al. 2005), and neo-angiogenesis (Summy and Gallick, 2006). Additionally, the SH3, SH2, and tyrosine kinase domains can have specific, but varying roles during protein activity. In many instances of Src-family kinase activity the specific roles for the SH3, SH2, and TK domains have not been established. We are using the *Drosophila* Src-family kinase *Src64* to study Src-family kinase activity, and hope to identify specific roles for the SH3, SH2, and TK domains.

The $Src64^{\Delta 17}$ mutation has been used to confirm Src64 protein activity during the process of cellularization (Dodson et al., 1998; O'Reilly et al., 2006; Thomas and Weischaus, 2004). However, these have provided little information on the specifics of Src64 protein activity. Due to this, the precise role that *Src64* plays during these processes is still unknown. We propose that Src64 protein domains could function in a variety of different ways during embryo development, and hypothesize that Src64 protein activity could be different during the different developmental processes in which it is involved. Specifically, we wish to determine how Src64 protein is active during the process of cellularization and microfilament ring constriction.

To test this hypothesis we analyzed the effects of mutations in *Src64* that impaired the activity of specific domains. We used the TILLING (Targeting Induced Lesions Localized in Genomes) method in order to locate specific mutations to *Src64* located within the SH3, SH2, and tyrosine kinase domains (Henikoff et al., 2004). The Seattle TILLING project has approximately 5000 lines of chromosome 3 ethyl methanesulfonate mutated flies. Using the primers defined by our lab (Chapter 2, Section 2.5) they amplified the *Src64* coding region in their mutated lines of flies and screened for mutations. Mutation screening was performed in pooled batches of amplified DNA. Specific mutations were identified by restriction mapping (Henikoff et al., 2004). We

obtained mutant strains of flies confirmed to have a mutation in *Src64* from the Seattle TILLING project and the University of Washington. Previous data suggested a mutation rate of one G/C to A/T transition per 300kbp (Henikoff et al., 2004). Factoring in chromosome size, percent euchromatin, and intronic DNA they estimate approximately 10 damaging mutations per chromosome spaced out over approximately 5000 genes on chromosome 3 (Henikoff et al., 2004). In order to reduce the effect of background mutations we performed a recombination cross with the mutant line *rucuca* to replace the majority of the mutant chromosome (Chapter 2, Section 2.5). We analyzed *Src64* mutants for defects in nuclear fallout, progression of the cellularization front, microfilament rings circularity during early cellularization, microfilament ring circularity during late cellularization, microfilament ring constriction, embryo size, embryo count, and hatch rate.

4.2 Results

4.2.1 Ten mutations in *Src64* were located by the TILLING method

We located ten mutations in *Src64* by using the TILLING method with primers encompassing the majority of the SH3 domain and the entire SH2 and tyrosine kinase domains (Figure 2.3) (Table 2.1). Five mutations were located in the SH2 domain, and five mutations were located in the tyrosine kinase domain (Table 4.1). No mutations were located in the SH3 domain. The $Src64^{D404N}$ mutation is a mutation of the catalytic aspartate in the tyrosine kinase domain. This mutation should remove all kinase activity from the affected protein while leaving the SH3 and SH2 domains fully functional. Each mutation was analyzed for the likelihood it alters the specific domain structure. This analysis was performed by the Seattle TILLING Project and was provided to our lab along with the mutant strains of flies. For each mutation The Seattle TILLING Project measured the PSSM (Position Specific Scoring Matrix) difference and SIFT (Sorting Intolerant From Tolerant) score, two measures of the probability that a given mutation is deleterious to the overall structure and activity of the protein or domain (Altschul et al. 1997; Ng and Henikoff, 2003) (Table 4.2). The PSSM difference is determined by aligning similar sequences produced by BLAST and comparing the sequences. The

PSSM value is calculated as the ratio of the probability of finding a specific amino acid at a particular position to the probability of finding it in a random background model. The higher the PSSM difference, the more likely it is that a given mutation will cause a significant change in the overall domain structure (Altschul et al. 1997). The SIFT score is calculated by comparing a given mutation to the amino acid sequence of known homologous sequences. The lower the SIFT score is the more likely it is that a mutation will have a detrimental effect on the structure and activity of a protein or specific domain. A mutation with a SIFT score of less than 0.05 is predicted to have an impact on the domain structure (Ng and Henikoff, 2003). In addition to this data we were provided with specific restriction sites lost or generated for each mutation that would allow us verify the presence of the mutant chromosome by restriction mapping (Table 4.2).

The mutations were provided to our lab in the form of balanced heterozygous stocks. The $Src64^{R217C}$ and $Src64^{P190L}$ mutations were provided in single mutant chromosome stocks while the remaining mutations were provided in stocks with a mixed population of mutant chromosomes. We isolated the desired mutant chromosome in the mixed mutant stocks, and confirmed the presence of the mutant chromosome in the progeny using a combination of restriction mapping and direct sequence analysis (Chapter 2, Section 2.5) (Figure 2.4). The recombination cross was performed on the ten *Src64* mutant strains as well as the $Src64^{KO}$ strain (Chapter 2, Section 2.5). We identified recombinants in 10 of the 11 crosses that had recombined at the ideal location, between 66D and 72D on chromosome 3L (ru^+ h^+ *th st cu sr* e^s *ca*). We did not find a $Src64^{S440F}$ recombinant that had recombined between 66D and 72D; however, we did locate a $Src64^{S440F}$ recombinant that had recombined between 72D and 73D (ru^+ h^+ th^+ *st cu sr es ca*). Recombinations were confirmed by standard PCR of DNA isolated from the recombinant stocks and by either restriction mapping, or direct sequencing analysis (Chapter 2, Section 2.5). Recombinations in the $Src64^{P190L}$, $Src64^{G208E}$, $Src64^{D372N}$, $Src64^{H402L}$, $Src64^{R403C}$, and $Src64^{S440F}$ lines were confirmed by restriction mapping (Figure 4.1). The presence of the recombinant chromosome is represented by the appearance of an extra band in the mutant sample when compared to a wild-type sample. Recombinations in the $Src64^{D204V}$, $Src64^{R217C}$, and $Src64^{C259Y}$ lines were confirmed by

direct sequence analysis of DNA isolated from the heterozygous stocks. Recombination in the *Src64*^{KO} line was confirmed by amplification of DNA isolated from recombinant stock with primers specific to the recombinant (Figure 4.2).

Homozygous recombinant Src64 mutants were assessed for viability. We determined that the *Src64*^{H402L}*/TM6B* stock did not produce homozygous progeny. Homozygous females are necessary for embryo analysis, so *Src64*^{H402L} was omitted from the remainder of the *Src64* mutant embryo analysis. The *Src64*^{D372N}*/TM6B* stock did produce homozygous flies; however the homozygous females did not produce live embryos and *Src64*^{D372N} was omitted as well. The *Src64*^{G208E}*/TM6B* and *Src64*^{D404N}*/TM6B* stocks produced homozygous flies. The homozygous females did produce live embryos that did lived past the period necessary for our analysis, but never hatched. The remaining *Src64* mutant lines were homozygous viable. From here, *Src64*^{m} will refer to homozygous *Src64*^{m} embryos derived from homozygous parents unless otherwise specified

4.2.2 The nuclear fallout defect was identified only in *Src64*$^{\Delta 17}$ embryos

Nuclear fallout is an embryonic defect that has previously been associated with defects in cytoskeletal genes (Sullivan et al., 1993). The defect is characterized as an increased number of nuclei in the region between the peripheral nuclei and the yolk nuclei during embryonic stage four. The nuclear fallout defect in *Src64*$^{\Delta 17}$ embryos has previously only been briefly mentioned (Thomas and Wieschaus, 2004), and has yet to be characterized or quantified in *Src64*$^{\Delta 17}$ embryos. The first step in our analysis of nuclear fallout in *Src64* mutants was to characterize and quantify the defect in *Src64*$^{\Delta 17}$ embryos (Chapter 2, Section 2.6).

We identified a significant increase ($P<0.001$) in the number of fallout nuclei in *Src64*$^{\Delta 17}$ embryos compared to wild-type embryos during nuclear division cycles 12, 13, and 14 of stage four (Table 4.3; Figure 4.3). The greatest difference was identified during cycle 13 of stage four during which wild-type embryos had average of 10.06 (+/- 5.13) fallout nuclei while *Src64*$^{\Delta 17}$ embryos had in cycle 13 had an average of 34.77 (+/- 14.22) fallout nuclei ($P=5.54E-11$) (Table 4.3).

We compared nuclear fallout in $Src64^{KO}$, $Src64^{P190L}$, $Src64^{D204V}$, $Src64^{G208E}$, $Src64^{R217C}$, $Src64^{C259Y}$, $Src64^{R403C}$, $Src64^{D404N}$, and $Src64^{S440F}$ embryos to wild-type and $Src64^{\Delta 17}$ embryos during cycle 13 of stage four. All of the embryos analyzed, including $Src64^{KO}$, embryos showed no indication of the increased incidence of nuclear fallout (Table 4.4). From our statistical analysis of the results we determined that the number of fallout nuclei in all *Src64* mutant embryos, with the exception of $Src64^{\Delta 17}$, was not statistically different (P>0.05) than the number of fallout nuclei in wild-type embryos (Table 4.4). These results suggest that the nuclear fallout defect identified in $Src64^{\Delta 17}$ embryos may not be a result of the reduction in Src64 protein and that there may be some other element present in the $Src64^{\Delta 17}$ strain that leads to the nuclear fallout defect

4.2.3 Defects in embryo length and embryo width were identified related to mutations in *Src64*

Embryo size is a relatively non-specific trait of embryos that could be affected by mutations to *Src64* by way of ring canal defects during oogenesis. Defects to embryo size have not yet been linked to mutations to *Src64*. We analyzed embryo length and embryo width in wild-type, $Src64^{\Delta 17}$, $Src64^{KO}$ $Src64^{P190L}$, $Src64^{D204V}$, $Src64^{G208E}$, $Src64^{R217C}$, $Src64^{C259Y}$, $Src64^{R403C}$, $Src64^{D404N}$, and $Src64^{S440F}$ embryos.

In our analysis of embryo length we identified an average embryo length of 493.53µm (+/-19.18m) in wild-type embryos. We identified a significant reduction in embryo length (P<0.001) in $Src64^{\Delta 17}$, $Src64^{KO}$ and all of the *Src64* point mutations with the exception of $Src64^{G208E}$ and $Src64^{S440F}$ (Table 4.5). The greatest reduction in embryo length was seen in the $Src64^{KO}$ and $Src64^{\Delta 17}$ embryos. $Src64^{KO}$ embryos had an average length of 385.60µm (+/-26.26µm), or 78% of wild-type embryo length (Table 4.5).

In our analysis of embryo width we identified an average embryo width of 194.30µm (+/-9.31m) in wild-type embryos (Table 4.6). We identified a significant reduction in embryo width (P<0.01) in $Src64^{\Delta 17}$ and $Src64^{KO}$ embryos. The most severe defect to embryo width was identified in $Src64^{KO}$ embryos with an average embryo width of 174.24µm (+/-10.30µm), or 90%of wild-type embryowidth (Table 4.6). We did not identify any significant reduction of embryo width in the *Src64* point mutations (P>0.05) (Table 4.6).

These results suggest that Src64 may have some function during embryogenesis that relates to embryo size, and that both the SH2 domain and tyrosine kinase domain may be involved in this process. However, embryo size is a complex trait, and these results do not provide any information as to the specifics of *Src64* activity related to embryo size.

4.2.4 Cellularization front defects were identified in $Src64^{KO}$, $Src64^{R217C}$, and $Src64^{D404N}$ embryos

Defects in the cellularization have previously been described in $Src64^{\Delta 17}$ embryos (Thomas and Wieschaus, 2004). The cellularization front defect appears as a wavy, distorted cellularization front in $Src64^{\Delta 17}$ embryos compared to the smooth and uniform cellularization front in wild-type embryos (Chapter 1, Section 1.4). Our analysis of the cellularization front included an analysis of $Src64^{KO}$, $Src64^{P190L}$ (SH2 domain), $Src64^{G208E}$ (SH2 domain), $Src64^{R217C}$ (SH2 domain), $Src64^{R403C}$ (TK domain), $Src64^{D404N}$ (TK domain catalytic aspartate), $Src64^{S440F}$ (TK domain) embryos with wild-type, $Src64^{\Delta 17}$, and *rucuca* embryos included as controls.

We identified four, early cellularization, wild-type embryos (Figure 4.5). Our results indicated, as previously reported by Thomas and Wieschaus (Thomas and Wieschaus, 2004), that the cellularization front in wild-type embryos was straight, uniform, and lacked any apparent defects. We identified six early cellularization $Src64^{\Delta 17}$ embryos and analyzed the embryos for defects in the cellularization front (Figure 4.6). Each of the embryos exhibited some form of defect in the progression of the cellularization front that ranged from a general wrinkled appearance of the cellularization front (Figure 4.6 A-C) to acute defects that appeared as dents or hitches in the cellularization front (Figure 4.6 D-F). From an analysis of embryos during late cellularization we determined that the defect appears less pronounced as the cellularization front progresses past the nuclei. During late cellularization wild-type and $Src64^{\Delta 17}$ cellularization fronts become indistinguishable (Figure 4.7: A, B).

We identified four *rucuca* embryos in early cellularization (Figure 4.8: A, B, C, D), and found no indication of defects in the cellularization. The cellularization front in each of the *rucuca* embryos identified appeared smooth, uniform, and similar the wild-

type cellularization front (Figure 4.8). This confirmed that any defects identified in *Src64* mutants recombined to *rucuca* were not due to the *rucuca* chromosome.

Src64^{KO}, three *Src64* SH2 domain mutants, and three *Src64* TK domain mutants were included in our analysis of the cellularization front. We identified three *Src64*^{KO} embryos in the process of early cellularization. The embryos exhibited defects similar to those seen in *Src64*$^{\Delta 17}$ embryos (Figure 4.9). The cellularization front in each of the embryos analyzed had a wavy, wrinkled appearance and lacked the uniform appearance of the wild-type cellularization front (Figure 4.9: A, B, C). In some cases the defect appeared more severe than the defect observed in *Src64*$^{\Delta 17}$(Figure 4.9: B, C).

Of the three SH2 domain mutants analyzed, we identified a defect to the cellularization front only in *Src64*^{R217C} embryos. The cellularization front in *Src64*^{P190L} and *Src64*^{G208E} embryos appeared smooth, uniform, and similar to a wild-type cellularization front (Figure 4.10 A, B). However; the cellularization front in *Src64*^{R217C} appeared wavy and disorganized, similar to the cellularization front in *Src64*$^{\Delta 17}$ embryos (Figure 4.10 C).

Of the three TK domain mutants analyzed, we identified a defect to the cellularization front only in *Src64*^{D404N} embryos. The cellularization front in *Src64*^{R403C} and *Src64*^{S440F} embryos appeared similar to the wild-type cellularization front (Figure 4.11 A, B). However, the cellularization front in *Src64*^{D404N} (the catalytic aspartate mutation) embryos appeared wavy, slack, and disorganized (Figure 4.11 C, D). As in *Src64*^{KO} embryos, some of the embryos exhibited a defect to the cellularization front that appeared more severe than the defect identified in *Src64*$^{\Delta 17}$ embryos (Figure 4.11 D)

The defect to the cellularization front was identified in early cellularization *Src64*$^{\Delta 17}$, *Src64*^{KO}, *Src64*^{R217C}, and *Src64*^{D404N} embryos (Figure 4.7; Figure 4.9; Figure 4.10; Figure 4.11). These results suggest that both the SH2 domain and the tyrosine kinase domain are involved in Src64 activity during cellularization. Additionally, the possibility of a more severe defect in *Src64*^{KO} and *Src64*^{D404N} embryos suggests a critical role for the tyrosine kinase domain during Src64 activity while the SH2 domain may have some redundant or accessory function, or that the *Src64*^{R217C} mutation does not completely eliminate the function of the SH2 domain

4.2.5 Microfilament ring circularity defects were identified in *Src64*^{KO}, *Src64*^{R217C}, and *Src64*^{D404N} embryos

Microfilament ring defects have previously been described in *Src64*$^{\Delta 17}$ embryos (Thomas and Wieschaus, 2004). The microfilament ring defect appears as a reduced circularity of microfilament rings in *Src64*$^{\Delta 17}$ embryos during early and late cellularization compared to microfilament rings in wild-type embryos (Chapter 1, Section 1.4). Our analysis of the microfilament rings included an analysis of microfilament ring circularity in early and late cellularization (Figure 4.12) from *Src64*^{KO}, *Src64*^{P190L} (SH2 domain) (no data from late cellularization), *Src64*^{G208E} (SH2 domain), *Src64*^{R217C} (SH2 domain), *Src64*^{R403C} (TK domain), *Src64*^{D404N} (TK domain catalytic aspartate), *Src64*^{S440F} (TK domain) embryos with wild-type, *Src64*$^{\Delta 17}$, and *rucuca* embryos included as controls.

We identified four early cellularization wild-type embryos and three late cellularization wild-type embryos, and calculated a wild-type embryo early cellularization microfilament ring circularity of 0.88 (+/- 0.046) in microfilament rings and a late cellularization microfilament ring circularity of 0.91 (+/-0.032) (Table 4.7; Table 4-8; Figure 4.13). From our analysis of *Src64*$^{\Delta 17}$ embryos we confirmed the previously identified defect to microfilament ring circularity. We calculated an early cellularization microfilament ring circularity of 0.84 (+/-0.044), and a late cellularization microfilament ring circularity of 0.85 (+/-0.052) in *Src64*$^{\Delta 17}$ embryos (Table 4.7; Table 4-8). Statistical analysis confirmed that microfilament ring circularity was significantly reduced in *Src64*$^{\Delta 17}$ embryos compared to wild-type embryos during early ($P<0.01$) and late ($P<0.01$) cellularization (Table 4.7; Table 4-8). From our analysis of microfilament ring circularity in *rucuca* embryos we calculated an early cellularization microfilament ring circularity of 0.90 (+/-0.030) and a late cellularization microfilament ring circularity of 0.90 (+/-0.021). We determined that microfilament ring circularity in *rucuca* embryos was not statistically different than microfilament ring circularity in wild-type embryos during both early ($P>0.05$) and late ($P>0.05$) cellularization (Table 4.7; Table 4.8; Figure 4.13).

In our analysis of early cellularization microfilament ring circularity, we identified a reduced microfilament ring circularity in *Src64*^{KO} and *Src64*^{D404N} (TK domain catalytic aspartate) embryos. Microfilament ring circularity in early cellularization *Src64*^{KO} embryos was calculated as 0.81 (+/-0.027) (Table 4.7; Figure 4.14). Microfilament ring circularity in early cellularization *Src64*^{D404N} embryos was calculated as 0.80 (+/-0.047). We determined that microfilament ring circularity in *Src64*^{KO} and *Src64*^{D404N} embryos is significantly reduced ($P<0.001$) from microfilament ring circularity in wild-type embryos (Table 4.7; Figure 4.14). We also determined that the microfilament ring defect in early cellularization *Src64*^{KO} and *Src64*^{D404N} embryos is significantly more severe that the defect identified in *Src64*$^{\Delta 17}$ embryos ($P<0.01$), and that microfilament ring circularity in early cellularization *Src64*^{KO} and *Src64*^{D404N} embryos was not statistically different($P>0.05$) (Table 4.7). The remaining *Src64* mutations did not exhibit any reduction in microfilament ring circularity in early cellularization embryos (Table 4.7). From our statistical analysis (Chapter 2, Section 2.6), we classified the early cellularization microfilament ring defect in *Src64*$^{\Delta 17}$ embryos as a moderate defect, and the early cellularization microfilament ring defect in *Src64*^{KO} and *Src64*^{D404N} embryos as a severe defect (Table 4.7).

In our analysis of late cellularization microfilament ring circularity, we identified a reduced microfilament ring circularity in *Src64*^{KO}, *Src64*^{R217C} (SH2 domain), and *Src64*^{D404N} (TK domain catalytic aspartate) embryos. We calculated a microfilament ring circularity of 0.78 (+/-0.041) in late cellularization *Src64*^{KO} embryos, 0.84 (+/-0.043) in late cellularization *Src64*^{R217C} embryos, and 0.79 (+/-0.047) in late cellularization *Src64*^{D404N} embryos. We determined that microfilament rings in late cellularization *Src64*^{KO} and *Src64*^{D404N} embryos exhibited a severe defect ($P<0.001$) in microfilament ring circularity compared to wild-type embryos, and compared to the moderate defect exhibited in *Src64*$^{\Delta 17}$ and *Src64*^{R217C} embryos. As in early cellularization, microfilament ring circularity in late cellularization *Src64*^{KO} and *Src64*^{D404N} embryos was not statistically different ($P>0.05$). Interestingly, statistical analysis of microfilament rings in late cellularization *Src64*^{R217C} embryos indicated a significant, though moderate, defect to microfilament ring circularity ($P<0.01$) (Table 4.8). Microfilament ring circularity in late

cellularization *Src64*^{R217C} embryos was not statistically different than microfilament ring circularity in late cellularization *Src64*$^{\Delta 17}$ embryos (P>0.05) (Table 4.8). The remaining *Src64* mutations did not exhibit any reduction in microfilament ring circularity in late cellularization embryos (Table 4.8). From our statistical analysis (Chapter 2, Section 2.6), we classified the microfilament ring defect in *Src64*$^{\Delta 17}$ and *Src64*^{R217C} embryos as a moderate defect, and the microfilament ring defect in *Src64*^{KO} and *Src64*^{D404N} embryos as a severe defect (Table 4.8).

We identified a reduced microfilament ring circularity in early cellularization *Src64*$^{\Delta 17}$, *Src64*^{KO}, and *Src64*^{D404N} embryos (Figure 4.13; Figure 4.14); and in late cellularization *Src64*$^{\Delta 17}$, *Src64*^{KO}, *Src64*^{R217C}, and *Src64*^{D404N} embryos (Figure 4.13; Figure 4.15). These results suggest that both the SH2 domain and the tyrosine kinase domain are involved in Src64 activity related to microfilament ring circularity. Importantly, these results also suggest that Src64 activity may be different during early cellularization and late cellularization. The normal microfilament ring circularity in early cellularization *Src64*^{R217C} embryos, and reduced microfilament ring circularity in late cellularization *Src64*^{R217C} embryos suggest a Src64 activity during early cellularization that is independent of the SH2 domain, and a Src64 activity during late cellularization that does involve the SH2 domain (Figure 4.16; Figure 4.17)

4.2.6 Microfilament ring constriction defects were identified in *Src64*$^{\Delta 17}$, *Src64*^{KO} and *Src64*^{D404N} embryos

In addition to a reduction in microfilament ring circularity, some data suggests a possible defect in microfilament ring constriction from early to late cellularization (Thomas and Wieschaus, 2004). As the embryo enters late cellularization, and the cellularization front passes the inner edge of the peripheral nuclei, microfilament rings within the cellularization front constrict and begin the process of closing off the basal edge of the new cells (Figure 4.12) (Chapter 1, Section 1.3). We measured microfilament ring constriction in wild-type, *rucuca*, *Src64*^{KO}, *Src64*^{G208E} (SH2 domain), *Src64*^{R217C} (SH2 domain), *Src64*^{R403C} (TK domain), *Src64*^{D404N} (TK domain), and *Src64*^{S440F} (TK domain), embryos. Statistical analysis was not performed on microfilament ring constriction data due to the speed of microfilament ring constriction and difficulties in matching the exact age of embryos.

Our analysis of wild-type embryos indicated a 33% reduction in the area encompassed by microfilament rings from early to late cellularization (Table 4.9). Similar to wild-type embryos, *rucuca* embryos showed a 32% decrease in the area encompassed by microfilament rings from early to late cellularization (Table 4.9). We identified the most severe defect to microfilament ring constriction in $Src64^{KO}$ embryos. We identified a microfilament ring constriction of only 3% in $Src64^{KO}$ embryos (Table 4.9). Moderate reductions in microfilament ring constriction were identified in $Src64^{\Delta 17}$, and $Src64^{D404N}$ embryos. Microfilament rings in $Src64^{\Delta 17}$ embryos constricted an average of 23% from early to late cellularization, and microfilament rings in $Src64^{D404N}$ embryos constricted an average of 17% from early to late cellularization (Table 4.9). Microfilament rings in $Src64^{R217C}$ embryos constricted an average of 28% (Table 4.9). This value is inconclusive, and falls within the range identified in wild-type and $Src64^{\Delta 17}$ embryos.

We identified a reduced microfilament ring constriction in $Src64^{\Delta 17}$, $Src64^{KO}$, $Src64^{D404N}$ embryos, and possibly $Src64^{R217C}$ and $Src64^{R403C}$ embryos. The severely reduced microfilament ring constriction in $Src64^{KO}$ embryos suggests a critical role for *Src64* during microfilament ring constriction. Microfilament ring constriction in $Src64^{D404N}$ embryos was not reduced to the level in $Src64^{KO}$ embryos suggesting that elimination of tyrosine kinase function is not sufficient to result in the $Src64^{KO}$ phenotype, and that there may be a tyrosine kinase independent function for Src64 during microfilament ring constriction.

4.2.7 A range of embryo yield and hatch rate defects were identified related to mutations in *Src64*

Defects in embryo yield and hatch rate have previously been associated with the $Src64^{\Delta 17}$ and $Src64^{KO}$ mutations (Chapter 1, Section 1.4) (Dodson et. al., 1998; O'Reilly et al., 2006). The $Src64^{\Delta 17}$ and $Src64^{KO}$ mutations caused a reduction in embryo yield and hatch rate suggesting a role for *Src64* in the process of embryogenesis and early embryo development before the onset of zygotic transcription. We measured embryo yield and hatch rate in wild-type, $Src64^{\Delta 17}$, $Src64^{KO}$, $Src64^{P190L}$ (SH2 domain), $Src64^{D204V}$ (SH2 domain), $Src64^{G208E}$ (SH2 domain), $Src64^{R217C}$ (SH2 domain), $Src64^{C259Y}$ (SH2

domain), *Src64*^{R403C} (TK domain), *Src64*^{D404N} (TK domain), *Src64*^{S440F} (TK domain), and *rucuca* flies and embryos. In our analysis of embryo yield and hatch rate, Src64m represents the maternal genome that is controlling oogenesis and early embryo development, and not the embryonic genome (Chapter 2, Section 2.6).

We measured embryo yield and hatch rate until the females in a specific cross stopped producing embryos. The results from our analysis of both embryo yield and embryo hatch rate indicated low values at the beginning of each cross (Figure 4.18). Additionally, after day ten the results became erratic in many of the crosses (Figure 4.18). Due to this we performed our statistical analysis on data gathered from day three to ten of the embryo collection.

In our analysis of embryo yield we calculated an average embryo yield of 35.18 (+/-4.17) embryos per wild-type female (day 3-10) (Table 4.10). *Src64*$^{\Delta 17}$ females did not exhibit any defect in embryo yield with an average embryo yield of 33.99 (+/-3.50) embryos per *Src64*$^{\Delta 17}$ female (day 3-10) (Table 4.10). We did identify a moderate defect in embryo yield ($P<0.001$) in *rucuca* females. We calculated an average embryo yield of 15.48 (+/-2.23) embryos per *rucuca* female (day 3-10) (Table 4.10). Due to the defect identified in *rucuca* females, statistical analysis compared embryo yield in the *Src64* mutations recombined to *rucuca* to the embryo yield calculated from *rucuca* females. We identified defects in embryo yield more severe than the defect identified in *rucuca* females in *Src64*^{KO} and *Src64*^{G208E} females (Figure 4.19). We calculated an average embryo yield of 2.83 (+/-1.45) embryos per *Src64*^{KO} female, and an average embryo yield of 2.49 (+/-0.90) embryos per *Src64*^{G208E} female (Table 4.10). These values are statistically more severe than the embryo yield value calculated from *rucuca* females ($P<0.001$). The embryo yield calculated from the remaining *Src64* mutants was less than wild-type embryo yield, but statistically similar ($P>0.05$) to the embryo yield calculated from *rucuca* females (Table 4.10; Figure 4.19).

In our analysis of hatch rate we calculated an average hatch rate of 84.21% (+/-6.01%) in embryos laid by wild-type females (day 3-10) (Table 4.11). We identified a moderate defect in hatch rate ($P<0.001$) in embryos laid by *Src64*$^{\Delta 17}$ females. We calculated a hatch rate of 44.52% (+/-12.77%) from embryos laid by *Src64*$^{\Delta 17}$ females

(Table 4.11). We did not identify any defect in hatch rate in embryos laid by *rucuca* females. Embryos laid by *rucuca* females hatched at a rate of 72.13% (+/-9.27%) (Table 4.11), and we determined that the hatch rate in embryos laid by wild-type females and rucuca females are not statistically different (P>0.05). The *Src64* mutants exhibited a wide range of defects to hatch rate. The most severe defect to hatch rate was identified in embryos laid by $Src64^{KO}$ females which hatched at a rate of 11.78% (+/-7.47%) (Table 4.11; Figure 4.20). A similar hatch rate was identified embryos laid by $Src64^{D404N}$ females which hatched at a rate of 16.12% (+/-3.88%) (Table 4.11; Figure 4.20). Hatch rate defects in the remaining *Src64* mutants ranged from no defect (P>0.05) ($Src64^{G208E}$, and $Src64^{S440F}$), to a moderate defect in hatch rated similar to the hatch rate of embryos laid by $Src64^{\Delta 17}$ females ($Src64^{P190L}$, $Src64^{D204V}$, $Src64^{R217C}$, $Src64^{C259Y}$, $Src64^{R403C}$) (Table 4.11; Figure 4.20).

The most severe defect in embryo yield was identified in $Src64^{KO}$ and $Src64^{G208E}$ females. These results suggest a critical role for the Src64 SH2 domain during embryogenesis, and another possible tyrosine kinase independent function for Src64. Additionally, the $Src64^{G208E}$ mutation caused a defect in embryo yield, while the $Src64^{R217C}$ mutation did not. This suggests that the $Src64^{G208E}$ and $Src64^{R217C}$ mutations affect the SH2 domain function in different ways, possibly by affecting binding affinity or substrate binding. The $Src64^{G208E}$ mutation affects SH2 domain function and Src64 activity during embryogenesis, while the $Src64^{R217C}$ mutation affects SH2 domain function and Src64 activity during cellularization.

The most severe defect in hatch rate was identified in $Src64^{KO}$ and $Src64^{D404N}$ embryos. These results suggest that Src64, and specifically the Src64 tyrosine kinase domain, has a crucial role in early embryo development, and that a likely elimination of tyrosine kinase activity is sufficient to result in the $Src64^{KO}$ phenotype. Additionally, the reduced hatch rate in Src64 SH2 domain mutants suggests some role for the SH2 domain during early embryo development, but that a reduction in SH2 domain function is not sufficient to result in the $Src64^{KO}$ phenotype.

Table 4.1: Mutations located by the Seattle TILLING Project: nucleotide change, amino acid change, and domain

Mutant line	Nucleotide change	Amino acid change	Domain
Z3-0989	C315T	P190L	SH2
Z3-1066	A357T	D204V	SH2
Z3-1792	G369A	G208E	SH2
Z3-0327	C395T	R217C	SH2
Z3-1745	G589A	C259Y	SH2
Z3-0399	G988A	D372N	TK
Z3-4912	A1079T	H402L	TK
Z3-6137	C1081T	R403C	TK
Z3-3707	G1084A	D404N*	TK
Z3-3573	C1193T	S440F	TK

* The *Src64*^{D404N} changes the catalytic aspartate of the tyrosine kinase domain to asparagine and should remove all kinase activity

Table 4.2: Restriction sites and predictive statistics for *Src64* mutations located by the Seattle TILLING Project

Src64 allele	Restriction site lost	PSSM difference	SIFT score
Src64^{P190L}	*Eco57I*	-	0.00
Src64^{D204V}	*	-	0.00
Src64^{G208E}	*BccI*	-	0.81
Src64^{R217C}	*	16.0	0.00
Src64^{C259Y}	*	29.4	0.00
Src64^{D372N}	*BccI*	-	0.27
Src64^{H402L}	*BccI*	36.9	0.00
Src64^{R403C}	*BccI*	9.3	0.03
Src64^{D404N}	*NruI*	16.1	0.01
Src64^{S440F}	*MboI*	12.4	0.00

* No restriction site was lost from these mutations. Verification of the mutant chromosome was performed by sequencing analysis.

\- No data given for PSSM score

Table 4.3: Statistical analysis of nuclear fallout in wild-type and *Src64*$^{\Delta 17}$ embryos during cycles 10-14

Cycle number	Number of WT embryos analyzed	WT: average number of fallout nuclei (standard dev.)	Number of *Src64*$^{\Delta 17}$ embryos analyzed	*Src64*$^{\Delta 17}$: Average number of fallout nuclei (standard dev.)	P value
10	19	2.47 (2.31)	15	3.33 (3.45)	0.208
11	17	4.00 (3.42)	21	3.38 (4.18)	0.309
12	22	3.54 (3.48)	33	11.96 (11.22)	0.0001*
13	30	10.06 (5.13)	30	34.76 (14.22)	5.54 E-11*
14	26	11.73 (5.77)	21	27.81 (17.08)	0.0002*

* Nuclear fallout was significantly increased in *Src64*$^{\Delta 17}$ embryos during cycles 12, 13, and 14. The greatest difference in nuclear fallout between WT and *Src64*$^{\Delta 17}$ embryos was seen during cycle 13 of stage 4

Table 4.4: Statistical analysis of nuclear fallout in *Src64* mutant embryos compared to wild-type embryos during cycle 13 of stage 4

Src64 allele	Number of embryos analyzed	Average nuclear fallout	P value
Src64$^{\Delta 17}$	30	34.76	P<0.01
Src64^{KO}	3	6.33	P>0.05
Src64^{P190L}	10	11.80	P>0.05
Src64^{D204V}	6	11.16	P>0.05
Src64^{G208E}	5	5.80	P>0.05
Src64^{R217C}	17	11.7	P>0.05
Src64^{C259Y}	6	10.0	P>0.05
Src64^{R403C}	5	9.20	P>0.05
Src64^{D404N}	5	20.5	P>0.05
Src64^{S440F}	7	7.57	P>0.05

No significant increase in nuclear fallout (P<0.001) was seen in any of the *Src64* alleles

Table 4.5: Analysis of embryo length in wild-type and *Src64* mutant embryos

Src64 allele	Number of embryos measured	Average embryo length in μm (standard dev.)	Statistical grouping
WT	114	493.53 (19.18)	A
$Src64^{\Delta 17}$	120	439.44 (25.07)	B
$Src64^{KO}$	11	385.60 (26.26)	B
$Src64^{P190L}$	36	456.79 (30.58)	B^{+}
$Src64^{D204V}$	26	462.27 (20.46)	B^{+}
$Src64^{G208E}$	10	472.28 (20.93)	A^{+}
$Src64^{R217C}$	56	462.18 (24.16)	B^{*+}
$Src64^{C259T}$	21	452.72 (25.25)	B
$Src64^{R403C}$	17	446.17 (27.02)	B
$Src64^{D404N}$	11	430.47 (27.39)	B
$Src64^{S440F}$	21	469.97 (20.04)	A^{+}

A) No significant reduction in length compared to WT ($P>0.05$)
B) Significant reduction in embryo length ($P<0.001$)
* Significantly larger embryo width compared to $Src64^{\Delta 17}$ embryo width ($P<0.01$)
$^{+}$ Significantly larger embryo width compared to $Src64^{KO}$ embryo width ($P<0.01$)

Table 4.6: Analysis of embryo width in wild-type and *Src64* mutant embryos

Src64 allele	Number of Embryos measured	Average embryo width in μm (standard dev.)	Statistical grouping
WT	114	194.30 (9.31)	A
$Src64^{\Delta 17}$	120	179.44 (10.30)	B
$Src64^{KO}$	11	174.24 (14.09)	B
$Src64^{P190L}$	36	202.80 (15.14)	A*$^{+}$
$Src64^{D204V}$	26	203.54 (14.43)	A*$^{+}$
$Src64^{G208E}$	10	200.48 (16.14)	A*$^{+}$
$Src64^{R217C}$	56	202.38 (14.18)	A*$^{+}$
$Src64^{C259T}$	21	198.72 (12.45)	A*$^{+}$
$Src64^{R403C}$	17	193.20 (20.48)	A*
$Src64^{D404N}$	11	187.41 (18.26)	A
$Src64^{S440F}$	21	201.69 (16.63)	A*$^{+}$

A) No significant reduction in embryo width ($P<0.05$)
B) Significant reduction in embryo length compared to WT ($P<0.01$)
* Significantly larger embryo width compared to $Src64^{\Delta 17}$ embryo width ($P<0.01$)
$^{+}$ Significantly larger embryo width compared to $Src64^{KO}$ embryo width ($P<0.01$)

Table 4.7: Analysis of microfilament ring circularity during early cellularization

Src64 allele	Rings measured[+]	Early cellularization (standard dev.)	Statistical grouping
WT	40	0.88 (0.046)	A
rucuca	30	0.90 (0.03)	A
$Src64^{\Delta 17}$	30	0.84 (0.044)	B
$Src64^{KO}$	10	0.81 (0.027)	C*
$Src64^{P190L}$	10	0.90 (0.032)	A
$Src64^{G208E}$	40	0.89 (0.029)	A
$Src64^{R217C}$	30	0.88 (0.033)	A
$Src64^{R403C}$	10	0.90 (0.033)	A
$Src64^{D404N}$	20	0.80 (0.047)	C*
$Src64^{S440F}$	20	0.89 (0.035)	A

[+] 10 rings measured per embryo

A) No significant reduction in circularity index of microfilament rings ($P>0.05$)

B) Moderate reduction in circularity index of microfilament rings ($P<0.01$)

C) Severe reduction in circularity index of microfilament rings ($P<0.001$)

* Circularity index of microfilament rings in $Src64^{KO}$ and $Src64^{D404N}$ are statistically similar ($P>0.05$)

Table 4.8: Analysis of microfilament ring circularity during late cellularization

Src64 allele	Rings measured[+]	Average circularity index (standard dev.)	Statistical grouping
WT	30	0.91 (0.032)	A
rucuca	10	0.90 (0.021)	A
$Src64^{\Delta 17}$	20	0.85 (0.052)	B*
$Src64^{KO}$	30	0.78 (0.041)	C[+]
$Src64^{G208E}$	10	0.89 (0.044)	A
$Src64^{R217C}$	50	0.84 (0.043)	B*
$Src64^{R403C}$	10	0.88 (0.022)	A
$Src64^{D404N}$	30	0.79 (0.047)	C[+]
$Src64^{S440F}$	30	0.89 (0.032)	A

[+] 10 rings measured per embryo

A) No significant reduction in circularity index of microfilament rings ($P>0.05$)

B) Moderate reduction in circularity index of microfilament rings ($P<0.01$)

C) Severe reduction in circularity index compared to statistical grouping B ($P<0.001$)

* Circularity index of microfilament rings measured in $Src64^{\Delta 17}$ and $Src64^{R217C}$ are statistically similar ($P>0.05$)

[+] Circularity index of microfilament rings measured in $Src64^{KO}$ and $Src64^{D404N}$ are statistically similar ($P>0.05$)

\- No data collected from $Src64^{P190L}$ during late cellularization

Table 4.9: Analysis of microfilament ring constriction from early and late cellularization

Src64 allele	Early cellularization rings measured	Early cellularization microfilament ring mean area (standard dev.) in μm^2	Late cellularization rings measured	Late cellularization microfilament ring mean area (standard dev.) in μm	Percent change from early to late cellularization
WT	40	0.73 (0.07)	30	0.49 (0.10)	33%
rucuca	30	0.73 (0.10)	10	0.56 (0.07)	32%
$Src64^{\Delta 17}$	30	0.75 (0.11)	20	0.58 (0.13)	23%
$Src64^{KO}$	10	0.62 (0.06)	30	0.60 (0.18)	03%
$Src64^{G208E}$	40	0.72 (0.08)	10	0.31 (0.06)	57%
$Src64^{R217C}$	30	0.64 (0.14)	50	0.46 (0.10)	28%
$Src64^{R403C}$	10	0.69 (0.07)	10	0.51 (0.07)	26%
$Src64^{D404N}$	20	0.76 (0.07)	30	0.63 (0.07)	17%
$Src64^{S440F}$	20	1.01 (0.07)	30	0.67 (0.70)	33%

No statistical analysis could be performed on microfilament ring constriction data. Microfilament ring constriction occurs rapidly during late cellularization. We were unable to correlate data between sample sets; however we observed a reduced constriction of microfilament rings in $Src64^{KO}$ and $Src64^{D404N}$ mutants.

Table 4.10: Analysis of embryo yield in wild-type and *Src64* mutants

Src64 allele	Number of days measured	Average embryo yield (standard dev.)	3-10 day average embryo yield (standard dev.)	Statistical grouping[+]
WT	34	25.65 (9.91)	35.81 (4.17)	A
rucuca	29	12.45 (4.43)	15.48 (2.23)	B
$Src64^{\Delta 17}$	23	23.12 (13.42)	33.99 (3.50)	A
$Src64^{KO}$	13	2.76 (1.71)	2.83 (1.45)	C
$Src64^{P190L}$	16	6.83 (4.72)	7.50 (5.25)	B
$Src64^{D204V}$*	12	23.05 (5.68)	23.47 (4.80)	B
$Src64^{G208E}$	19	1.84 (1.07)	2.49 (0.90)	C
$Src64^{R217C}$*	12	11.67 (3.88)	13.27 (2.11)	B
$Src64^{C259Y}$*	19	11.58 (4.04)	11.48 (2.54)	B
$Src64^{R403C}$*	12	19.91 (8.64)	23.56 (10.20)	B
$Src64^{D404N}$	18	7.97 (4.33)	10.47 (3.04)	B
$Src64^{S440F}$	13	26.56 (15.27)	20.18 (10.16)	B

* Analysis of these mutants did not continue to the end of embryo production; however, enough data was gathered for the 3-10 day statistical analysis

[+] Statistical comparisons made between days 3-10 only. One way ANOVA with a Tukey-Kramer Multiple Comparison test was used for statistical analysis

A) No statistical deviation in embryo yield from wild-type ($P>0.05$)

B) Embryo yield significantly reduced from wild-type ($P<0.001$), but statistically similar to *rucuca* ($P>0.05$)

C) Embryo yield significantly reduced from wild-type ($P<0.001$), and rucuca ($P<0.001$)

Table 4.11: Analysis of hatch rate in wild-type and *Src64* mutants

Src64 allele	Number of days measured	Average hatch rate (standard dev.)	3-10 day average hatch rate (standard dev.)	Statistical grouping[+]
WT	34	77.96 (26.36)	84.21 (6.01)	A
rucuca	29	50.91 (32.20)	72.13 (9.27)	A
$Src64^{\Delta 17}$	23	35.04 (20.86)	44.52 (12.77)	B
$Src64^{KO}$	13	10.86 (7.99)	11.78 (7.47)	C
$Src64^{P190L}$	16	33.14 (17.56)	30.87 (15.26)	B
$Src64^{D204V}$*	12	49.53 (14.02)	54.97 (18.46)	B
$Src64^{G208E}$	19	68.11 (24.16)	72.49 (11.61)	A
$Src64^{R217C}$*	12	32.61 (15.62)	37.14 (7.35)	B
$Src64^{C259Y}$*	19	44.31 (15.53)	46.90 (17.36)	B
$Src64^{R403C}$*	12	30.98 (16.24)	32.14 (8.78)	B
$Src64^{D404N}$	18	11.91 (7.66)	16.12 (3.88)	C
$Src64^{S440F}$	13	75.75 (37.28)	67.09 (27.60)	A

* Analysis of these mutants did not continue to the end of embryo production; however, enough data was gathered for the 3-10 day statistical analysis

[+] Statistical comparisons made between days 3-10 only. One way ANOVA with a Tukey-Kramer Multiple Comparison test was used for statistical analysis

A) No statistical deviation in hatch rate from wild-type ($P>0.05$)

B) Hatch rate significantly reduced from WT ($P<0.001$)

C) Hatch rate is significantly reduced from WT ($P<0.001$), *rucuca* ($P<0.001$), and $Src64^{\Delta 17}$ ($P<0.01$)

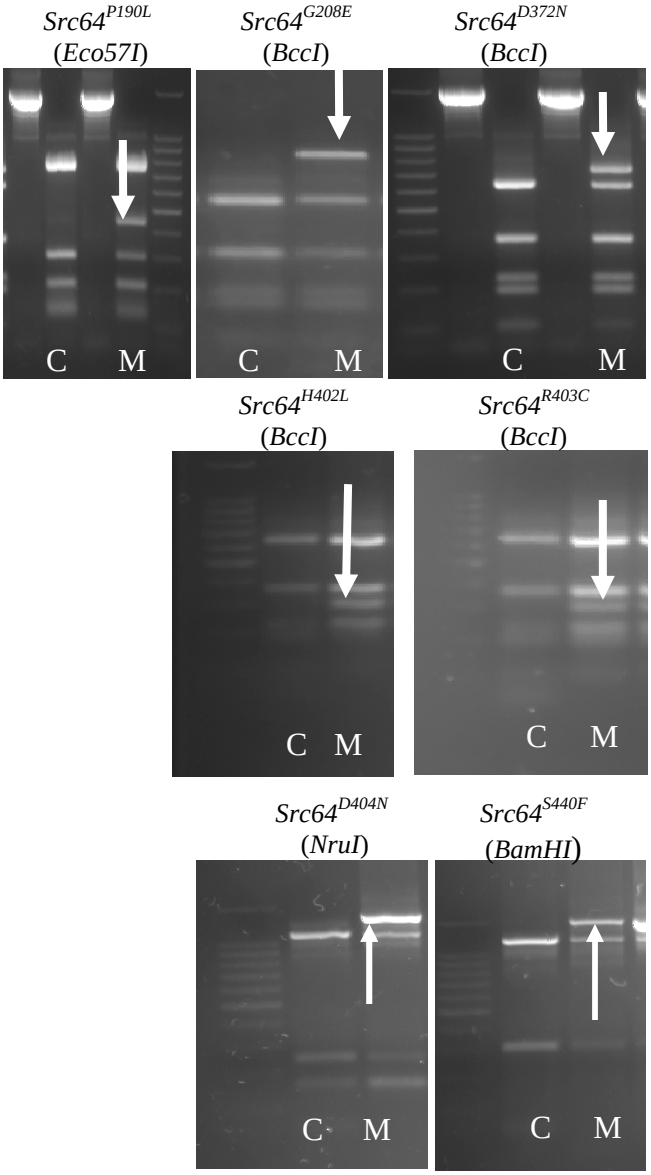

Figure 4.1: Restriction digest confirmation of recombination crosses. Proper recombination of *Src64*^{P190L}, *Src64*^{G208E}, *Src64*^{D372N}, *Src64*^{H402L}, *Src64*^{R403C}, *Src64*^{D404N}, and *Src64*^{S440F} was confirmed by restriction mapping. Isolated DNA was amplified with the same primers provided to the Seattle TILLING Project and digested with the appropriate restriction enzyme (M) along with a WT control (C). The digested DNA was run on a 2% agarose gel for maximum separation. An extra band in the mutant sample indicated the loss of a restriction site. Mutants *Src64*^{R217C}, *Src64*^{D204V}, and *Src64*^{C259Y} did not lose a restriction site. Confirmation of proper recombination of these mutants was done by sequencing of DNA isolated and amplified using the same primers provided to the TILLING lab.

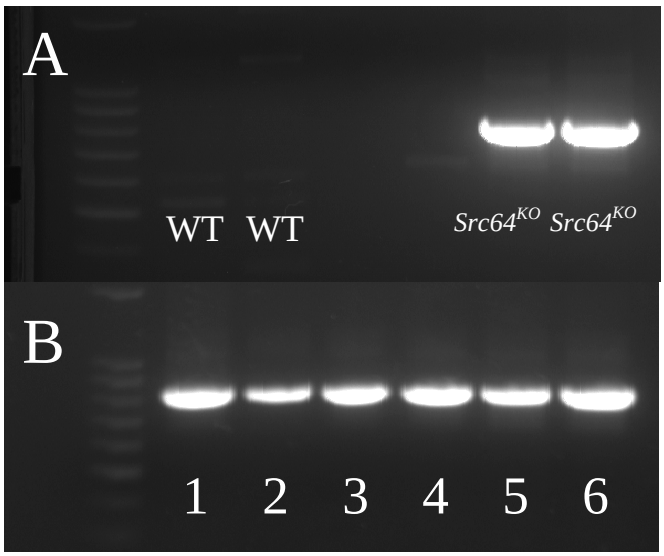

Figure 4.2: Confirmation of *Src64*^{KO} recombination. *Src64*^{KO} recombination was confirmed by amplification of isolated DNA with a specific set of primers designed to only amplify *Src64*^{KO} DNA. (A) Six *Src64*^{KO} recombinants were located. Each of the six recombinants was confirmed to have retained the *Src64*^{KO} gene. (B)

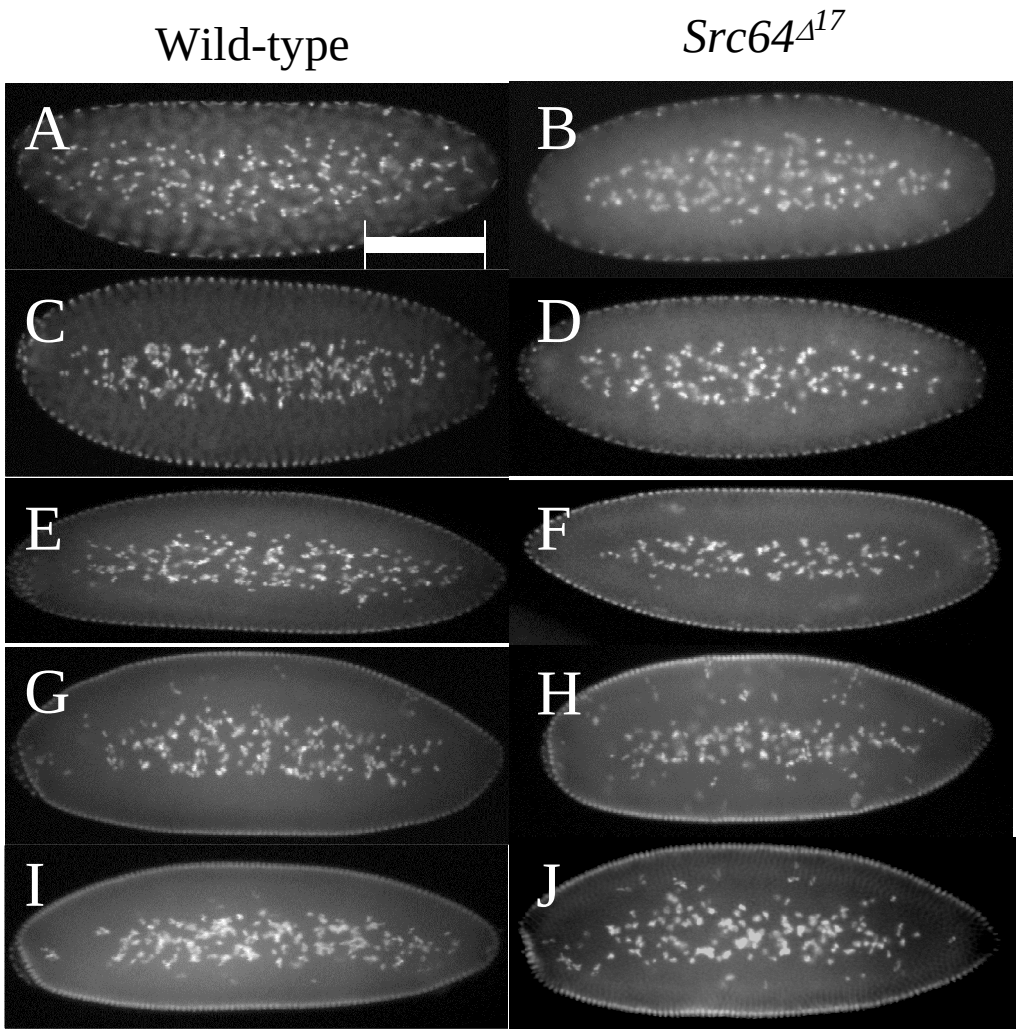

Figure 4.3: Analysis of nuclear fallout in wild-type and *Src64*$^{\Delta 17}$ embryos. Heat fixed embryos were stained for 3 minutes with Hoechst stain diluted 1:1000 in PTw. Images were taken at 200X magnification and analyzed using the ImageJ program. Stage four embryos were sorted into stage 4 cycle 10 (A, B), stage 4 cycle 11 (C, D), stage 4 cycle 12 (E, F), stage 4 cycle 13 (G, H), and stage 4 cycle 14 (I, J) for comparison of nuclear fallout. Analysis of nuclear fallout indicated a significantly higher amount of nuclear fallout in the *Src64*$^{\Delta 17}$ embryos during cycles 12, 13, and 14 with the greatest difference seen during cycle 13. Scale bar (A) is 125µm.

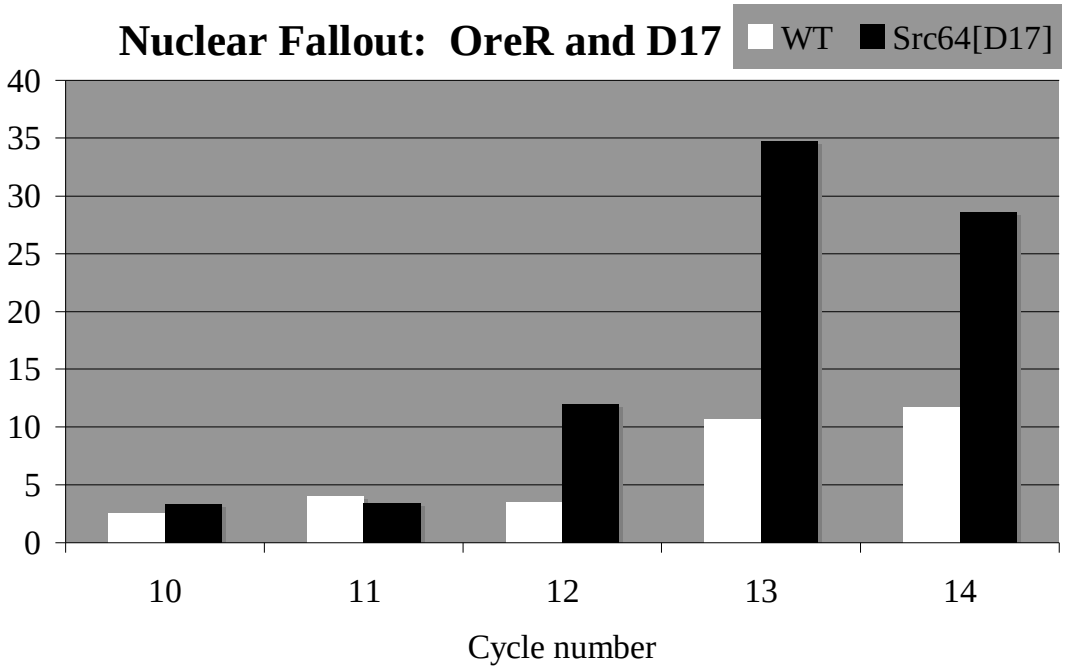

Figure 4.4: Average nuclear fallout comparison by cycle number in WT and *Src64*$^{\Delta 17}$ embryos. Significant differences in nuclear fallout were seen in cycles 12 (P=0.001), 13 (P= 5.54E-11), and 14 (P=0.0002) with *Src64*$^{\Delta 17}$ embryos exhibiting an increased amount of nuclear fallout. The greatest difference in nuclear fallout was seen in stage 4 cycle 13. From these results we decided to analyze the *Src64*^{KO} and *Src64* TILLING mutant embryos by comparison to wild-type and *Src64*$^{\Delta 17}$ embryos during cycle 13 of embryonic stage 4.

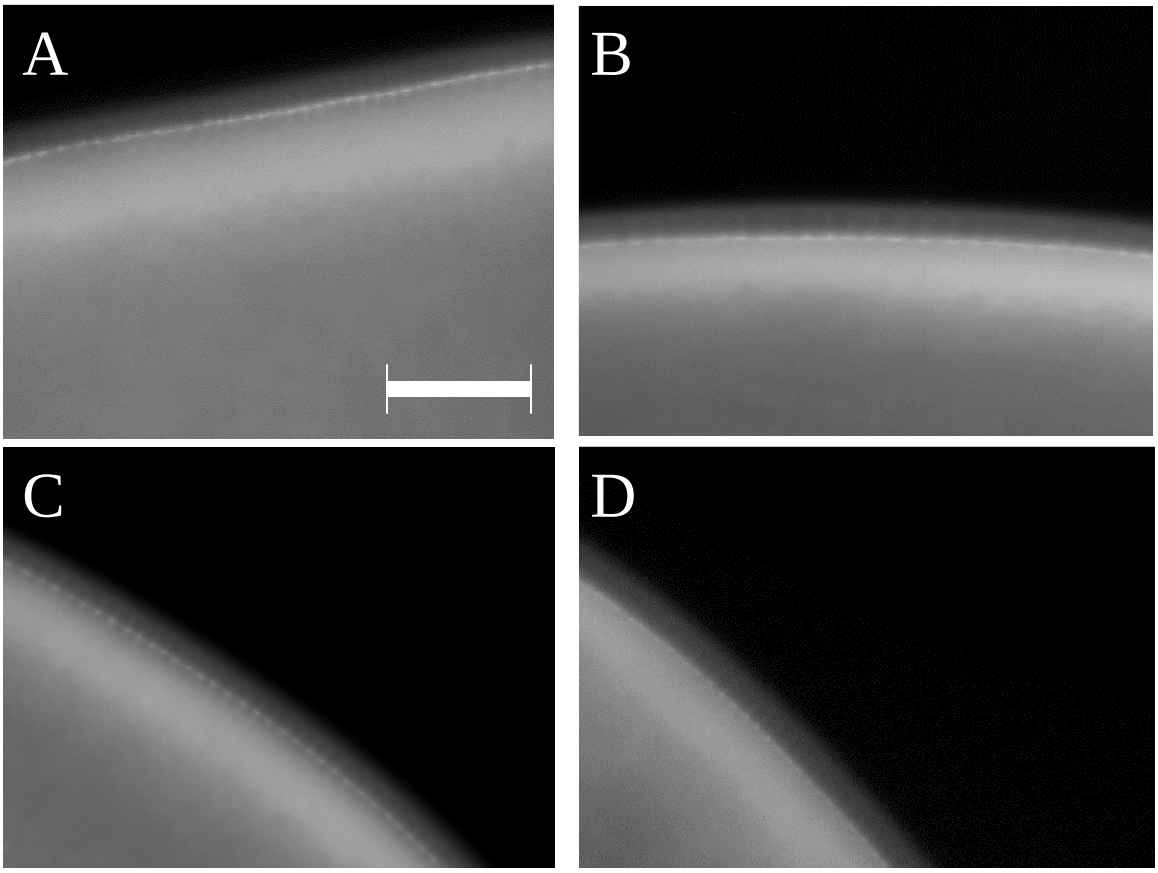

Figure 4.5: The cellularization front in wild-type embryos. We identified four wild-type embryos in the stage of early cellularization. (A-D) The cellularization fronts in the identified embryos exhibited a smooth, uniform appearance with no apparent defects. Scale bar (A) is 30µm.

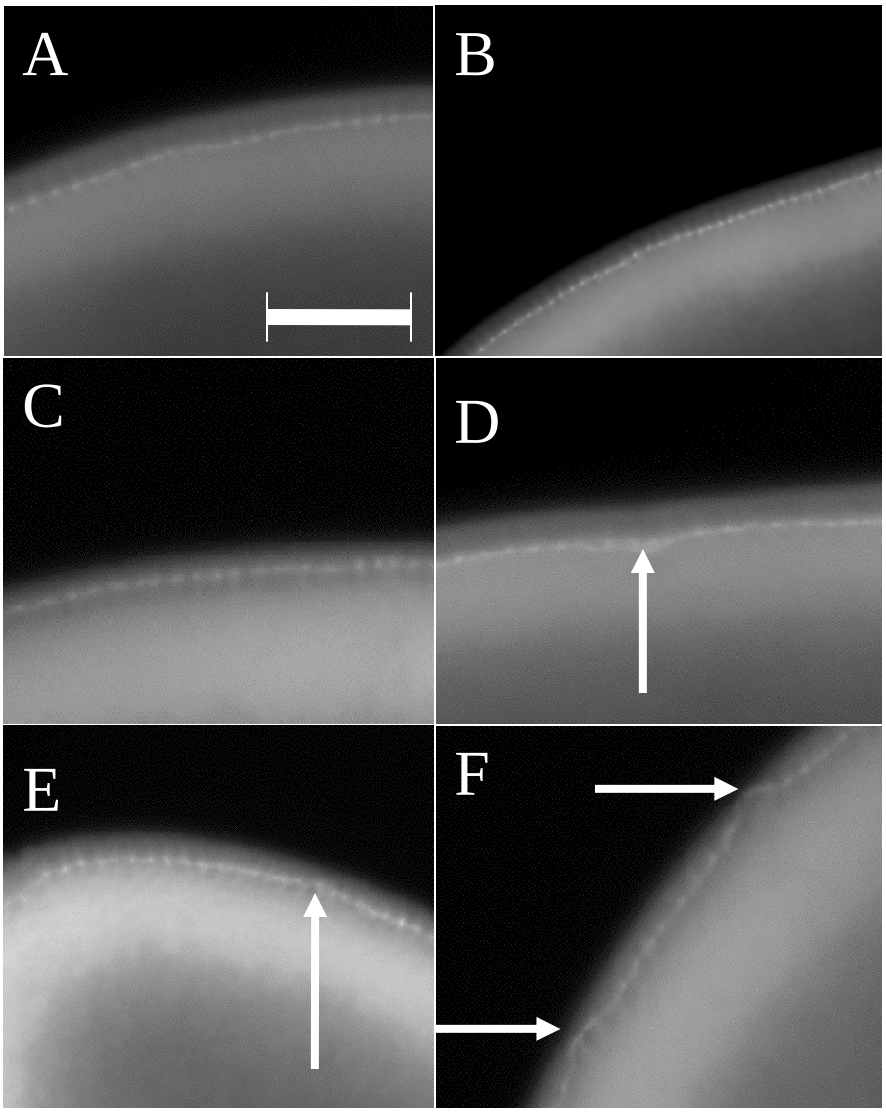

Figure 4.6: Analysis of cellularization front defects in *Src64*$^{\Delta 17}$ embryos. We identified six *Src64*$^{\Delta 17}$ embryos in early cellularization. Each of the embryos exhibited some form of defect to the cellularization front that ranged from a general wavy appearance (A, B, C) to acute dents or hitches in the cellularization front. (D, E, F) These defects were not seen in any of the wild-type embryos. Scale bar (A) is 30µm.

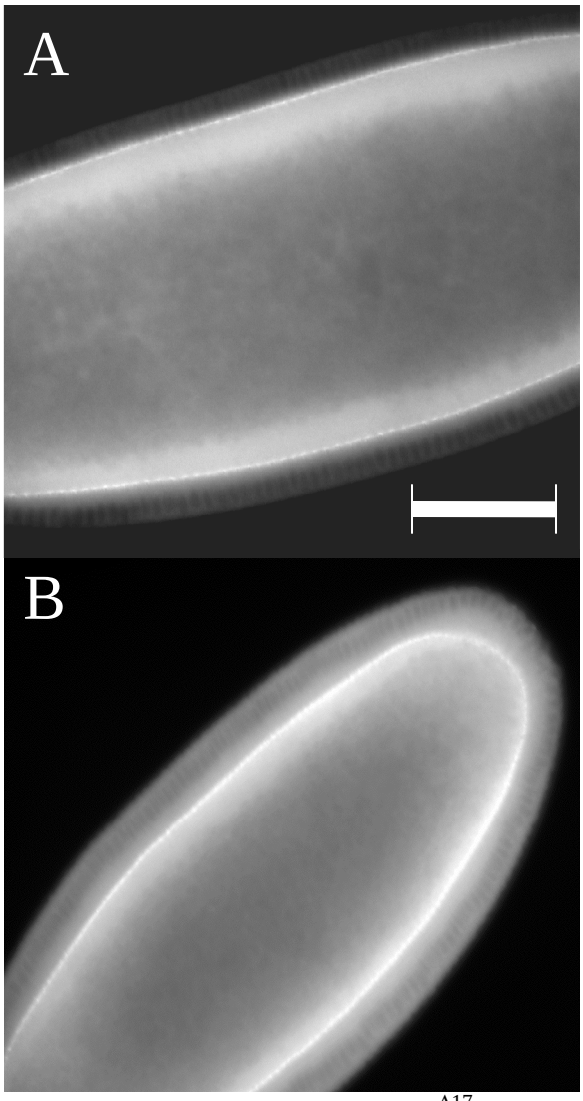

Figure 4.7: Wild-type and *Src64*$^{\Delta 17}$ cellularization fronts during late cellularization. As the embryo enters late cellularization and the cellularization front passes the basal edge of the nuclei the defect becomes less and less apparent. Eventually, wild-type (A) and *Src64*$^{\Delta 17}$ (B) cellularization fronts are indistinguishable. Scale bar (A) is 100µm.

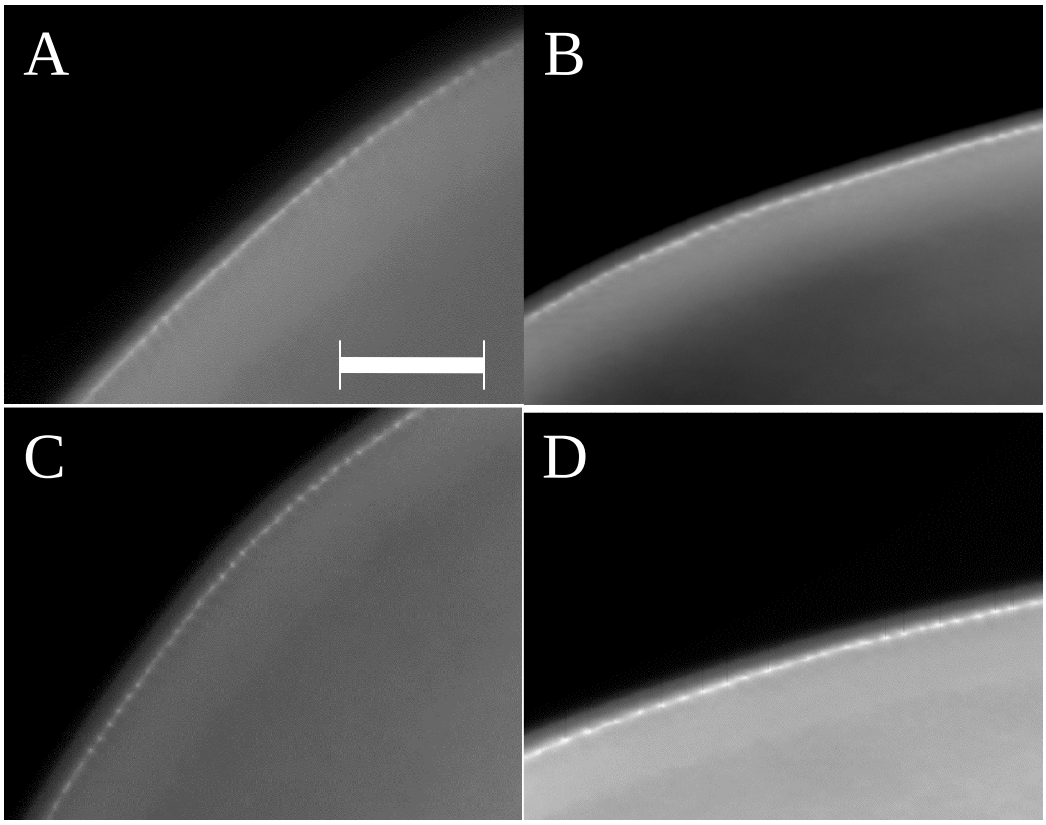

Figure 4.8: Analysis of cellularization front in early cellularization *rucuca* embryos. We identified four *rucuca* embryos in early cellularization (A-D). None of the *rucuca* embryos exhibited the defect to the cellularization front. In the four embryos located, the cellularization front appeared uniform and straight, similar to the cellularization front seen in wild-type embryos. This confirmed that any defects identified in the recombinants were not due to the *rucuca* chromosome used in the recombination cross. Scale bar (A) is 30µm.

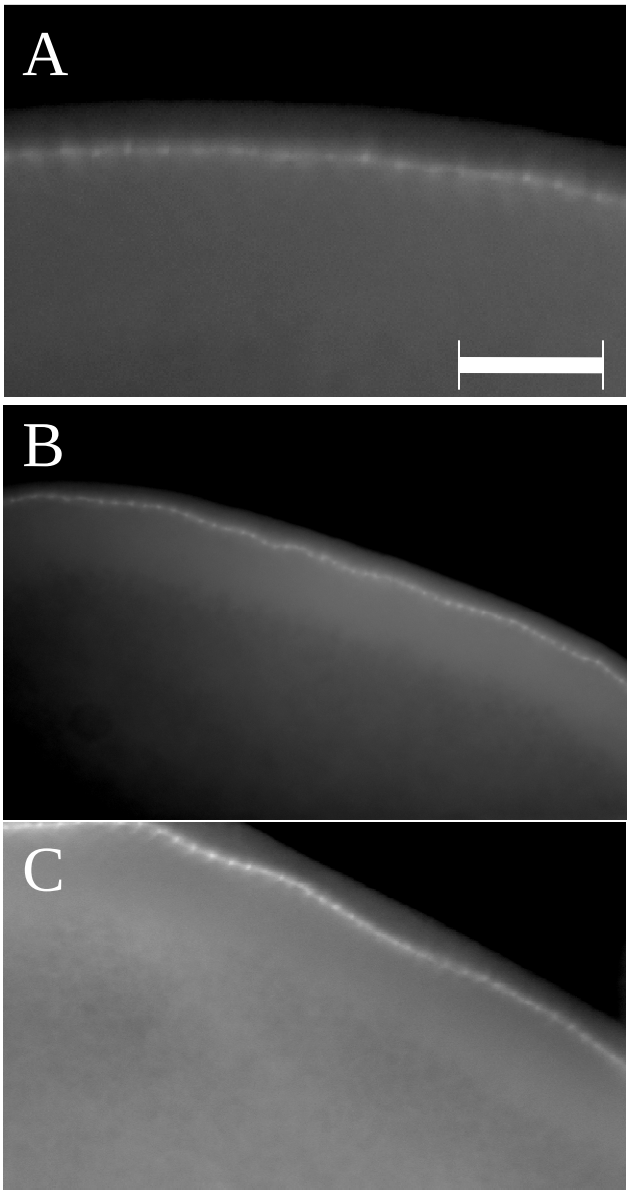

Figure 4.9: Analysis of the cellularization front in early cellularization *Src64*^{KO} embryos. All *Src64*^{KO} early cellularization front embryos identified exhibited the defect to the cellularization front (A, B, C). The cellularization front appeared wavy and disorganized. In some cases the defect to the cellularization front appeared worse than the defect seen in *Src64*$^{\Delta 17}$ embryos. (B, C). Scale bar (A) is 30µm.

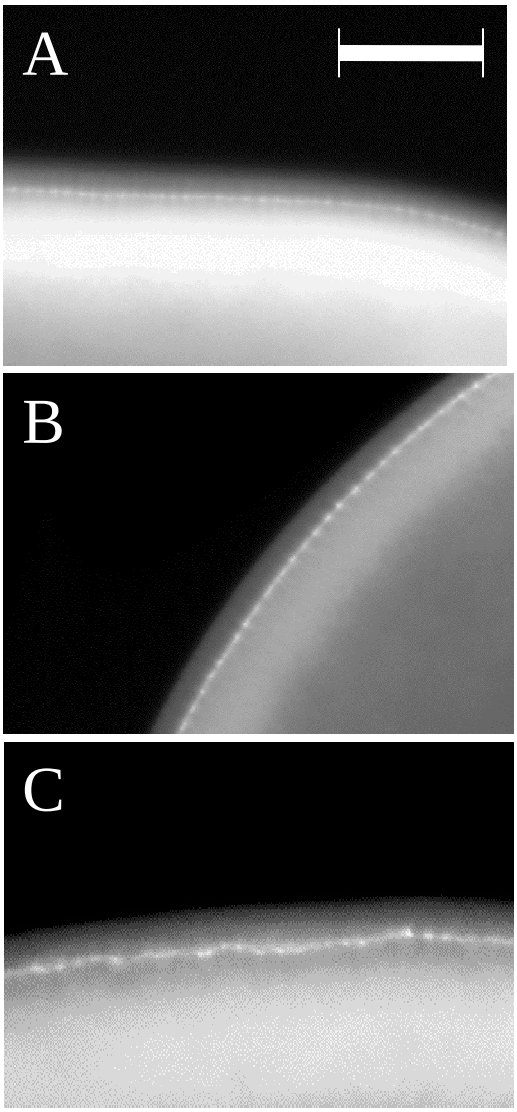

Figure 4.10: Analysis of the cellularization front in early cellularization *Src64* SH2 domain mutants. *Src64*^{P190L} (A), *Src64*^{G208E} (B), and *Src64*^{R217C} (C) embryos were analyzed for defects to the cellularization front. *Src64*^{P190L} and *Src64*^{G208E} embryos did not exhibit the defect. In the embryos identified, the cellularization front appeared similar to wild-type embryos (B, C). *Src64*^{R217C} embryos did exhibit the cellularization front defect similar to the defect seen in *Src64*$^{\Delta 17}$ and *Src64*^{KO} embryos. The cellularization front appeared wavy and wrinkled (C). Scale bar (A) is 30µm.

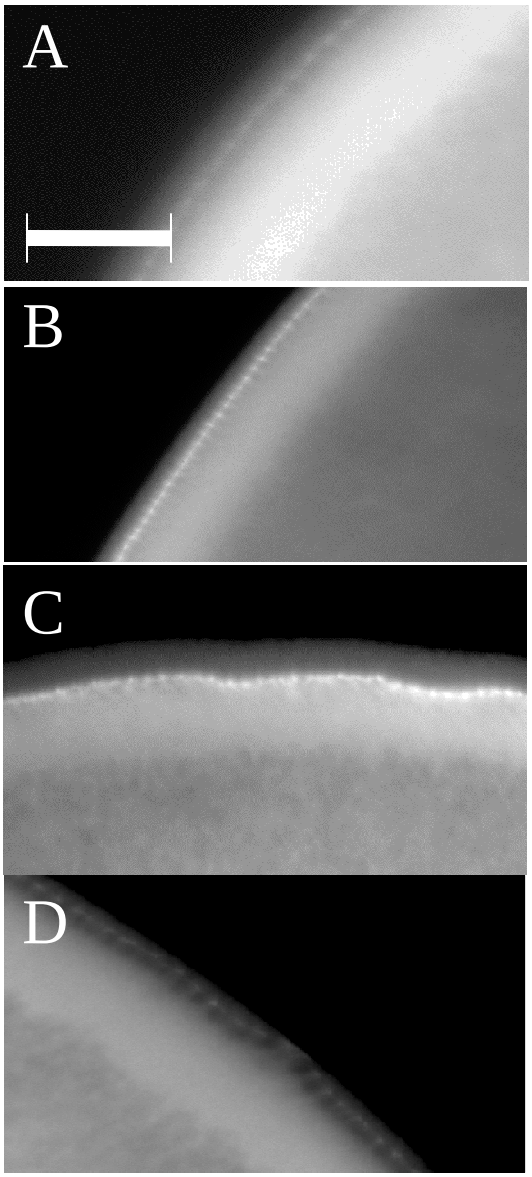

Figure 4.11: Analysis of the cellularization front in early cellularization *Src64* TK domain mutants. $Src64^{R403C}$ (A), $Src64^{S440F}$ (B), and $Src64^{D404N}$ (C, D) embryos were analyzed for defects in the cellularization front. The cellularization fronts in $Src64^{R403C}$ and $Src64^{S440F}$ embryos appeared similar to wild-type embryos, and did not appear to show any signs of the defect. The cellularization fronts were straight and uniform and did not appear to show any signs of the defect. (A, B) $Src64^{D404N}$ embryos did exhibit the defect in multiple embryos. The cellularization fronts in these embryos appeared similar to those seen in $Src64^{\Delta 17}$ and $Src64^{KO}$ embryos (C, D). In some cases the defect appeared more severe than that seen in $Src64^{\Delta 17}$ embryos and more similar to $Src64^{KO}$ embryos (C). Scale bar (A) is 30µm.

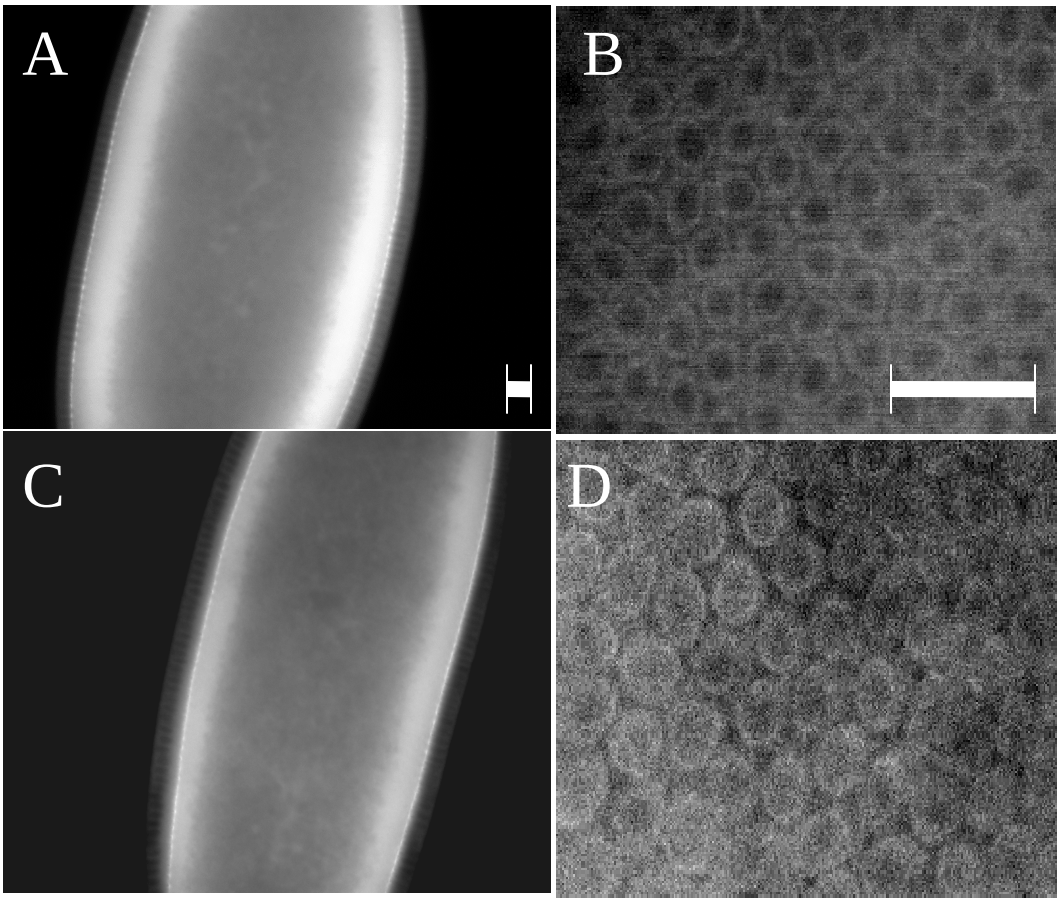

Figure 4.12: Wild-type microfilament rings during early and late cellularization. Microfilament ring circularity index and area measurements were taken from embryos separated into early and late cellularization. In early cellularization embryos the cellularization front has yet to pass the basal edge of the nuclei at the periphery of embryo (A, B). In late cellularization embryos the cellularization front has passed the peripheral nuclei and the cellularization front has begun to constrict (C, D). As the microfilament rings constrict more space can be seen around each ring (D). Images of the cellularization front were taken at 630X magnification, and zoomed in for better comparison (B, D). Scale bars (A, B) are 10µm.

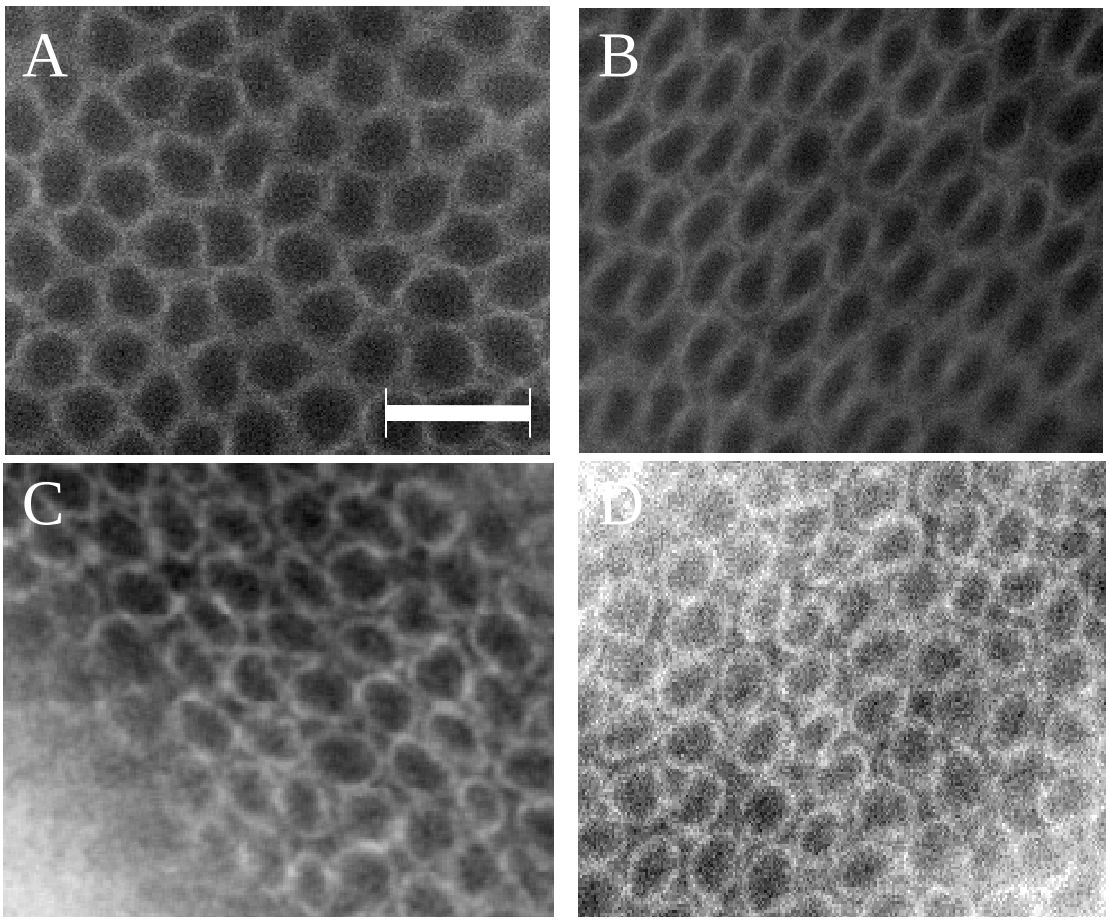

Figure 4.13: Microfilament ring defects in *Src64* mutants. Microfilament ring defects were seen in $Src64^{\Delta 17}$ (A), $Src64^{KO}$ (B), $Src64^{D404N}$ (C), and $Src64^{R217C}$ (D) embryos. In $Src64^{\Delta 17}$, $Src64^{KO}$ and $Src64^{D404N}$ embryos the defect could be seen in both early and late cellularization embryos. In $Src64^{R217C}$ embryos the defect was only apparent in late cellularization embryos. The defect appears as a reduced circularity to the microfilament rings. Ten rings were measured in a group from the mid-section of each embryo identified. Scale bar (A) is 10 µm

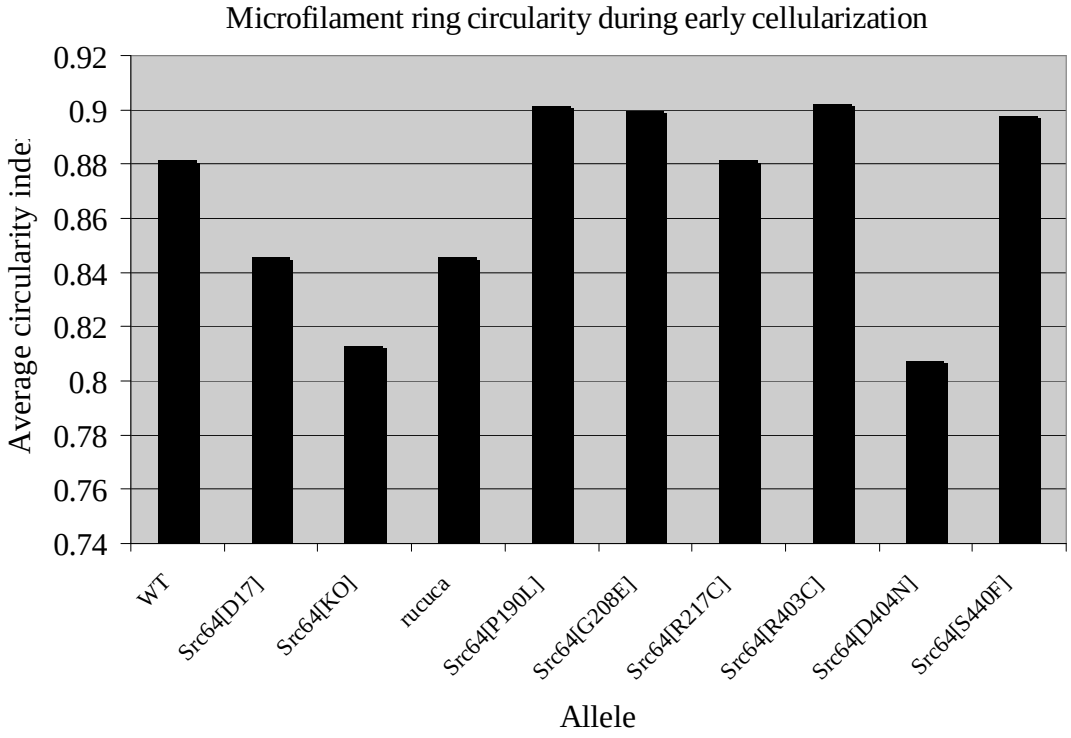

Figure 4.14: Comparison of microfilament ring circularity during early cellularization. Defects to microfilament ring circularity during early cellularization were seen in $Src64^{\Delta 17}$, $Src64^{KO}$, and $Src64^{D404N}$ embryos. $Src64^{\Delta 17}$ is a weak mutation that exhibits a moderate defect ($P<0.01$). $Src64^{KO}$ and $Src64^{D404N}$ are strong mutations that exhibit a severe defect to microfilament ring circularity ($P<0.001$).

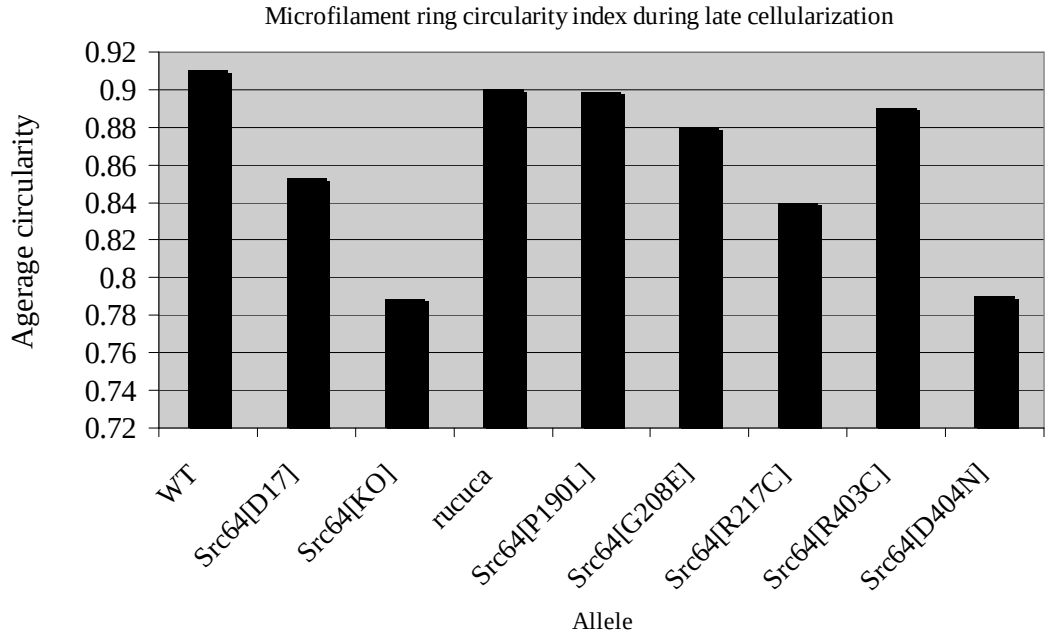

Figure 4.15: Comparison of microfilament ring circularity during late cellularization. Defects to microfilament ring circularity during early cellularization were seen in $Src64^{\Delta 17}$, $Src64^{KO}$, and $Src64^{D404N}$ embryos. $Src64^{\Delta 17}$ is a weak mutation that exhibits a moderate defect ($P<0.01$). $Src64^{KO}$ and $Src64^{D404N}$ are strong mutations that exhibit a severe defect to microfilament ring circularity ($P<0.001$).

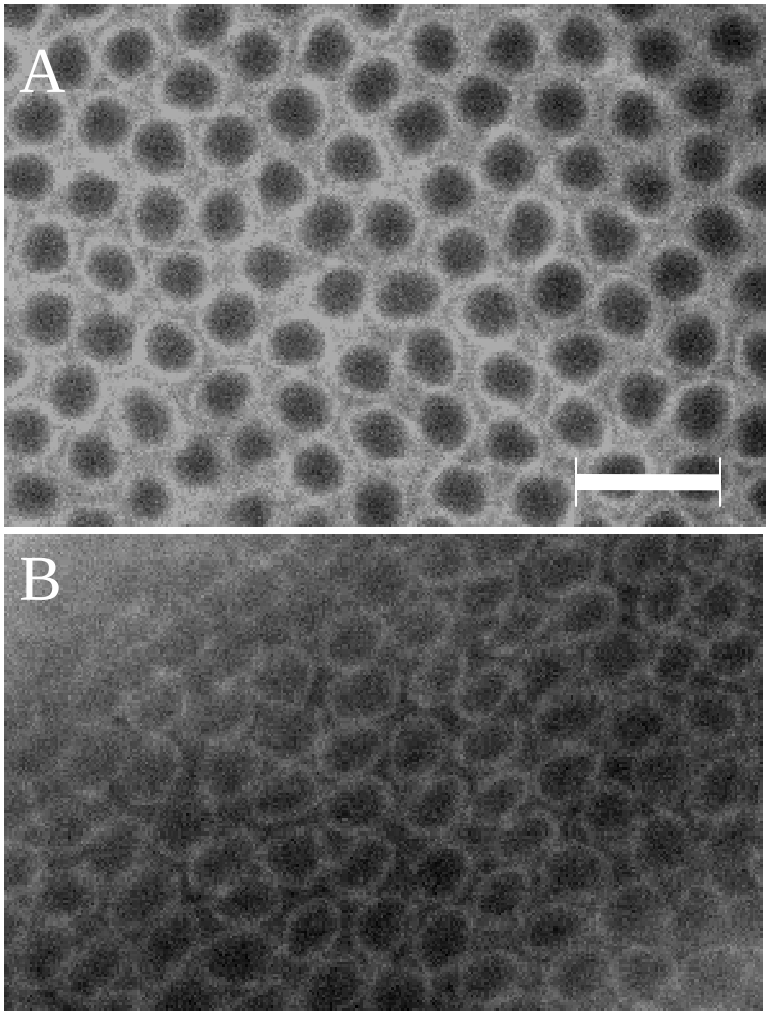

Figure 4.16: *Src64*^{R217C} microfilament rings during early and late cellularization. *Src64*^{R217C} microfilament rings do not exhibit the defect during early cellularization. The rings are statistically similar to wild-type microfilament rings (P>0.05) (A). During late cellularization *Src64*^{R217C} embryos exhibit a moderate defect to microfilament ring circularity and resemble *Src64*$^{\Delta 17}$ embryos (P>0.05) (B). Scale bar (A) is 10µm

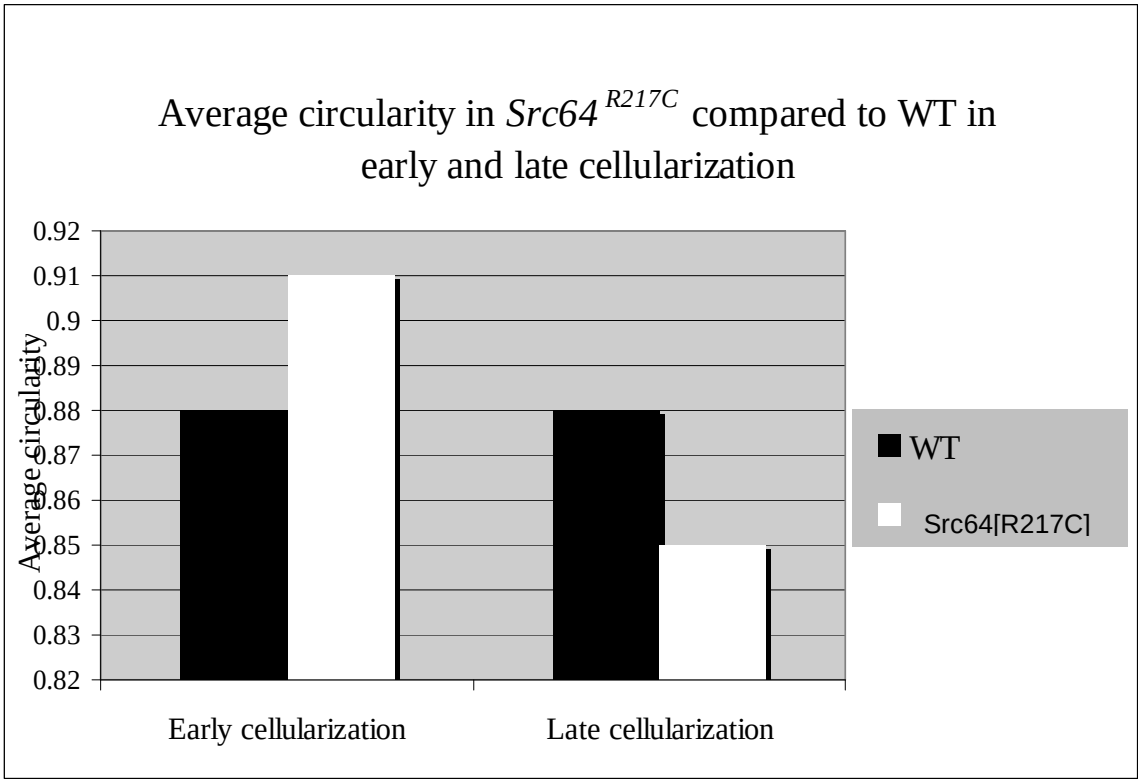

Figure 4.17: Comparison of *Src64*^{R217C} microfilament ring circularity in early and late cellularization. The average microfilament ring circularity in *Src64*^{R217C} embryos was statistically similar to WT during early cellularization ($P>0.05$). However, during late cellularization, *Src64*^{R217C} embryos exhibited a moderate defect to microfilament ring circularity ($P<0.01$). The late cellularization microfilament ring circularity defect is statistically similar to the defect seen in *Src64*$^{\Delta 17}$ embryos ($P>0.05$). This may suggest a different function for Src64 during early and late cellularization in which Src64 activity during early cellularization may be independent of the SH2 domain, but Src64 activity during late cellularization may involve the SH2 domain.

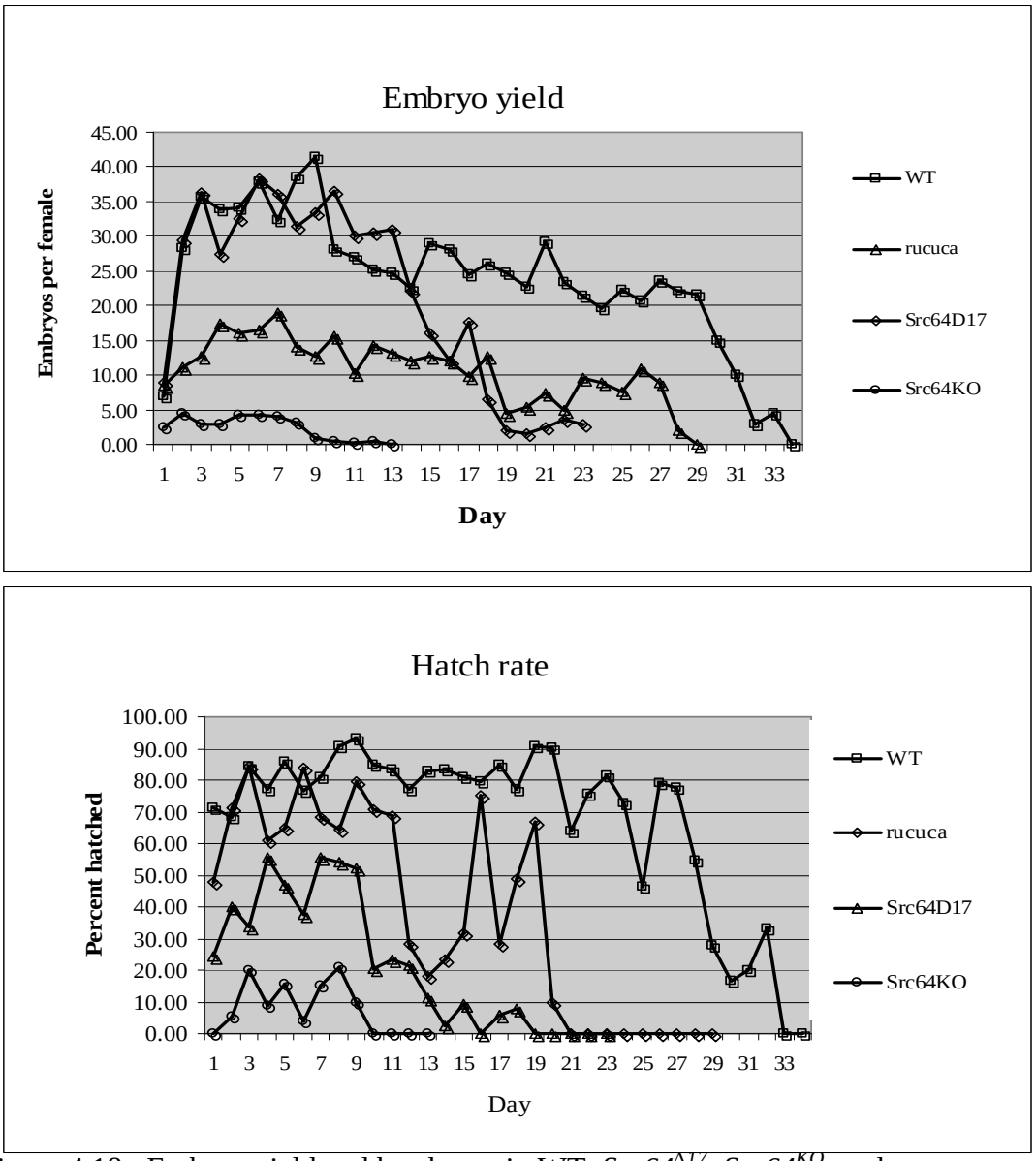

Figure 4.18: Embryo yield and hatch rate in WT, *Src64*$^{\Delta 17}$, *Src64*^{KO}, and *rucuca*. Analysis of embryo yield and hatch rate over the entire period of embryo productivity indicated reduced values during the first two (embryo yield in WT and *Src64*$^{\Delta 17}$) days and after ten days of analysis (embryo yield and hatch rate in *Src64*^{KO}). To make an accurate statistical comparison between the samples, we compared data between days 3 and 10.

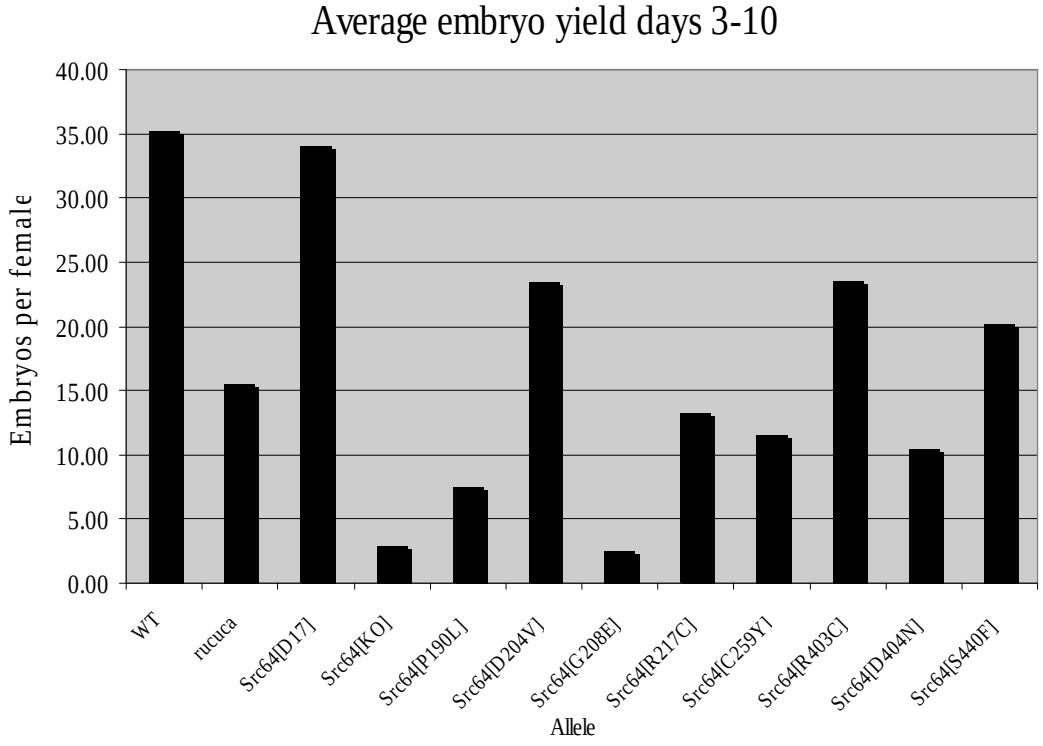

Figure 4.19: Comparison of average embryos yields from days 3-10. Statistical comparison was performed on embryo yields from days 3-10. Analysis of embryo yield indicated the most severe defect in $Src64^{KO}$ females ($P<0.001$). The defect to embryo yield in $Src64^{G208E}$ females was not statistically different ($P>0.05$) than the $Src64^{KO}$ defect, and was the most severe defect observed in the *Src64* point mutation embryos ($P<0.001$). Embryo yield in $Src64^{D404N}$ females was not statistically different than embryo yield in *rucuca* females ($P>0.05$).

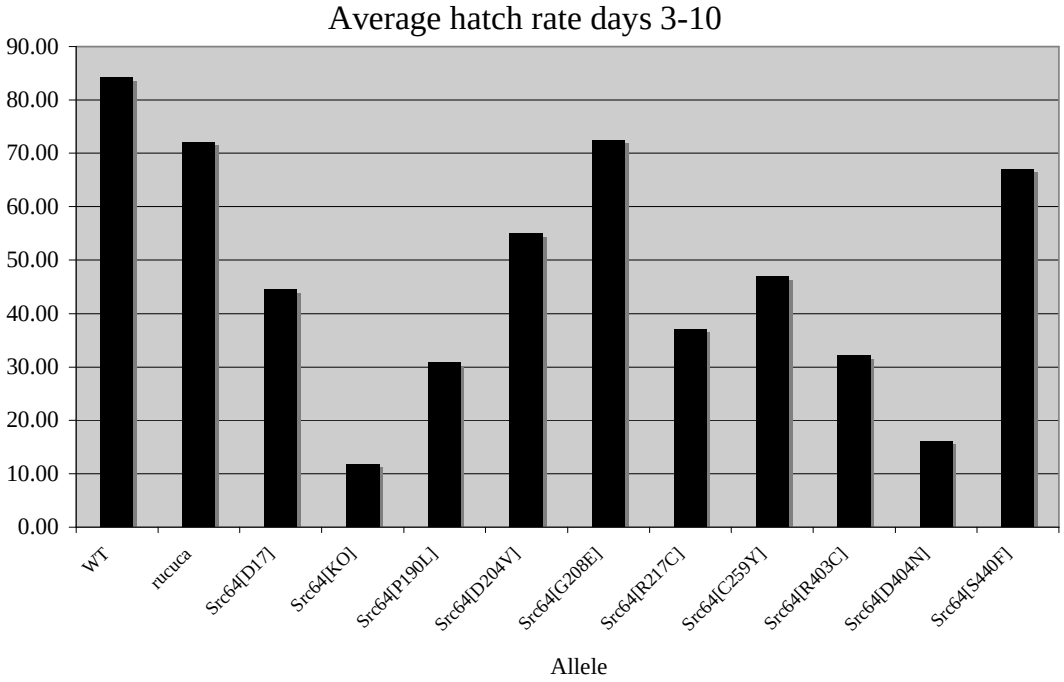

Figure 4.20: Comparison of average embryo hatch rates from days 3-10. Statistical comparison of hatch rate was performed on hatch rates gathered from days 3-10. Analysis of the hatch rates indicated the most severe defect in *Src64*^{KO} embryos ($P<0.001$). The defect to hatch rate identified in *Src64*^{D404N} embryos was statistically the same as the defect in *Src64*^{KO} embryos ($P>0.05$). The *Src64* mutant that exhibited the most severe defect to embryo yield, *Src64*^{G208E}, did not exhibit any defect in hatch rate ($P>0.05$).

CHAPTER V
DISCUSSION

5.1: Summary of Results

5.1.1 Molecular analysis of *Src64*

In the first step of our molecular analysis of *Src64* we determined that Src64mRNA was present in $Src64^{\Delta 17}$ embryos. Using semi-quantitative RT-PCR and primers that amplified specific transcripts of *Src64* we were able to determine that the level of *Src64* in $Src64^{\Delta 17}$ embryos was approximately 10% of the level seen in wild-type embryos (Table 3.1; Figure 3.3).

We performed a 5'RACE on RNA isolated from $Src64^{\Delta 17}$ embryos in order to locate the alternate transcriptional start site. We located the alternate transcriptional start site 13,100 base pairs downstream of the primary transcriptional start site (Figure 3.6). The alternate transcriptional start site is located in a previously undiscovered 108 base pair exon located 99 base pairs upstream of exon 3.

Locating the alternate transcriptional start site allowed us to make primers that specifically amplify mRNA derived from this start site. Using these primers we were able to compare the amount of mRNA derived from the alternate transcriptional start site in wild-type and $Src64^{\Delta 17}$ embryos (Figure 3.8). Our analysis detected no difference in the amount of mRNA derived from the alternate transcriptional start site in $Src64^{\Delta 17}$ embryos compared to wild-type embryos (Table 3.2).

5.1.2 Phenotypic analysis of *Src64* mutant embryos

For our phenotypic analysis of *Src64* mutant embryos we located ten point point mutations within the *Src64* coding region using the TILLING method. These ten mutations were located in the SH2 and TK domains. Our goal in locating these mutations was to knock out the function of specific domains of *Src64* and to determine how this affected *Src64* function during embryo development. In addition, we included $Src64^{\Delta 17}$ and $Src64^{KO}$ embryos in our phenotypic analysis. Our analysis of embryo development included an analysis of nuclear fallout, embryo size, progression of the cellularization

front, microfilament ring circularity, microfilament ring constriction, embryo yield, and hatch rate.

From our analysis of nuclear fallout in wild-type and $Src64^{\Delta 17}$ embryos we determined that nuclear fallout is significantly increased ($P<0.001$) in $Src64^{\Delta 17}$ embryos compared to wild-type embryos during nuclear division cycles 12, 13, and 14 of embryonic stage four (Table 4.3). In our analysis of $Src64^{KO}$, $Src64^{P190L}$, $Src64^{D204V}$, $Src64^{G208E}$, $Src64^{R217C}$, $Src64^{C259Y}$, $Src64^{R403C}$, $Src64^{D404N}$, and $Src64^{S440F}$ embryos we did not find any evidence of an elevated level of nuclear fallout. Nuclear fallout in these embryos was statistically similar ($P>0.05$) to the level of nuclear fallout in wild-type embryos (Table 4.4). These results suggest that the increased incidence of nuclear fallout identified in $Src64^{\Delta 17}$ embryos is likely not a result of the $Src64^{\Delta 17}$ mutation, and may be caused by some other element present in the $Src64^{\Delta 17}$ strain.

From our analysis of embryo size we determined that embryo length was significantly reduced ($P<0.001$) in $Src64^{\Delta 17}$, $Src64^{KO}$, $Src64^{P190L}$, $Src64^{D204V}$, $Src64^{R217C}$, $Src64^{C259Y}$, $Src64^{R403C}$, and $Src64^{D404N}$ embryos (Table 4.5). Additionally, we determined that embryo width was significantly reduced ($P<0.01$) in $Src64^{\Delta 17}$, $Src64^{KO}$ embryos (Table 4.6).

Our analysis of *Src64* mutant embryos for cellularization defects confirmed the previously identified defect in cellularization front progression in $Src64^{\Delta 17}$ embryos. In contrast to the uniform and smooth wild-type cellularization front, the cellularization front in $Src64^{\Delta 17}$ embryos appears wavy, wrinkled and disorganized (Figure 4.6). Additionally, we identified a similar defect in $Src64^{KO}$ embryos (Figure 4.9). We also identified the defect in $Src64^{R217C}$ and $Src64^{D404N}$ embryos (Figure 4.10; Figure 4.11). Although we were unable to quantify the defect to the cellularization front, the defect did appear more severe in $Src64^{KO}$ and $Src64^{D404N}$ embryos than in $Src64^{\Delta 17}$ and $Src64^{R217C}$ embryos.

From our analysis of microfilament ring circularity we determined that microfilament rings in early cellularization $Src64^{\Delta 17}$, $Src64^{KO}$, and $Src64^{D404N}$ embryos exhibit a reduced circularity compared to microfilament rings in early cellularization wild-type embryos (Table 4.7), and that microfilament rings in late cellularization

Src64$^{\Delta 17}$, *Src64*^{KO}, *Src64*^{R217C}, and *Src64*^{D404N} embryos exhibit a reduced circularity compared to microfilament rings in wild-type embryos (Table 4.8). Additionally, from our statistical analysis we determined that the defect in microfilament ring circularity in *Src64*^{KO} and *Src64*^{D404N} embryos is more severe ($P<0.001$) than the defect in *Src64*$^{\Delta 17}$ and *Src64*^{R217C} embryos ($P<0.01$) (Table 4.7; Table 4.8).

From our analysis of microfilament ring constriction we determined that microfilament ring constriction was severely reduced in *Src64*^{KO} embryos (table 4.9). Microfilament ring constriction also appeared to be reduced in *Src64*$^{\Delta 17}$, *Src64*^{D404N}, and possibly *Src64*^{R217C} and *Src64*^{R403C} embryos; however, due to difficulties in matching the exact age of the embryos, and the speed of microfilament ring constriction we were unable to make a statistical comparison of these results.

In our analysis of embryo yield we identified a severe defect ($P<0.001$) in embryo yield in *Src64*^{KO} and *Src64*^{G208E} females (table 4.10). Surprisingly, embryo yield in *Src64*^{D404N} embryos was statistically similar ($P>0.05$) to the embryo yield in the *rucuca* control (Table 4.10).

In our analysis of hatch rate in *Src64* mutants we identified a significantly reduced ($P<0.001$) hatch rate in *Src64*^{KO} and *Src64*^{D404N} mutants (Table 4.11). The remaining *Src64* mutants exhibited a defects in embryo hatch rate that ranged from statistically similar to the wild-type and *rucuca* hatch rates (*Src64*^{G208E}), to a moderate defect in hatch rate compared to the wild-type and *rucuca* embryo hatch rates (*Src64*$^{\Delta 17}$, *Src64*^{P190L}, *Src64*^{D204V}, *Src64*^{R217C}, *Src64*^{C259Y}, *Src64*^{R403C}) that was not reduced to the level seen in embryos laid by *Src64*^{KO} and *Src64*^{D404N} females (Table 4.11).

5.2 Discussion of results

5.2.1 Molecular analysis of *Src64*

Our hypothesis in the molecular analysis of *Src64* was that there is an alternate transcriptional start site for *Src64* that was responsible for the trace amounts of Src64 protein seen in *Src64*$^{\Delta 17}$ flies. We confirmed our hypothesis by identifying the alternate transcriptional start site and an alternate first exon. The alternate transcriptional start site codes for exactly the same protein as the primary transcriptional start site; however, an

alternate transcriptional start site does have implications for transcriptional regulation of Src64 protein levels.

Transcriptional control of Src-family kinases is especially important due to the role that Src-family kinases can play in cancer development and malignant transformation. An increase in Src activity can lead to increased cell motility, increased cell proliferation, promotion of neo-angiogenesis, and the presentation of a transformed phenotype. Elevated Src activity can result from the increased activity of up-stream Src activating proteins, a specific activating mutation to Src that prevents inhibition, or elevated levels of Src protein due to increased transcription. An alternate transcriptional start site provides another area for transcriptional control over the level of *Src64* present in a cell.

We confirmed the presence of *Src64* transcripts derived from the alternate transcriptional start site in both wild-type and $Src64^{\Delta 17}$ embryos, suggesting that the alternate transcriptional start site is responsible for at least a fraction of *Src64* transcription in wild-type embryos, and plays some role in normal biological functions. In $Src64^{\Delta 17}$ embryos, transcription via the alternate transcriptional start site is responsible for the low levels of Src64 protein, and is likely responsible for the phenotypic differences seen in $Src64^{\Delta 17}$ and $Src64^{KO}$ embryos. $Src64^{\Delta 17}$ homozygous flies produce viable embryos; while $Src64^{KO}$ flies do not produce viable embryos. Transcription of *Src64* via the alternate transcriptional start site is then likely sufficient to allow for embryo survival. We also determined that transcription via the alternate transcriptional start site is not limited to the embryo. The presence of the *Src64* transcripts derived from the alternate transcriptional start site in pre-cellularization and post-cellularization samples indicated that *Src64* derived from the alternate transcriptional start site is both maternally deposited and zygotically transcribed.

The specific role of the alternate transcriptional start site in embryonic development is still unknown. While we identified the alternate transcriptional start site in embryos at a very early stage of development before tissue differentiation begins, further research into the role of the alternate transcriptional start site may indicate importance in specific developmental processes. The alternate transcriptional start site,

located 13,100 base pairs downstream of the primary transcriptional start site, is far enough away from away from the primary transcriptional start site to have its own promoter region that could function independently of the primary transcriptional start site promoter region. This could allow for precise control over the amount of Src64 protein present in a particular type of cell, or during a particular developmental process. Additionally, an alternate transcriptional start site could allow for tissue specific transcription of Src64 protein.

We performed an analysis of the promoter binding sites located in the 1,000 base pairs upstream of the primary transcriptional start site and the alternate transcriptional start site using the TFSEARCH program (Table 5.1) (TFSEARCH, 1999). By comparing the two promoter regions we have identified a number of differences that could lead to preferential activation of the alternate transcriptional start site. Most importantly, we identified four TATA boxes in the 1,000 base pairs upstream of the alternate transcriptional start site while the primary transcriptional start site had none. Additionally, there were a number of promoter binding sites upstream of the alternate transcriptional start site that were not present upstream from the primary transcriptional start site. The Abd-D, Croc, and Ftz promoter binding sites were specific to the primary transcriptional start site, and AP-1, Elf-1, and GCM binding sites were specific to the alternate transcriptional start site. There are also significant differences in the number of binding sites for promoters known to be important in the early embryo. Specifically, there were 11 Dfd, 9 BR-C, and 5 Hb binding sites upstream of the primary transcriptional start site and 2 Dfd, 1 BR-C, and 1 Hb binding sites upstream of the alternate transcriptional start site. These data support the hypothesis that *Src64* transcription from the alternate transcriptional start site has a specific role in development, and the differences in the two promoter regions could lead to tissue specific transcription of *Src64*.

5.2.2 Phenotypic analysis of *Src64* mutants

In our analysis of the *Src64* mutants, we analyzed $Src64^{\Delta 17}$, $Src64^{KO}$, $Src64^{P190L}$, $Src64^{D204V}$, $Src64^{G208E}$, $Src64^{R217C}$, $Src64^{C259Y}$, $Src64^{R403C}$, $Src64^{D404N}$, and $Src64^{S440F}$

embryos. We were able to confirm our hypothesis that mutations in different domains of *Src64* would cause varying effects to the phenotype of developing embryos. Using the results from each of our analyses we can create an allelic series that ranks the strength of each mutation for each of the specific defects. This has allowed us to determine some specifics of Src64 activity in the developing embryo. (Table 5.2) Research into cancer treatment by Src inhibition has focused on inhibition of kinase activity. Successful kinase inhibitors have been developed; however, as our research, and previous research, has indicated, Src kinase activity is complex and multi-layered. Further research into Src-family kinase activity, and domain specific activity, is important to fully understanding the role that Src-family kinases play in proper development and in cancer progression.

In our analysis of the cellularization front we identified a defect in $Src64^{\Delta 17}$, $Src64^{KO}$, $Src64^{D404N}$, and $Src64^{R217C}$ embryos (Table 5.2). Additionally, we speculate that the defect may be more severe in the $Src64^{KO}$ and $Src64^{D404N}$ embryos; however, this is not based on a statistical analysis. From these results we determined that both the SH2 and TK domains are likely active in proper formation of the cellularization front, and that the TK domain may be more vital to this process than the SH2 domain. If *Src64* activity in the formation of the cellularization front is similar to human Src activity in the activation of focal adhesion kinase, the SH2 domain may be involved in localization of Src to the cellularization front, or in recruitment of downstream factors, while the TK domain is likely involved in activation of a downstream *Src64* target. Additionally, the SH2 and SH3 domains could have some redundant function, as seen in human Src activation of FAK, resulting in the apparently moderate defect identified in the SH2 domain mutant. The SH2 domain mutations could also reduce, but not entirely remove the binding ability of the SH2 domain. Such a reduction in binding affinity could result in the moderate defects observed in SH2 domain mutants.

Our results from the analysis of microfilament ring circularity correlate with the results of our cellularization front analysis. Again, defects were seen in $Src64^{\Delta 17}$, $Src64^{KO}$, $Src64^{D404N}$, and $Src64^{R217C}$ (Table 5.2). However, in this analysis we were able to quantify our results and confirm that the defects in $Src64^{KO}$ and $Src64^{D404N}$ embryos

are significantly more severe than the defects in *Src64*$^{\Delta 17}$ and *Src64*^{R217C} embryos. Our analysis of microfilament ring circularity also revealed some phenotypic differences between early and late cellularization. Specifically, *Src64*^{R217C} embryos exhibited the microfilament ring circularity defect during late cellularization, but not during early cellularization. These results suggest that there may be some difference in *Src64* activity between early and late cellularization, and that the SH2 domain may not be involved in microfilament ring formation during early cellularization, but becomes important during late cellularization. Again, the moderate defect in the SH2 domain mutants may be due to redundancy in SH2 and SH3 domain activity, or only a moderate reduction in the *Src64* SH2 domain binding affinity due to the mutations.

The results from our analysis of microfilament ring constriction support the hypothesis that *Src64* activity is different during different developmental processes (Table 5.2). However, similar to our analysis of the cellularization front, analysis of microfilament ring constriction is not based on a statistical comparison, but on a direct analysis of the data. As we determined in our analysis of the cellularization front and microfilament rings, the most severe defect in microfilament ring constriction was seen in *Src64*^{KO} embryos. *Src64*^{D404N} embryos exhibited a moderate defect to microfilament ring constriction, while neither *Src64*^{R217C} embryos nor any other *Src64* mutant embryos exhibited any defect in microfilament ring constriction. These results suggest that while the TK domain is likely involved in microfilament ring constriction, a reduction in TK domain activity is not sufficient to reduce microfilament ring constriction to the level seen in *Src64*^{KO}. Additionally, the SH2 domain is likely not involved in microfilament ring constriction. One possibility is that the SH3 domain works with the TK domain during microfilament ring constriction in a process that is independent of any SH2 domain activity.

Our analysis of *Src64* mutants indicated a role for the SH2 and tyrosine kinase domains at the cellularization front and in microfilament rings; however, until additional targets of Src64 activity at these locations are determined we can not determine why mutations to *Src64* cause such defects. Knowing how Src64 is active in the formation of ring canals, we can speculate on how Src64 may be active in the cellularization front and

microfilament rings. Src64 may be involved in recruitment or activation of an actin-polymerizing protein to the cellularization front. Activation of an actin polymerizing protein at the cellularization front could lead to an increased level of actin organization at the plasma membrane near the cellularization front. This could provide the necessary anchoring point progression of the myosin-rich cellularization front, and constriction of the microfilament rings. Mutations to *Src64* could lead to a decreased recruitment or activation of downstream proteins that could lead to a decreased actin polymerization near the cellularization front. Without sufficient actin polymerization at the cellularization front myosin mediated progression of the cellularization front and constriction of the microfilament rings may be disrupted.

Our analysis of embryo yield and hatch rate also indicated varying phenotypes depending on the specific mutation (Table 5.2). As seen in our previous analyses, $Src64^{KO}$ caused the most severe defect in both embryo yield and hatch rate. $Src64^{G208E}$ females, with an SH2 domain mutation, exhibited a defect in embryo yield statistically similar to $Src64^{KO}$ females, while $Src64^{D404N}$ females only exhibited a moderate defect to embryo yield. These results suggest that the SH2 domain is vital to embryo production, while the TK domain may have some redundant function, or have only an accessory role. It is possible that Src64 may have a role in oogenesis that is independent of the TK domain function. $Src64^{D404N}$ caused a defect in hatch rate statistically similar to $Src64^{KO}$ embryos, while $Src64^{G208E}$ embryos did not exhibit any defect to hatch rate. These results suggest that *Src64* may play two distinct roles in development, with the SH2 domain being vital in embryo yield and the TK domain being vital to hatch rate. A mutation to either the SH2 domain or the TK domain is not sufficient to reduce both embryo yield and hatch rate to the levels seen in $Src64^{KO}$ females and embryos. The role of *Src64* during these processes is not fully known; however, defects in ring canal formation are likely to result from at least one of the mutations. Ring canal defects could explain the decrease in hatch rate seen in $Src64^{KO}$ and $Src64^{D404N}$ embryos. Defective ring canals likely impede maternal deposition of transcription factors and RNA transcripts, possibly enough to lower the hatch rate. The role that the SH2 domain plays in maintaining normal embryo yield is unknown; however this could involve ring canals as well.

Interestingly, different SH2 domain mutations caused two distinct defects (Table 5.2). *Src64*^{G208E} exhibited the defect to embryo yield but no defect to the cellularization front, while *Src64*^{R217C} exhibited defects to the cellularization front and microfilament rings, but did not show any signs of defects to embryo yield. *Src64* likely acts on different target proteins in these two roles, and we suggest that the two different SH2 mutations reduce SH2 domain binding affinity in different ways. The *Src64*^{G208E} mutation may disrupt binding to a target protein involved in embryogenesis, while the *Src64*^{R217C} mutation may disrupt binding to a target protein involved in the cellularization front and microfilament rings. Until the binding partners of *Src64* have been identified during these processes we will not be able to determine how these mutations specifically affect SH2 domain binding affinity.

5.3 Future research directions

5.3.1 Molecular analysis of *Src64*

The first step in the continued analysis of the *Src64* alternate transcriptional start site should be the confirmation of our results by real-time quantitative RT-PCR. These experiments could confirm our results and give us a better understanding of the level of *Src64* transcription from the alternate transcriptional start site. Additionally, real-time quantitative RT-PCR may be precise enough to determine if there is any elevated or decreased *Src64* transcription from the alternate transcriptional start site related to embryo age.

The next step in the analysis of the alternate transcriptional start site would be an analysis of its potential biological importance. Our experiments were focused on locating the alternate transcriptional start site, and not on its potential role in developments. *in situ* hybridization experiments could be used to localize *Src64* transcripts derived from the alternate transcriptional start site, and determine if the alternate transcriptional start site is a tissue specific transcript involved in specific developmental processes. Expanding the molecular analysis to embryos later in embryo development could identify specific roles for the alternate transcriptional start site. Additionally, the alternate transcriptional start site may have a specific role in adult flies.

5.3.2 Phenotypic analysis of *Src64* mutants

The first step that we have discussed in continuing with the phenotypic analysis of *Src64* mutants is expanding the analysis to include SH3 domain mutants, and double mutants. Our analysis thus far has identified some potential roles for the SH3 domain, specifically in microfilament ring constriction; however, this hypothesis is based on the lack of a defect in SH2 domain mutants that would account for the differences in microfilament ring constriction between $Src64^{KO}$ and $Src64^{D404N}$ embryos. Direct analysis of SH3 domain mutants could confirm this hypothesis. We have discussed the creation of an SH3-knockout mutant that could be created and expressed in $Src64^{KO}$ flies. Using the UAS-Gal4 expression system and a promoter active in the early embryo we could express *Src64* lacking the SH3 domain in the early embryo. This could be used to determine if the SH3 domain is involved in microfilament ring constriction or possibly identify other roles for the SH3 domain.

Additionally, we have discussed expanding the analysis of the mutants that we already have obtained. An analysis of ring canals in the egg chamber could determine if the $Src64^{G208E}$ and $Src64^{D404N}$ mutations disrupt the proper formation of ring canals. Analysis of the ring canals could also help determine why the SH2 domain mutation in $Src64^{G208E}$ females causes such a severe defect to embryo yield. The results from our analysis of embryo yield strongly suggest a tyrosine kinase domain function for Src64 during the process of oogenesis. Analysis of ring canals in female flies could help in the identification of such a process. .

Additionally, further research is needed into the downstream targets of *Src64*. In many of the processes in which we have analyzed Src64 activity, the specific target or targets of *Src64* are not known. One area that our lab is actively researching is the role of the protein cortactin in the cellularization front and microfilament rings. Cortactin is a known target of human Src, and may be involved in the microfilament reorganization taking place in the cellularization front and microfilament rings.

Table 5.1 Analysis of promoter binding sited 1000 base pairs upstream of the primary transcriptional start site and the alternate transcriptional start site

Promoter	Gene	Binding sites in the primary transcriptional start site	Binding sites in the alternate transcriptional start site
TATA Box	-	0	4
Abd-B	*Abdominal-B*	1	0
AP-1	*AP-1*	0	2
BR-C Z	*Broad-Complex Z3*	9	1
CF2-II	*CF2-II*	14	8
Croc	*Crocodile*	2	0
Dfd	*Deformed*	11	2
dl	*dorsal*	1	1
Elf-1	*Elf-1*	0	1
Ftz	*Fushi tarazu*	1	0
GCM	*glial cells missing*	0	1
Hb	*Hunchback*	1	5
Hsf	*Heat Shock factor*	22	32
Ttk-69	*Tramtrack-69K*	0	3

Table 5.2: Allelic series for defects to the cellularization front, microfilament rings during early and late cellularization, microfilament ring constriction, embryo yield, and hatch rate

	Strength of defect compared to WT					
Src64 Allele	Cellularization front*	Microfilament ring circularity during early cellularization	Microfilament ring circularity during late cellularization	Microfilament ring constriction*	Embryo yield	Hatch rate
$Src64^{\Delta 17}$	Moderate	Moderate	Moderate	WT	WT	Moderate
$Src64^{KO}$	Severe	Severe	Severe	Severe	Severe	Severe
$Src64^{P190L}$	WT	WT	-	-	Moderate	Severe
$Src64^{D204V}$	-	-	-	-	Moderate	Moderate
$Src64^{G208E}$	WT	WT	WT	WT	Severe	WT
$Src64^{R217C}$	Moderate	WT	Moderate	WT	Moderate	Moderate
$Src64^{C259Y}$	-	-	-	-	Moderate	Moderate
$Src64^{R403C}$	WT	WT	WT	WT	Moderate	Moderate
$Src64^{D404N}$	Severe	Severe	Severe	Moderate	Moderate	Severe
$Src64^{S440F}$	WT	WT	WT	WT	Moderate	WT

* Rankings not based on statistical analysis

\- No data for this mutant in this specific defect

REFERENCES

Akiyama, Y. (1999). *TFSEARCH: Searching transcription factor binding sites (ver. 1.3).* Retrieved March 28, 2007 from http://www.cbrc.jp/research/db/TFSEARCH.html.

Ali, N., Yoshizumi, M., Fujita, Y., Izawa, Y., Kanematsu, Y., Ishizawa, K., Tsuchiya, K., Yano, S., Sone, S., and Tamaki, T. (2005). A novel Src kinase inhibitor, M475271, inhibits VEGF-induced human umbilical vein endothelial cell proliferation and migration. *Journal Pharmacol Sci, 98,* 130-141.

Altschul, S. F., Madden, T. L., Schaffer, A. A., Zhang, Z., Miller, W., and Lipman, D. J. (1997). Gapped BLAST and PSI-BLAST; a new generation of protein database search programs. *Nucleic Acids Res, 25,* 3389-3402.

Baumeister, U., Funke, R., Ebnet, K., Vorschmitt, R., Koch, S., and Vestweber, D. (2005). Association of Csk to VE-cadherin and inhibition of cell proliferation. *The EMBO Journal, 24,* 1686-1695.

Bishop, J. M. (1985). Viral oncogenes. *Cell, 42,* 23-38.

Boggon, T. J. and Eck, M. J. (2004). Structure and regulation of Src family kinases. *Oncogene, 23,* 7918-7927.

Brody, T. B. (1995). The *Interacttive Fly*. Retrieved May 15th, 2006 from http://www.sdbonline.org/fly/cytoskel/src64-1.htm.

Dodson, G. S., Guarnieri, D. J., and Simon, M. A. (1998). Src64 is required for ovarian ring canal morphogenesis during Drosophila oogenesis. *Development, 125,* 2883-2892.

Edgar, B. A., and Schubinger, G. (1986). Parameters controlling transcriptional activation during early Drosophila development. *Cell, 44,* 871-877.

Frame, M. C., Finchman, V. J., Carragher, N. O., and, Wyke, J. A. (2002). v-Src's hold over actin and cell adhesions. *Nature Reviews Molecular Cell Biology, 3,* 233-245.

Fullilove, S. L., and Jacobsen, A. G. (1971). Nuclear elongation and cytokinesis in Drosophila montana. *Developmental Biology, 26,* 560-570.

Gigliotti, S., Rotoli, D., Manzi, A., Graziani, F., and Malva, C. (2000). Female sterile mutations and egg chamber development in Drosophila melanogaster. *Int Jour Dev Bio, 44,* 581-589.

Gong, W. J., and Golic, K. G. (2003). Ends-out, or replacement, gene targeting in Drosophila. *Proc. Natl. Acad. Sci. USA, 100:* 2556-2561.

Gottardi, C. J., and Gumbiner, B. M. (2001). Adhesion signaling; how β-catenin interacts with its partners. *Curr. Biology, 11,* R792-R794.

Guarnieri, D.J., Dodson, G.S., and Simon, M.A. (1998). Src64 regulates the localization of a Tec-family kinase required for Drosophila ring canal growth. *Mol. Cell, 1,* 831-841.

Henikoff, S., Till, B. J., and Comai, L. (2004). TILLING. traditional mutagenesis meets functional genomics. *Plant Physiology, 135,* 11-17.

Higgs, H. N., and Pollard, T. D. (2001). Regulation of actin filament network formation through ARP2/3 complex: activation by a diverse array of proteins. *Annual Review Biochemistry, 70,* 767-776.

Huang, C., Ni, Y., Wang, T., Gao, Y., and Haudenschild, C. C. (1997). Zhan, X. Down-regulation of the filamentous actin cross-linking activity of cortactin by Src-mediated tyrosine phosphorylation. *Journal of Biological Chemistry, 272,* 13911-13915.

Irby, R. B., Mao, W., Coppola, D., Kang, J., Loubeau, J. M., Trudeau, W., Karl, R., Fujita, D. J., Jove, R., and Yeatman, T. (1999). Activating SRC mutations in a subset of advanced human colon cancers. *Nature Genetics, 21,* 187-190.

Irby, R. B., and Yeatman, T. J. (2000). Role of Src expression and activation in human cancer. *Oncogene, 19,* 5636-5642.

Kaplan, K. B., Swedlow, J. R., Morgan, D. O., and Varmus, H. E. (1995). c-Src enhances the spreading of Src -/- fibroblasts on fibronectin by a kinase-independent mechanism. *Genes Dev., 9,* 1505-1517.

Kaplan, K. B., Bibbins, K, B., Sewdlow, J. r., Arnaud, M., Morgan, D., and Varmus, H. E. (1994). Association of the amino-terminal half of c-Src with focal adhesions alters their properties and is regulated by phosphorylation of tyrosine 527. *The EMBO Journal, 13,* 4745-4756.

Kelso, J. R., Hudson, A. M., and Cooley, L. (2002). Drosophila Kelch regulates actin organization via *Src64*-dependent tyrosine phosphorylation. *JBC, 156,* 703-713.

Lu, N., Guarnieri, D., and Simon, M. A. (2004). Localization of Tec29 to ring canals is mediated by Src64 and PtdIns(3,4,5)P_3-dependent mechanisms. *The EMBO Journal, 23,* 1089-1100.

Mead, D. A., Pey, N. K., Herrnstadt, C., Marcil, R. A., and Smith, L. M. (1991). A universal method for direct cloning of PCR amplified nucleic acid. *Biotechnology, 9,* 657-663.

Ng, P.C., and Henikoff, S. (2001). Predicting deleterious amino acid substitutions. *Genome Res. 11,* 863-874.

O'Reilly, A.M., Ballew, A.C., Miyazawa, B., Stocker, H., Hafen, E., and Simon, M.A. (2006). *Csk* differentially regulates *Src64* during distinct morphological events in Drosophila germ cells. *Development, 133,* 2627-2638.

Parsons, J. T. (2003). Focal adhesion kinase: the first ten years. *Journal of Cell Science, 116,* 1409-1416.

Pawson, Tony. (2004). Specificity in signal transduction; from phosphotyrosine-SH2 domain interactions to complex cellular systems. *Cell, 116,* 191-203.

Pedraza, L. G., Stewart, R. A., Li, D., and Xu, T. (2004). Drosophila Src family kinases function with *Csk* to regulate cell proliferation and apoptosis. *Oncogene, 23,* 4754-4762.

Roberts, D. B. (1998). *Drosophila: A Practical Approach*. New York: Cold Spring Harbor Laboratory Press,

Robinson, D. N., and Cooley, L. (1996). Stable intercellular bridges in development: the cytoskeleton lining the tunnel. *Trends Cell Biology, 6,* 474-479.

Roskoski, R. J. (2004). Src protein-tyrosine kinase structure and regulation. *Biochemical and Biophysical Research Communications, 324,* 1155-1164.

Royou, A., Field, C., Sisson, J. C., Sullivan, W., and Karess, R. (2004). Reassessing the role and dynamics of nonmuscle myosin II during furrow formation in early Drosophila embryos. *Molecular Biology of the Cell, 15,* 838-850.

Schaller, M. D. (2001). Paxillin; a focal adhesion-associated adapter protein. *Oncogene, 20,* 6459-6472.

Schaller, M. D., Hildebrand, J. D., and Parsons, J. T. (1999). Complex formation with focal adhesion kinase: a mechanism to regulate activity and subcellular localization of Src kinases. *Molecular Biology of the Cell, 10,* 3489-3505.

Schejter, E. D., and Wieschaus, E. (1993). Functional elements of the cytoskeleton in the early *Drosophila* embryo. *Annu. Rev. Cell. Biology, 9,* 67-99.

Schwartz, S. M., Gajdusek, C. M., and Selden, S. M. (1981). Vascular wall growth control: the role of the endothelium. *Arteriosclerosis, 1,* 107-126.

Sieg, D. J., Hauck, C. R., and Schlaepfer, D. D. (1999). Required role of focal adhesion kinase (FAK) for integrin-stimulated cell migration. *Cell, 112,* 2677-2691.

Smith, C. I., Islam, T. C., Mattsson, P. T., Mohamed, A. J., Nore, B. F., and Vihinen, M. (2001). The Tec family of cytoplasmic tyrosine kinases; mammalian Btk, Bmx, Itk, Tec, Tck and homologs in other species. *Bioassays, 23,* 436-446.

Somogyi, K, and Rorth, P. (2003). Cortactin modulates cell migration and ring canal morphogenesis during Drosophila oogenesis. *Mechanisms of Development, 121,* 57-64.

Sullivan, W., Fogarty, P., and Theurkauf, W. (1993). "Mutations affecting the cytoskeletal organization of syncitial Drosophila embryos. *Development, 118,* 1245-1254.

Summy, J.M., and Gallick, G. E. (2006). Treatment for advanced tumors: Src reclaims center stage. *Clinical Cancer Research, 12,* 1398-1401.

The Flybase Consortium. (2003). The flybase database of the Drosophila genome projects and community literature. *Nucleic Acids Research, 31,* 172-175.

Thomas, S. M., and Brugge, J. S. (1997). Cellular functions regulated by Src family kinases. *Annual Rev Cell Dev Biology, 13,* 513-609.

Thomas, J. and Weischaus, E. (2004). *Src64* and *Tec29* are required for microfilament contraction during drosophila development. *Development, 131,* 863-871.

Tillney, L. G., Tilney, M. S., and Guild, G. M. (1996). Formation of actin filament bundles in the ring canals of developing Drosophila follicles. *Journal of Cell Biology, 133,* 61-74.

Wallez, Y., Cand, F., Cruzalegui, F., Wernstedt, C., Souchelnytskyi, S., Vilgrain, I., and Huber, P. (2007). Src kinase phosphorylates vascular endothelial-cadherin in response to vascular endothelial growth factor; identification of tyrosine 685 as the unique target. *Oncogene, 26,* 1067-1077.

Wu, H., and Parsons, J. T. (1993). Cortactin, an 80/85-kilodalton pp60src substrate, is a filamentous actin-binding protein enriched in the cell. *Journal of Cell Biology, 120,* 1417-1426.

Yeo M.G., Partridge, M.A., Ezratty, E. J., Shen, Q., and Gunderson, G. G., and Marcantonio, E. E. (2006). Src Sh2 arginine 175 is required for cell motility: specific focal adhesion kinase targeting and focal adhesion assembly function. *Molecular and Cell Biology,* 4399-4409.

PERMISSION TO COPY

In presenting this thesis in partial fulfillment of the requirements for a master's degree at Texas Tech University or Texas Tech University Health Sciences Center, I agree that the Library and my major department shall make it freely available for research purposes. Permission to copy this thesis for scholarly purposes may be granted by the Director of the Library or my major professor. It is understood that any copying or publication of this thesis for financial gain shall not be allowed without my further written permission and that any user may be liable for copyright infringement.

Agree (Permission is granted.)

_____ _____

Student Signature Date

Disagree (Permission is not granted.)

Taylor Strong 3-04-2007

_____ _____

Student Signature Date